Report 41164R05

ADAPTIVE FULL-SPECTRUM SOLAR ENERGY SYSTEMS

Cross-Cutting R&D on adaptive full-spectrum solar energy systems for more efficient and affordable use of solar energy in buildings and hybrid photobioreactors

Semi-Annual Technical Progress Report
For Period Ending January 31, 2004

Byard D. Wood, Project Director
Mechanical and Aerospace Engineering
Utah State University
Logan, Utah 84322-4130

Jeff D. Muhs, Principal Investigator
Oak Ridge National Laboratory
P.O. Box 2008
Oak Ridge, TN 37831-6074

PREPARED FOR

NATIONAL ENERGY TECHNOLOGY LABORATORY
THE UNITED STATES DEPARTMENT OF ENERGY

DOE Award Number DE-FC26-01NT41164
Energy Crosscutting Science Initiative
Office of Energy Efficiency and Renewable Energy

April 2004

ABTRACT

This RD&D project is a three year team effort to develop a hybrid solar lighting (HSL) system that transports solar light from a paraboloidal dish concentrator to a luminaire via a large core polymer fiber optic. The luminaire can be a device to distribute sunlight into a space for the production of algae or it can be a device that is a combination of solar lighting and electric lighting. A benchmark prototype system has been developed to evaluate the HSL system. Sunlight is collected using a one-meter paraboloidal concentrator dish with two-axis tracking. A secondary mirror consisting of eight planar-segmented mirrors directs the visible part of the spectrum to eight fibers (receiver) and subsequently to eight luminaires. This results in about 8,200 lumens incident at each fiber tip. Each fiber can illuminate about 16.7 m^2 (180 ft^2) of office space. The IR spectrum is directed to a thermophotovoltaic (TPV) array to produce electricity.

During this reporting period, the project team made advancements in the design of the second generation (Alpha) system. For the Alpha system, the eight individual 12 mm fibers have been replaced with a centralized bundle of 3 mm fibers. The TRNSYS Full-Spectrum Solar Energy System model has been updated and new components have been added. The TPV array and non-imaging device have been tested and progress has been made in the fiber transmission models. A test plan was developed for both the high-lumen tests and the study to determine the non-energy benefits of daylighting. The photobioreactor team also made major advancements in the testing of model scale and bench top lab-scale systems.

PREFACE

This report is a joint effort between Oak Ridge National Laboratory and the University of Nevada, Reno, and as such it satisfies the reporting requirements for the University and ORNL as the M&O for this project. This is the fifth semi-annual report for this technology development project. This report is posted on web site www.energy.unr.edu/lighting.htm

TABLE OF CONTENTS

LIST OF FIGURES

LIST OF TABLES

PARTICIPATING ORGANIZATIONS

Organization	Abbreviation	Principal Investigator
University of Nevada, Reno Mechanical Engineering-312 University of Nevada Reno, NV 89557	UNR	Daniel Dye
Utah State University Mechanical and Aerospace Engineering Utah State University Logan, Utah 84322-4130	USU	Byard Wood
Oak Ridge National Lab P.O. Box 2009, MS-8058 Oak Ridge, TN 32831	ORNL	Jeff Muhs
JX Crystals, Inc. 1105 12th Avenue NW, Suite A2 Issaquah, WA 98027	JXC	Lewis Fraas
Ohio University Dept. of Mechanical Engineering 248 Stocker Center Athens, OH 45701-2979	OU	David Bayless
Rensselaer Polytechnic Institute Lighting Research Center 21 Union Street Troy, NY 12180-3352	RPI	Nadarajah Narendran
Science Application International Corporation 9455 Towne Centre Drive San Diego, California 92121	SAIC	Robin Taylor
3M Company 3M Corporate Process Technology Center St. Paul, MN 55144-1000	3M	Jennifer Sahlin
TVA Public Power Institute 1101 Market Street, MR 2T Chattanooga, TN 37402-2801	TVA	David Dinse
University of Arizona Department of Agricultural and Biosystems Engineering 507 Shantz Building Tucson, AZ 85721	UA	Joel Cuello
University of Wisconsin Solar Energy Lab 1500 Johnson Dr. Madison, WI 53706	UW	William Beckman

The contributions of each of these individuals and their colleagues in the preparation of this report are gratefully acknowledged.

EXECUTIVE SUMMARY

This RD&D project is a three year team effort to develop a hybrid solar lighting (HSL) system that transports day light from a paraboloidal dish concentrator to a luminaire via a large core polymer fiber optic. The luminaire can be a device to distribute sunlight into a space for the production of algae or it can be a device that is a combination of solar lighting and electric lighting for a wide spectrum of commercial lighting applications. This report describes the technical progress from August 1, 2003 through January 31, 2004.

The overall objectives for this project are:

1. Use a Benchmark Prototype System to assess technical feasibility of using full-spectrum solar energy systems to enhance the overall sunlight utilization in buildings and biomass production rates of photobioreactors;

2. Through experiments and analyses, determine the commercial viability of using full-spectrum solar energy systems to enhance the overall sunlight utilization in buildings and biomass production rates of photobioreactors. (Alpha System)

3. Develop a pre-commercial prototype HSL system (Beta System) that illustrates substantial progress towards the project's cost and performance goals.

During the reporting period, the project team made advancements in the design of the Alpha system with acentralized small-fiber bundle, updated and added components to the TRNSYS Full-Spectrum Solar Energy System model, tested the Thermophotovoltaic (TPV) array and non-imaging device, made changes and advancements in the high-lumen test system, and made changes to the fiber transmission models. A test plan was developed for both the high-lumen tests and the study to determine the non-energy benefits of daylighting. The photobioreactor team also made major advancements in the testing of model scale and bench top lab-scale systems. Accomplishments for this period are:

1. Work was performed on the high-lumen test system and mechanical durability test device. Different brands of fibers were selected and acquired for both tests, and bending fatigue tests are underway. The high-lumen test system has undergone some revisions, and tests are not underway yet. A test plan has been laid out that outlines the steps that will be taken to perform the tests and analyze the data that are obtained.

2. Tests of the TPV array were performed and a publication was generated and submitted to the ISEC 2004 conference. The TPV array generated 26.7W and demonstrated 12% conversion efficiency. The results were compared with laboratory test data, and when the intensity differences of the light sources and characteristics of the cells are taken into consideration, the laboratory and outdoor tests are in agreement.

3. The light transmission of arbitrary lengths of fiber optic cables was investigated and models are being built with FORTRAN code and TracePro. The effects of interface roughness on light transmission were investigated, a sensitivity analysis of light transmission through a straight optical fiber was performed, and it is shown that the core-cladding interface roughness term is necessary for approximating experimental results. A study of light transmission using results generated from FORTRAN code is also shown.

4. Updates and additions were also made to the TRNSYS model. Chromaticity modeling, correlated color temperature (CCT), and spectral power distribution were studied and are being added to the TRSNSYS system model. Definition and calculation of the color rendering index is also presented.

5. Bioreactor light distribution tests, population and harvesting tests, and model scale tests were performed. There are very encouraging results from the model scale tests in terms of organism growth rates and the final tests necessary to meet our project goals have been started.

6. A bench top lab-scale membrane-based photobioreactor was developed. This system is designed to grow microalgae on a membrane surface. Experiments were described and results presented.

7. Several new, lower cost concentrating and tracking components were investigated. A lower-cost system, built by Edtek, Inc., was chosen for the Alpha system. An extremely low-cost stamped steel mirror, by Fortec, was purchased and analyzed for possible use in the Beta system. A small-fiber bundle was optimized for use in the Alpha system, along with a non-imaging device. A simple large-fiber bundle was also built and will be tested soon.

8. A test plan for the experiment proposed to address the non energy benefits of daylight was finalized and is presented. Details of how the experiment will be performed and the location of the experiment are discussed.

9. A solar energy lab at UNR was acquired for use as the Alpha and Beta systems test facility. An outdoor testing platform was built to mount the HSL system and High-Lumen test system adjacent to the lab. The team is now designing the data acquisition system in order to monitor the light transmission, thermal management of the fibers, luminaire power consumption, and power consumption of the two different tracking systems.

PROJECT DESCRIPTION

This project is part of the FY 2000 Energy Efficiency Science Initiative that emphasized Cross-Cutting R&D in Solicitation No.: DE-PS36-00GO10500. It is a three year research project that addresses key scientific hurdles associated with adaptive, full-spectrum solar energy systems and associated applications in commercial buildings and new hybrid solar photobioreactors. The goal of this proposal is to demonstrate that full-spectrum solar energy systems can more than double the affordability of solar energy in commercial buildings and hybrid solar photobioreactors used in CO_2 mitigation and compete favorably with existing alternatives.

This project is a multi-team effort to develop a hybrid solar lighting (HSL) system that transports solar light from a paraboloidal dish concentrator to a luminaire via a large core polymer fiber optic. The luminaire can be a device to distribute sunlight into a space for the production of algae or it can be a device that is a combination of solar lighting and fluorescent lighting for office lighting. In this project, the sunlight is collected using a one-meter paraboloidal concentrator dish with two-axis tracking. The secondary mirror consists of eight planar-segmented mirrors that direct the visible part of the spectrum to eight fibers (receiver) and subsequently to eight luminaires. This results in about 8,200 lumens incident at each fiber tip. The IR spectrum is directed to a thermophotovoltaic array to produce electricity. This report describes the technical progress from August 1, 2003 through January 31, 2004.

SCOPE OF WORK

The key scientific hurdles are being addressed in a three-phase effort, viz.:

Phase I. Assess Technical Feasibility

Determine technical feasibility of using full-spectrum solar energy systems to enhance the overall sunlight utilization in buildings and biomass production rates of photobioreactors. This will be accomplished by developing a benchmark prototype system that can evaluate the solar lighting technology that was outlined in the original proposal.

Phase II. Assess Commercial Viability

Determine the commercial viability of using full-spectrum solar energy systems to enhance the overall sunlight utilization in buildings and biomass production rates of photobioreactors. This will be accomplished by determining those aspects that characterize performance efficiency, reliability, durability and ultimately minimum cost potential. This phase will culminate with the design and construction of an Alpha system that shows significant improvement in the performance cost ratio.

Phase III. Assess System Affordability

Demonstrate the HSL technology in a building application and a photobioreactor application. The emphasis in developing the demonstration systems will be to meet performance objectives at minimum cost via a Beta system or pre-commercial prototype system.

PROGRESS TOWARDS PROJECT OBJECTIVES

The emphasis during this reporting period has been on the following items:

1. Fiber Durability Tests
2. Thermophotovoltaic System Testing
3. Prediction of attenuation loss for Plastic Optical Fibers (POF)
4. TRNSYS: Chromaticity modeling, Correlated Color Temperature (CCT) Algorithm, Spectral Power Distribution, SMARTS2 and TRNSYS, Definition and Calculation of the Color Rendering Index
5. Bioreactor Re-design, Light Data, Population & Harvesting Testing, and Model Scale Tests
6. Development of Bench Top Lab-Scale Photobioreactor
7. Collector/receiver and light deliver
8. Non-Energy Benefits of Daylighting
9. UNR Solar Energy Lab and Alpha System Test Facility

A summary of each investigation is given below.

1. Fiber Durability Tests

The fiber durability tests are comprised of the high-lumen test system and the mechanical durability, or bending fatigue, test system.

1.1 High-Lumen Test

1.1a High-Lumen Test System

A detailed discussion of the progress for this task is given in Appendix A "High Lumens Screening Test Setup for Optical Fiber Used in Hybrid Solar Lighting System". A brief summary is given below.

> *A research team led by Oak Ridge National Laboratory has designed a Hybrid Solar Lighting System for transporting daylight to building interiors via optical fibers [3]. Light carrying capacity, flexibility, and cost are important design factors for choosing an appropriate fiber, and these factors have pointed to the use of large-core plastic fibers. For the hybrid approach to be practical, the fibers must perform well for approximately 20 years, thus long-term transmission data are needed.*
>
> *This paper describes the design and analysis of two experimental apparatuses. One of these two has been chosen to evaluate the long-term optical performance of three different brands of large core fiber as a screening test for the Hybrid Lighting System. The test setup must supply a specified amount of lumens, protect the fiber from heat, and allow for periodic degradation measurements to be taken easily. This is a comparison and screening test only.*

1.1b: High-Lumen Test Plan

A test plan for the High Lumen testing was also developed and is presented below.

Experiment objective:

Compare the long-term transmission and attenuation of three different types of optical fibers used for illumination when exposed to high lumens.

Selected fiber brands to be tested:
3M
Poly Optic
Lumenyte

Instrumentation/background:
Three main factors that affect degradation in optical fibers are: incident angle of light at fiber tip, heat, and impurities in the fiber.

For each of the possible test options (see test options section below), overall lumens as well as the transmission at 2nm intervals over the 250nm to 900nm range will be measured. Lumens will be measured using a 4" integrating sphere and a hand-held spectrometer by Labsphere. The photopic curve is the commonly accepted definition of the wavelengths the average human eye responds to. The lumen is a measurement of wavelengths in the visible region, weighted by the photopic curve, so a good way to measure overall transmission is the number of lumens at various distances down an optical fiber. Transmission at various wavelengths will be measured using a spectroradiometer by StellarNet Inc. In order to generate a useful attenuation graph, it is recommended that attenuation be measured at 2nm to 5nm intervals. The transmission data will be taken for each length of fiber and written to an Excel sheet for post processing. Since the lumen is weighted towards λ=0.55μm, color shift is not really taken into account. However, differences in red and blue wavelengths are observable to humans, so both total lumens and absolute irradiance will be measured. The cutback method will be used at the end of each test because it has been adopted as the standard approach for measuring attenuation in fibers.

Light source:
A Cogent high intensity discharge light with voltage regulator will be the light source used for each test. This source will be allowed 10 minutes warm up time to stabilize.

Testing options:
Option 1
Place 10m length of fiber in the high lumen test setup, expose it to high lumens, measure both overall lumen output and spectral transmission frequently (time interval will be based on change in readings). After fiber has been exposed for a pre-selected time, the length of fiber will be cut back, 1m at a time until 1m remains, then cut back 10 cm at a time until 0.5m remains, then cut back 5cm at a time, and transmission measured at each length. This test will require more fiber than option 2, and will therefore be more expensive. It will take more time (a total of 30 polishes and measurements will need to be made), but will offer an opportunity to check the quality control of the fiber since there are more chances for impurities with longer lengths. It may also provide more data on the color shift, and it will still supply all the information available in option 2. The cost of instrumentation will be the same in both cases, as will the cost of the setup, so the only added costs are the price of the fiber itself and the additional labor.

Option 2
Place 2m length of fiber in the high lumen test setup, expose it to high lumens, measure both overall lumen output and spectral transmission frequently (time interval will be based on change in readings). After fiber has been exposed for a pre-selected time, 2m length of fiber will be cut back to 1m, then cut back 10 cm at a time until 0.5m remains, then cut back 5cm at a time, and transmission measured at each length. This will give an idea of how long the entrance region really is. The advantage this option has is that it will be cheaper than option 1 because it will require less fiber. It will also take less time to measure, but this is not a great factor because the measurements will be almost instantaneous with the spectroradiometer.

Option 3
Perform 2m test on all fiber except 3M, perform 10m test on 3M to determine if useful information is gained. Repeat test using option 1 if necessary.

A control piece of each type of fiber will be placed aside for comparison, and the same fiber cutter and polishing technique will be used on every fiber. At the end of the test, the 5cm segments from the entrance region of each fiber will be sent to Oak Ridge National Laboratory for hardness tests.

Prerequisite tests:
1) Use TracePro/Mathcad to determine length of quartz necessary to protect each fiber based on manufacturer's maximum recommended temperature. Verify with thermocouples to see if fiber is staying below that temp. Record length of quartz necessary and keep in consideration for final fiber recommendation.

2) Test/model quartz for loss- if little light is lost in the quartz itself then for simplicity it might be better to use the same length of quartz for each fiber as long as the one with the lowest maximum recommended temperature is adequately protected.

Expectations:
Most of the degradation will occur in the first ~15cm
Most of the degradation will occur within the first few days of the test.

1.2 Mechanical Durability Tests

The fiber bender was modified to speed up testing time. As shown in Fig. 1, it was modified to bend three fibers simultaneously and count the cycles each fiber completes individually, but due to the amount of torque put on the bending arm it was changed to only bend two fibers at a time. Since the three fibers were held on one side only, a ¼" grade eight bolt kept shearing off. With only two fibers this bolt has not broke. Tests are ongoing and different brands are now being tested. Durability data from each of the fiber brands should be available by the end of BP2.

Fig. 1: Fiber fatigue testing device

2. TPV System Testing

This Task is summarized in a paper accepted for publication in the ISEC 2004 Solar Energy Conference: "Demonstration of Thermophotovoltaics for a Full-Spectrum Solar Energy System". The abstract from this paper is shown below, and the full version of the paper can be found in Appendix B.

A non-imaging (NI) device and thermophotovoltaic (TPV) array for use in a full-spectrum solar energy system has been designed, built, and tested [1,2,3]. This system was designed to utilize the otherwise wasted infrared (IR) energy that is separated from the visible portion of the solar spectrum before the visible light is harvested. The IR energy will be converted to electricity via a gallium antimonide (GaSb) TPV array. The experimental apparatus for the testing of the IR optics and TPV performance is described. Array performance data will be presented, along with a comparison between outdoor experimental tests and laboratory flash tests. An analysis of the flow of the infrared energy through the collection system will be presented, and recommendations will be made for improvements. The TPV array generated a maximum of 26.7 W, demonstrating a conversion efficiency of the IR energy of 12%.

3. Prediction of attenuation loss for Plastic Optical Fibers (POF):

3.1 Interface Roughness Effect on Light Transmission

The attenuation of 3M's fiber was compared with that of TracePro for the same launching condition (given by the numerical aperture of the fiber), and power input to the fiber. The correction factor for TracePro result of 3M's attenuation under the same illumination conditions (3M's attenuation converted to absorption coefficient) is given in Fig. 2.

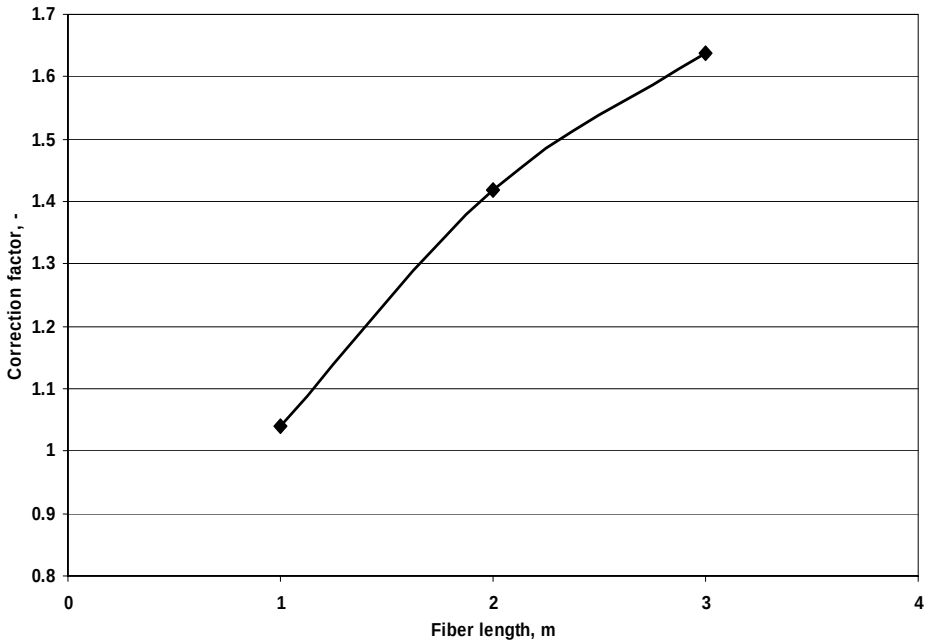

Fig.2: TracePro correction of 3M's fiber attenuation for straight fiber with no bends.

Figure 2 does not compare with 3M's experimental result after conversion of 3M's attenuation to absorption coefficient. The nature of increasing magnitude of correction factor was attributed to the lack of TracePro modeling of core-cladding interface roughness. The nature of this correction is not known for the same straight section of 3M fiber if that section follows a certain-radius bend and no correction factor was set for any bent section.

The result of Cates' et al. paper (Fig. 6) was compared with TracePro result. This is given in Fig. 3. Although TracePro result shows a small-slope linear decline with incident angle, it does not converge to the exponential decay given by Cates' et al.

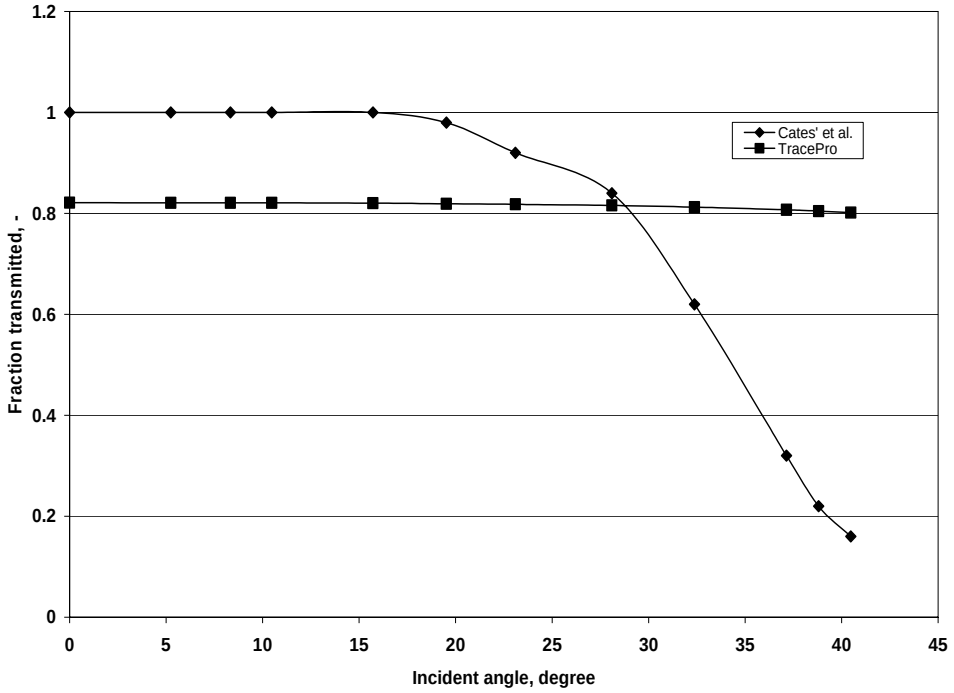

Fig. 3: TracePro result comparison of Cates' et al. paper (Fig. 6).

It was seen that the effect of core-cladding interface roughness on light transmission, verified experimentally with the work of Cates et al. and theoretically with the work of Remillard et al., is an important contributor, thus, needs to be properly modeled on TracePro.

3.2 Fortran Program Comparison with TracePro

A novel Fortran code has been written to analyze the light loss on a straight light pipe and the results were compared with the result of TracePro (See Fig. 4).

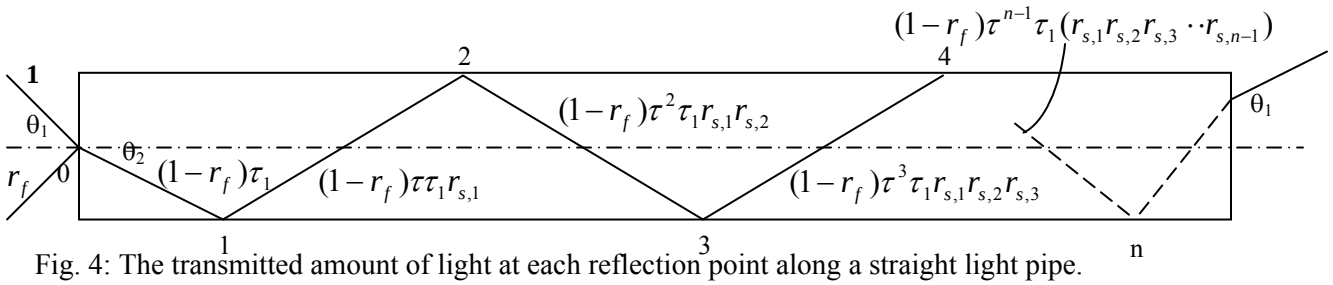

Fig. 4: The transmitted amount of light at each reflection point along a straight light pipe.

The model written in Fortran did not include the interface roughness loss but only bulk absorption, and bulk scattering losses. Figure 5 shows the comparison between the two models.

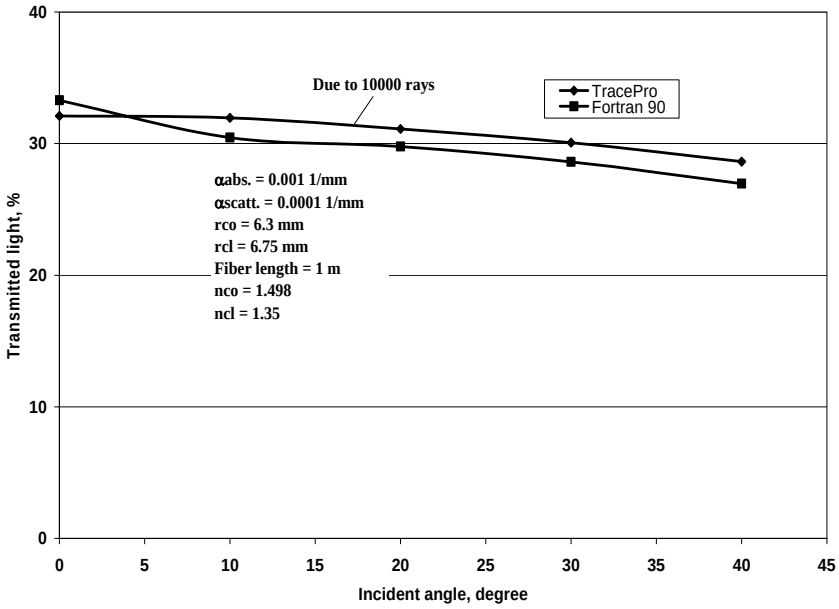

Fig. 5: Fortran 90 program compared to TracePro.

Figure 6 gives the difference between the results of Fig. 4. It is seen that the new written Fortran code matches the result of TracePro.

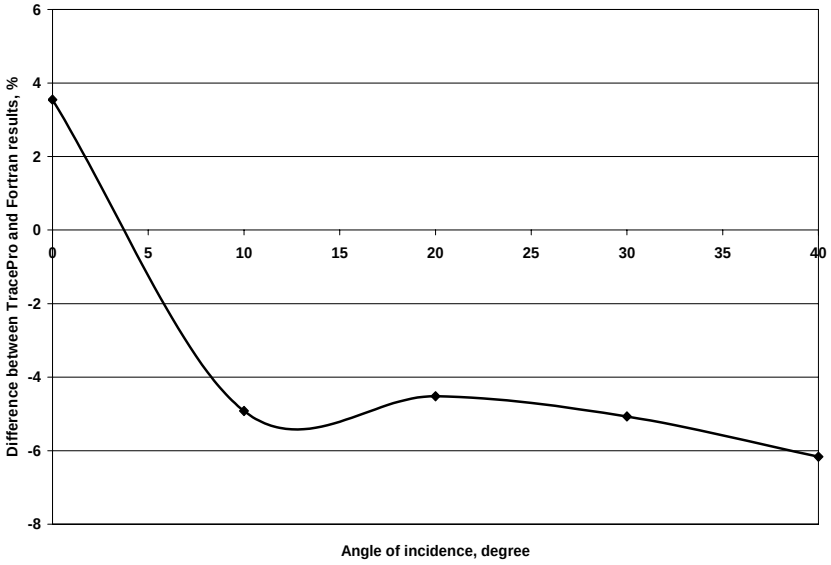

Fig. 6: Difference between the results of Fortran program and TracePro.

It was seen based on the straight fiber loss that the results of the written Fortran program and the TracePro do not differ substantially. The present model is now being written for multi-ray case on a straight light pipe. The bent section will be analyzed next.

3.3 Sensitivity Analysis of Light Transmission through a Straight Optical Fiber

Sensitivity analysis for the light transmission of straight optical fiber was completed.

$$\frac{P_{exit}(\lambda,\theta_2,r_{co})}{P_{in}(\lambda)} = [1-r_f]^2 \cdot (r_{s,1} \cdot r_{s,2} \cdots r_{s,n}) \cdot \exp\left\{-\alpha_e(\lambda) \cdot \begin{bmatrix} [r_{co} \cdot (2 \cdot n - 1) + r] / \sin\theta_2 + \\ (L_t - x_n) / \cos\theta_2 \end{bmatrix}\right\} \quad (1)$$

The light transmission equation given in Eq. (1) was derivated according to the factors, $\theta_1 = \theta_{inc}$, L_t, α_{abs}, α_{scatt}, r_{core}, and r where respective factors mean incident angle, fiber length, absorption coefficient, scattering coefficient, core radius, and local radius. Eqn. (2) shows the rule used in the sensitivity analysis where X denotes each of the factors mentioned above. In the derivation of Eq. (1) and further in comparison of the sensitivity coefficients, Fresnel reflectivity counting not more than 4% and the product of interface reflectivity terms $(r_{s,1} \cdot r_{s,2} \cdots r_{s,n})$ were taken constant. This is shown with A in Eq. (2).

$$\frac{1}{A} \cdot \left| \frac{\Delta \tau_{overall}}{\Delta X} \right| = \frac{\Delta}{\Delta X} \left| \exp\{-\alpha_e(\lambda) \cdot [r_{co} \cdot (2 \cdot n - 1) + r] / \sin\theta_2 + (L_t - x_n) / \cos\theta_2\} \right| \quad (2)$$

Although the sensitivity analysis used the 3M fiber's core and clad radii, the analysis results are valid on any optical fiber in order to get an idea about the most important factor affecting the light transmission.

Figures 7-13 show the sensitivity coefficient for each factor affecting the light transmission.

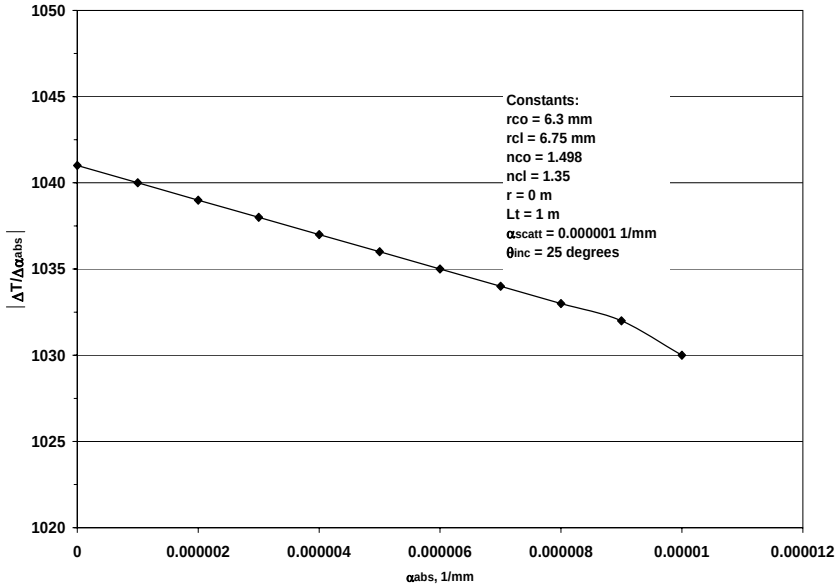

Fig. 7: Sensitivity coefficient of α_{abs} .

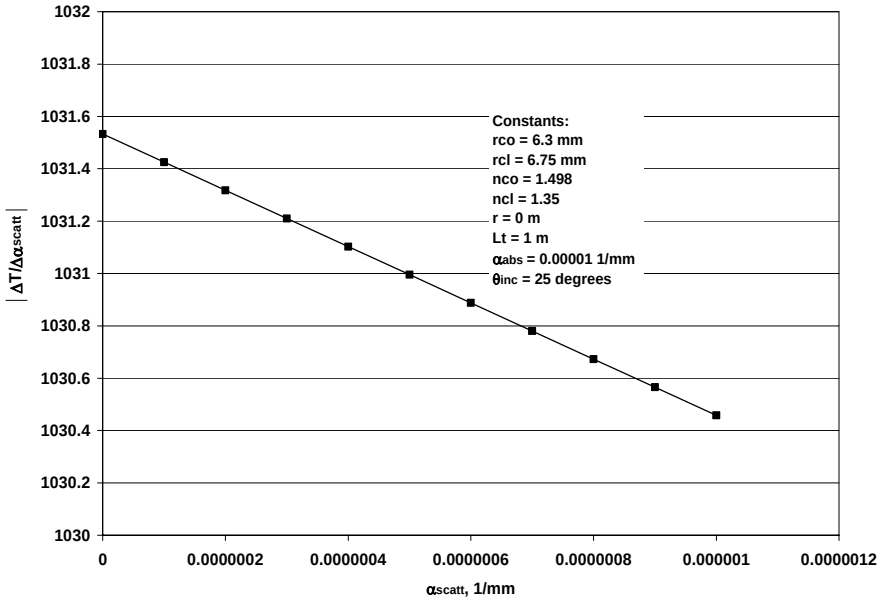

Fig. 8: Sensitivity coefficient of α_{scatt} .

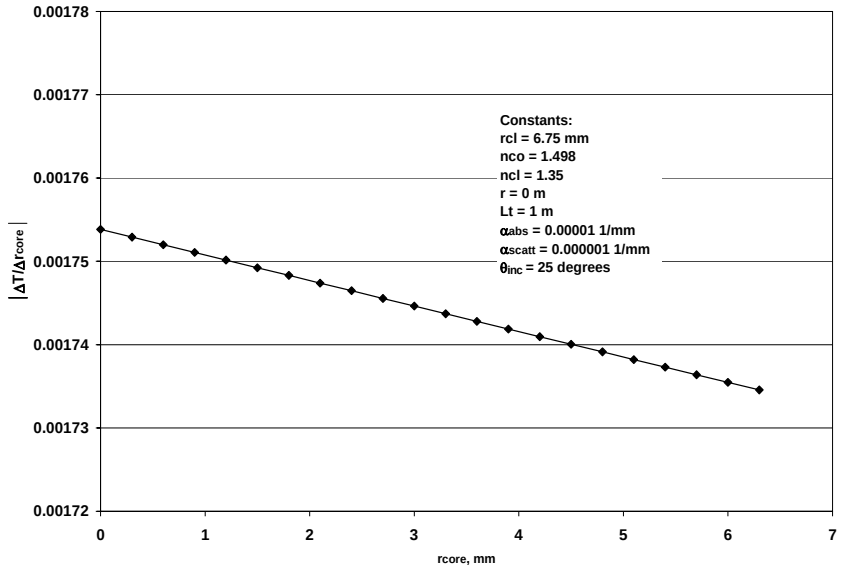

Fig. 9: Sensitivity coefficient of r_{core}.

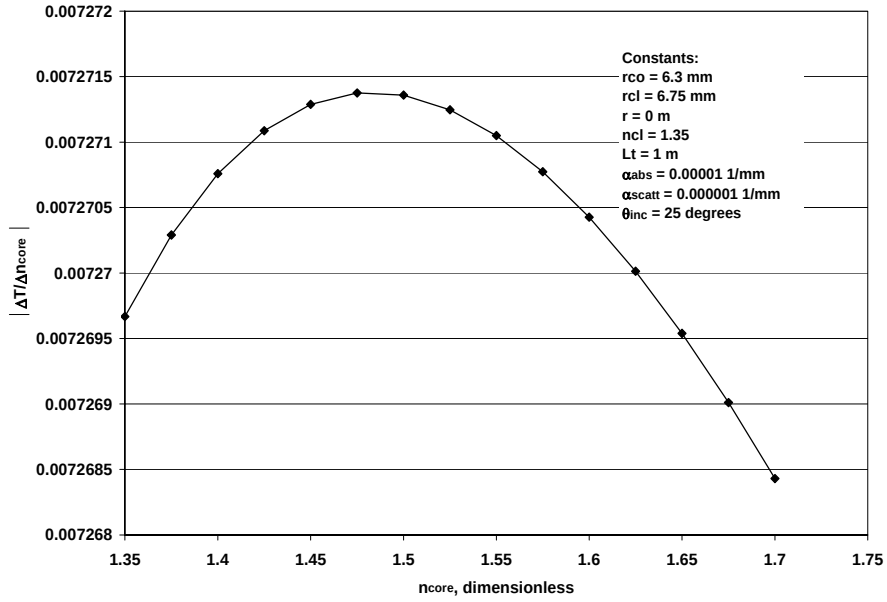

Fig. 10: Sensitivity coefficient of n_{co}.

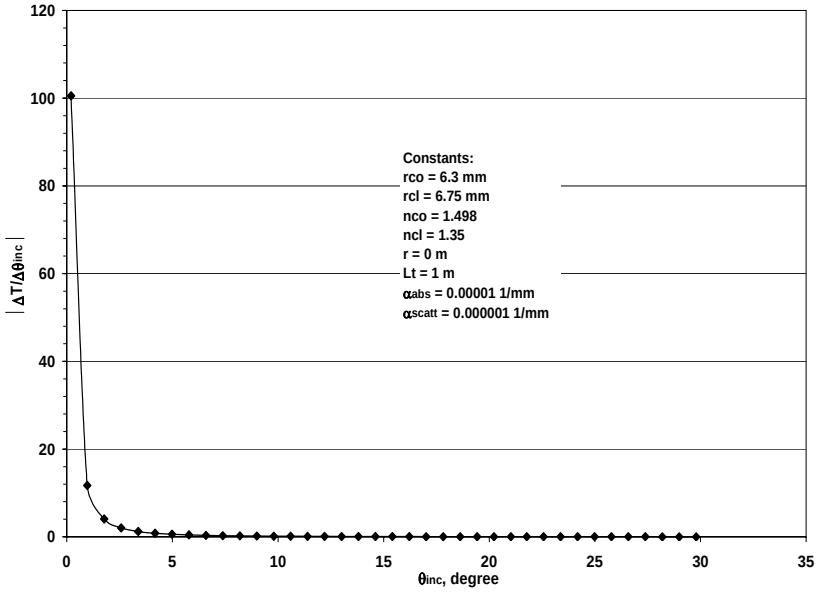

Fig. 11: Sensitivity coefficient of θ_{inc} .

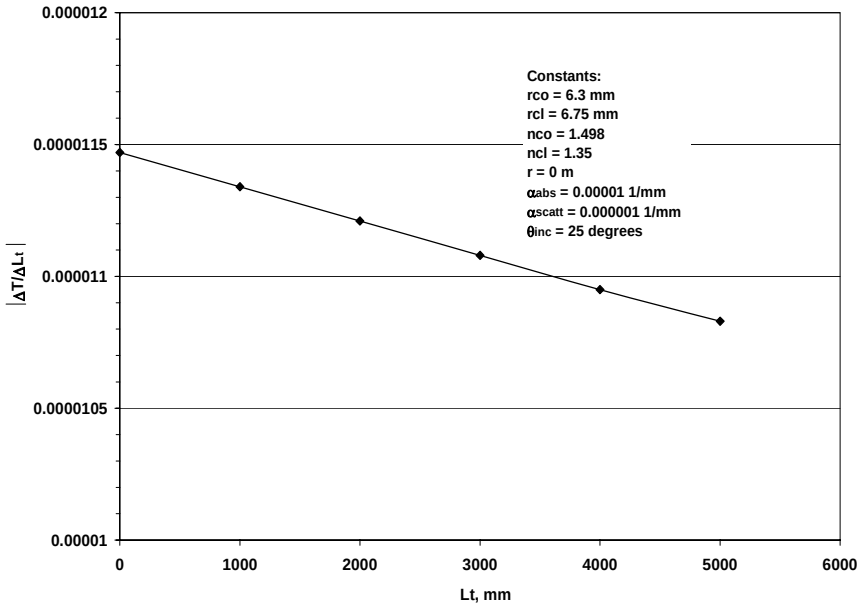

Fig. 12: Sensitivity coefficient of L_t .

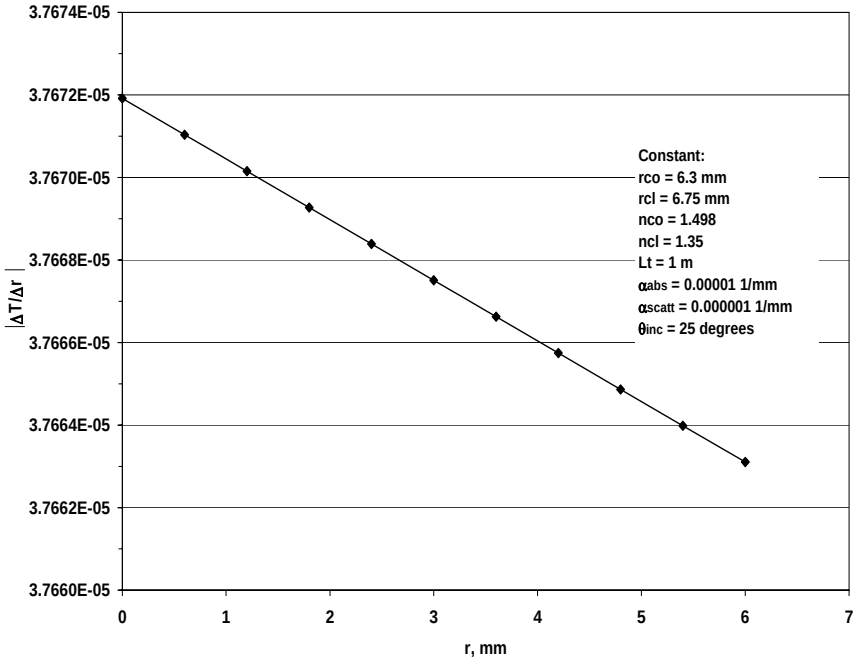

Fig. 13: Sensitivity coefficient of r.

According to Figures 7-13, except n_{co} factor which attains an optimum value at the concave peak, the sensitivity of the light transmission decreases with increasing magnitude of these factors. It was seen based on the magnitude of the sensitivity coefficients given that the light transmission through a straight light pipe is sensitive, from the most to the least, to factors α_{abs}, α_{scatt}, θ_{inc}, n_{co}, r_{co}, L_t, and r.

3.4 Experimental Result Is Better Approximated With Inclusion of Core-Clad Interface Roughness Term

Remillard et al.[1] gives the theoretical expression for the light loss of a straight light pipe via

$$\alpha(\varphi, d) = \frac{(\alpha_{abs} + \alpha_{scatt})}{\cos(\varphi)} + \frac{(1 - \exp[-(2k_{\perp}\sigma)^2])\tan(\varphi)}{2(r^2 - d^2)^{1/2}} + \frac{Dr}{2(r^2 - d^2)\cos(\varphi)} \quad (1)$$

where the first term on the rhs represent the light loss due to bulk absorption and scattering, second term represents the light loss due to interface roughness at the core-clad interface, and the last term represents the loss due to interface defects between core and cladding. D is the interface defects loss coefficient and $k_{\perp}$, the normal component of the wave vector at the core-clad interface given by

$$k_{\perp} = \frac{2\pi n_{co}\cos\theta}{\lambda} \quad (2)$$

[1] J. T. Remillard, M. P. Everson, and W. H. Weber, Loss Mechanisms In Optical Light Pipes, Applied Optics, Vol. 31, No. 34, December 1992, p 7232-7241

n_{co}, and λ being the core refractive index and the wavelength of the light in the air. (Refer to Fig. 1 for the explanation of φ, r, d, and θ).

Remillard et al. rewrites Eq. (1) with the inclusion of power reflection coefficient as

$$\alpha(\varphi,d)=\frac{(\alpha_{abs}+\alpha_{scatt})}{\cos(\varphi)}+\frac{\left(1-1/2\left(|r_s|^2+|r_p|^2\right)\exp[-(2k_\perp\sigma)^2]\right)\tan(\varphi)}{2(r^2-d^2)^{1/2}}+\frac{Dr}{2(r^2-d^2)\cos(\varphi)} \quad (3)$$

where r_s and r_p are the amplitude reflection coefficients for light polarized perpendicular and parallel to the plane of incidence.

Equation (3) is identical to Eq. (1) for total internal reflection rays. Figure 14 depicts the unit length, *h*, of a straight optical fiber used in the derivation of Eq. (1).

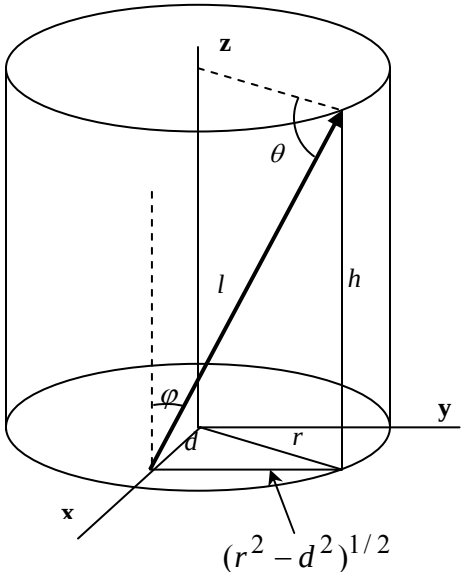

Fig. 14: Geometry for the ray path indicated by the bold arrow of length *l*; *r* is the pipe radius; the *z* axis is the pipe axis; and the *x* axis is chosen to lie along *d*.

Figure 15 shows the fraction of power transmitted for $\lambda = 0.55\mu m$ from Remillard et al. with incident angle at different rms (root-mean-square) interface roughness values.

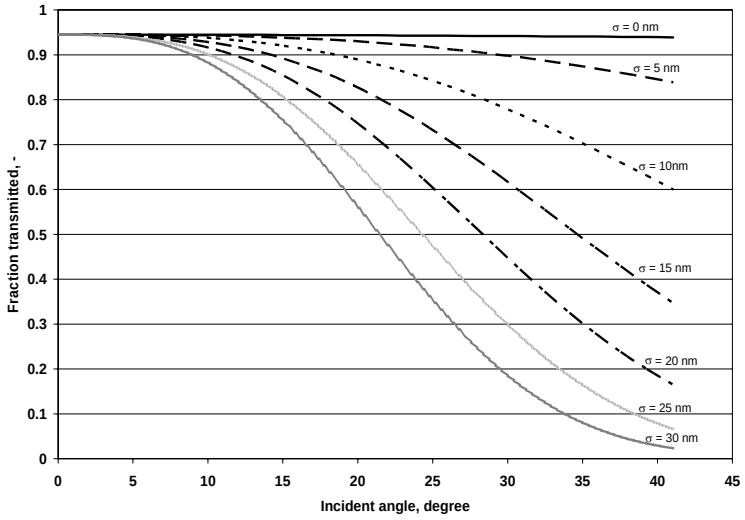

Fig. 15: Fraction of light transmitted with incident angle for different σ_{rms} values.

Figure 16 shows the Cates et al. result (Fig. 6 in their paper) compared to the result of Remillard et al. for rms (root-mean-square) interface roughness value of 23 nm. It is seen that an exponential decay is realized after about 20° degrees of incident angle. The difference between the experimental result and Remillard model was attributed to the facts that the latter was a theoretical model and that in the experiment the loss would drop below 1 after zero degrees of incident angle if the Fresnel reflectivity of light transmission were considered.

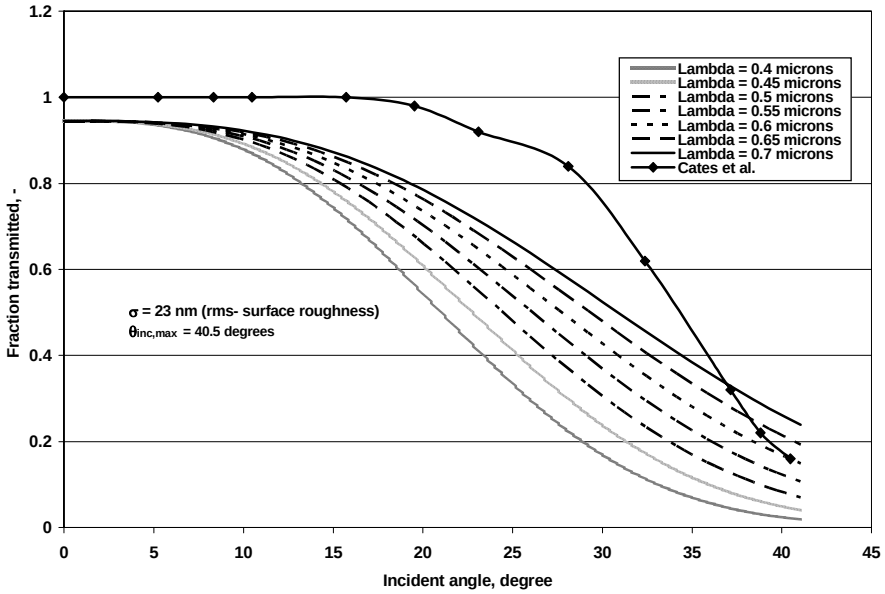

Fig. 16: Cates et al. result compared to the result of Remillard et al. ($L_t = 0.533m$).

Figure 17 shows the difference between Cates et al. result and the Remillard et al. result at different wavelength values. It is seen better agreement up to about 20-25 degrees of incidence angle.

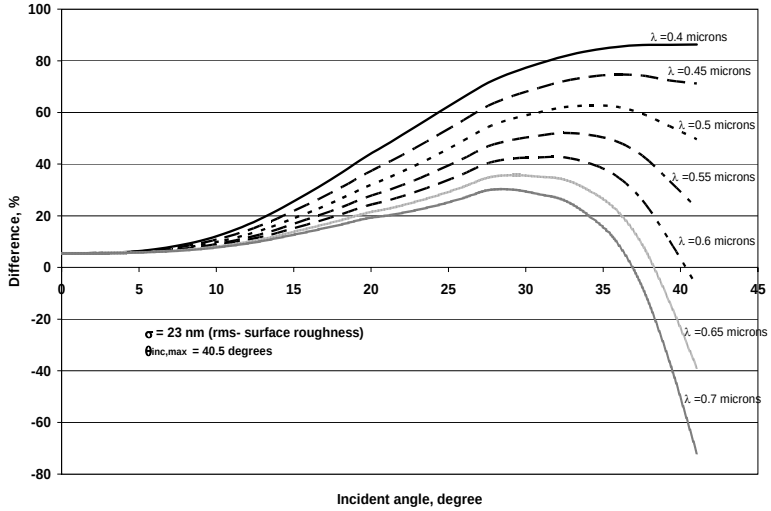

Fig. 17: Difference between Cates et al. result and Remillard et al. result.

Figure 18 shows the comparison between 3M experimental result and the result of Remillard et al. theoretical model after application of Simpon's integration over all possible wavelengths (visible), incident angle and local radius *d* (See Fig. 14)

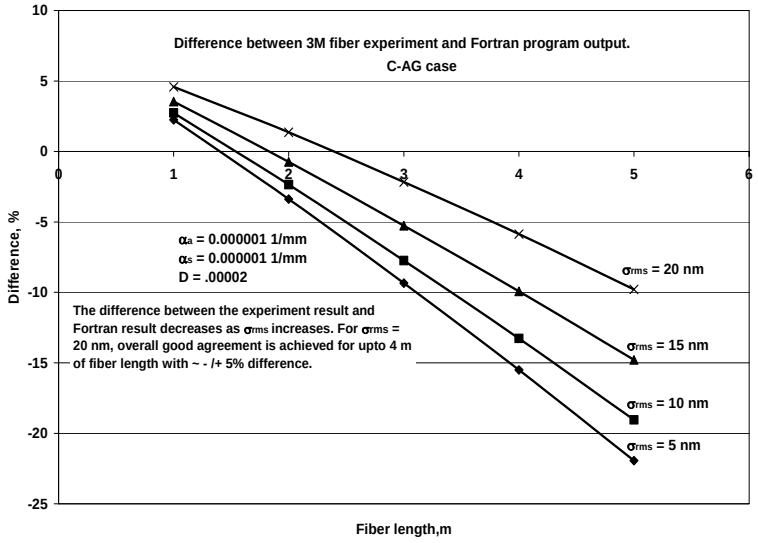

Fig. 18: Difference between 3M experiment result and the Remillard model.

In the result of Fig. 5, fiber absorption coefficient α_a, scattering coefficient α_s, rms interface roughness σ, and interface defects coefficient D were estimated. It is seen from Fig. 5 that application of the theoretical model gives a good estimation for up to 4 m of fiber for σ = 20 nm with a resulting μ 5% difference in the overall light transmission.

3.5 Study of Light Transmission for an HSL system

The study of light transmission estimation was completed by using the FORTRAN program. In the code, the straight light pipe loss was estimated from the expression given in the paper by Remillard et al.[2] from

$$\alpha(\varphi,d)=\frac{(\alpha_a+\alpha_s)}{\cos(\varphi)}+\frac{\left(1-1/2\left(|r_s|^2+|r_p|^2\right)\exp[-(2k_\perp\sigma)^2]\right)\tan(\varphi)}{2(r_{co}^2-d^2)^{1/2}}+\frac{Dr_{co}}{2(r_{co}^2-d^2)\cos(\varphi)} \quad (1)$$

where the first term on the rhs represents the light loss due to bulk absorption and scattering, second term represents the light loss due to interface roughness at the core-clad interface, and the last term represents the loss due to interface defects between core and cladding. α_a is the absorption coefficient, α_s is the scattering coefficient, σ is the rms value of the interface roughness, r_{co} is the core radius of the fiber, d is the local core radius, r_s and r_p are the amplitude reflection coefficients for light polarized perpendicular and parallel to the plane of incidence, D is the interface defects loss coefficient and $k_\perp$, the normal component of the wave vector at the core-clad interface given by

$$k_\perp=\frac{2\pi n_{co}\cos\theta}{\lambda} \quad (2)$$

n_{co}, and λ being the core refractive index and the wavelength of the light in the fiber core.

Figure 19 shows the simulation result compared to the experimental data of 3M fiber. An rms interface roughness height of 15 nm produced close estimate of the experiment. A correction factor of 1.10 applied on the simulation result predicts the straight pipe loss based on the experimental data available. In the simulation, the straight section light transmission was treated due to the sum of length of straight sections. For example, if a light distribution system is comprised of straight sections having 0.5-m, 1-m, 2-m, 1.5-m length, the overall straight section light loss was estimated for a total length of 5-m.

2 J. T. Remillard, M. P. Everson and W. H. Weber, "Loss Mechanisms in Optical Light Pipes", Applied Optics, Vol. 31, No. 34, 1992, 7232-7241.

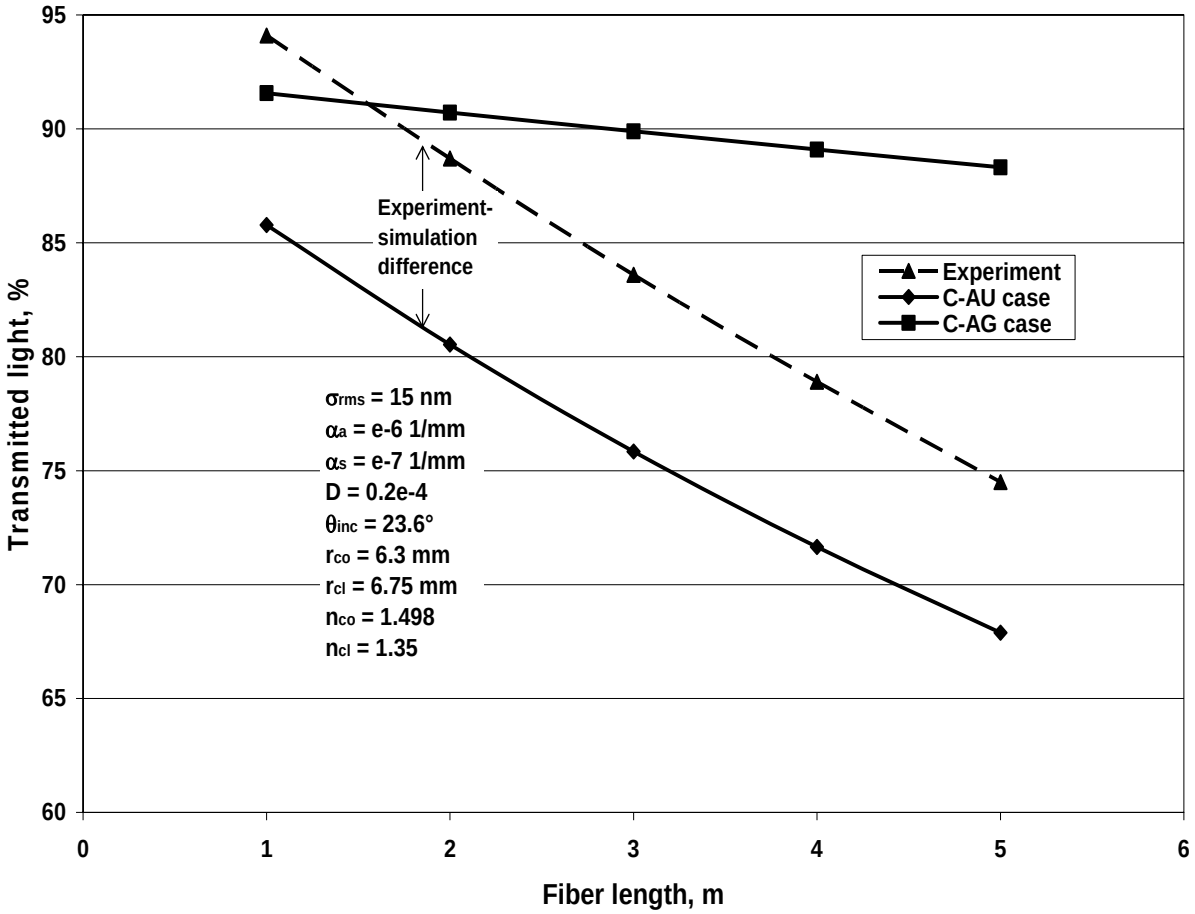

Fig. 19: Simulation result for the straight fiber light transmission compared to the experiment (3M's fiber data used).

The bent loss was determined from the light refraction equation given by

$$T(\theta) = \frac{4\sin\theta(\sin^2\theta - \sin^2\theta_{cr})^{1/2}}{[\sin\theta + (\sin^2\theta - \sin^2\theta_{cr})^{1/2}]} \tag{3}$$

applied at each turning point around the bend. Figure 20 shows the torus function values and method used in the location of next turning point. A method similar to binary-sectioning was used. The number of locations at the fiber entrance tip where the rays were launched was 50 (angular) x 50 (radial) = 2,500 locations. This number produced accurate enough results after comparing several combinations, e.g., 10 (angular) x (10 (radial) = 100 locations. Figure 21 shows the experimental and the simulation result in the bent fiber case. It is seen that the simulation underestimates the experiment for small bending radii, e.g $R/r_{cl} < 30$, and it overpredicts the experiment for large bending radii, e.g. $R/r_{cl} > 30$. A bending angle of 90 degrees was used on both parts although the simulation can be run for different bending angles, e.g., 50°, 110°, or 135°.

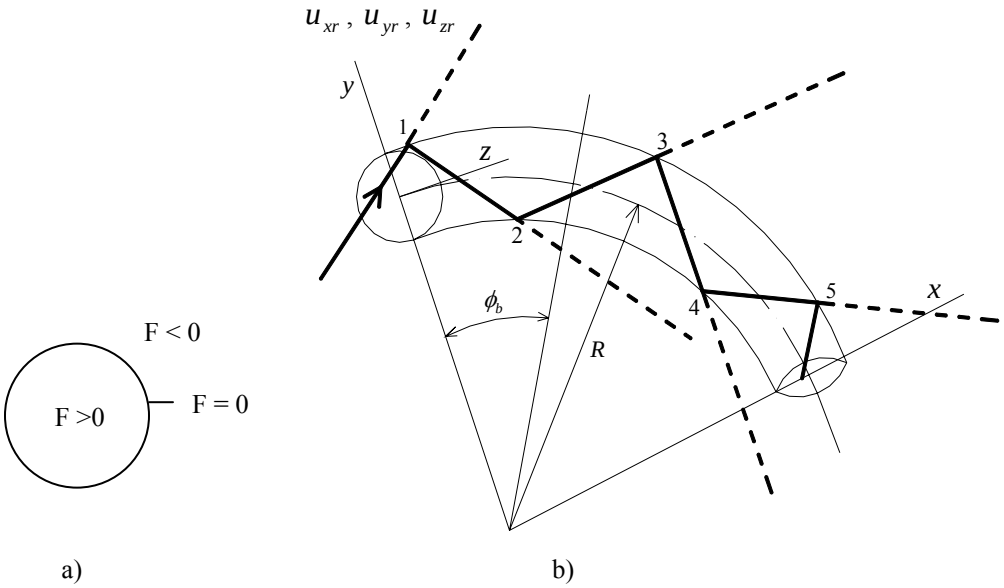

Fig. 20: a) The torus function at y, z-plane showing values. b) Direction vectors used to find the next turning point.

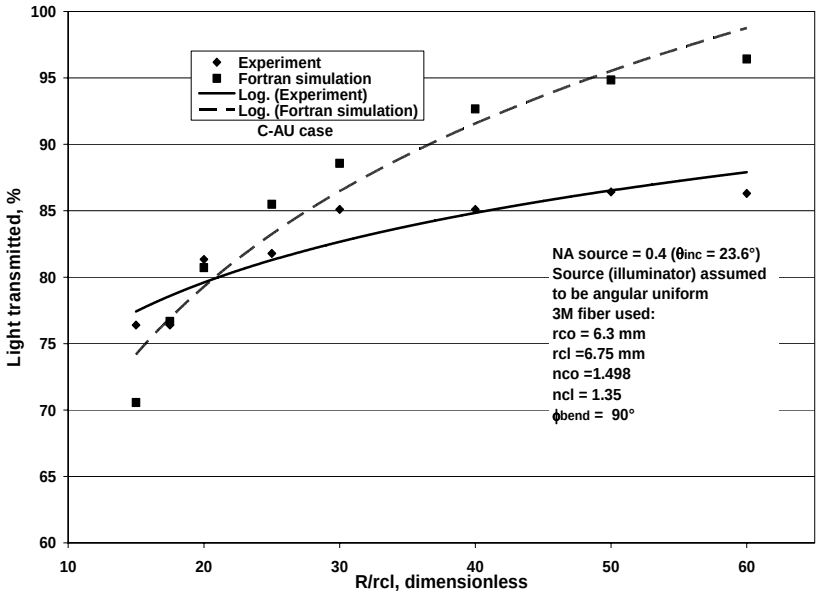

Fig. 21: Experimental and the simulation light transmission values in the bent fiber case, $\varphi_b = 90^{\circ}$

Example 1.

Let us determine the light transmitted through a light distribution system that uses the 3M's fiber having the following optical and geometrical properties:

$r_{co} = 6.3mm$, $r_{cl} = 6.75mm$,

$n_{co} = 1.498$, $n_{cl} = 1.35$,

$\alpha_a = e^{-6} 1/mm$, $\alpha_s = e^{-5} 1/mm$, $\sigma = 5nm$, $D = 0.2 \cdot 10^{-4}$

$\theta_{inc} = \theta_{inc,\max} = a\sin(sqrt(n_{co}^2 - n_{cl}^2)) = 40^o$

$L_t = 5.5m$, Total length of the straight section

$R_1 / r_{cl} = 40$, $R_2 / r_{cl} = 30$, $R_3 / r_{cl} = 25$, $R_4 / r_{cl} = 35$, Four bends

$\phi_{b,1} = 120^o$, $\phi_{b,2} = 90^o$, $\phi_{b,3} = 90^o$, $\phi_{b,4} = 60^o$, Corresponding four bend angles

Example 2.

Let us assume a light distribution system having the following arbitrary optical and geometrical properties for the fiber:

$r_{co} = 10mm$, $r_{cl} = 10.5mm$,

$n_{co} = 1.3$, $n_{cl} = 1.18$,

$\alpha_a = e^{-6} 1/mm$, $\alpha_s = e^{-5} 1/mm$, $\sigma = 5nm$, $D = 0.2 \cdot 10^{-4}$

$\theta_{inc} = \theta_{inc,\max} = a\sin(sqrt(n_{co}^2 - n_{cl}^2)) = 33^o$

$L_t = 4.5m$, Total length of the straight section

$R_1 / r_{cl} = 40$, $R_2 / r_{cl} = 30$, $R_3 / r_{cl} = 25$, $R_4 / r_{cl} = 35$, Four bends ```

$\phi_{b,1} = 120^o$, $\phi_{b,2} = 90^o$, $\phi_{b,3} = 90^o$, $\phi_{b,4} = 60^o$, Corresponding four bend angles

Table 1 shows the results from the FORTRAN program for Examples 1 and 2. Tr_c indicates the component-level light transmission and Tr_o indicates the overall light transmission.

Table 1: The result of the FORTRAN program.

	First bend	Second bend	Third bend	Fourth bend	Straight section
R / r_{cl},–	40	30	25	35	-
φ_{bend}, degree	120	90	90	60	-
Tr_c,% (Ex. 1)	88	85	82	89	75
Tr_c,% (Ex. 2)	89	86	83	89	89
Tr_o,% (Ex. 1)	41				
Tr_o,% (Ex. 2)	50				

Assuming a total light input of 10,000 lumens (for converging arrangement of rays having angular uniform power input at the very straight section inlet), this translates into 4,100 lumens of light output in the first example and of 5,000 lumens of light output in the second example case.

4. TRNSYS: Chromaticity modeling, Correlated Color Temperature (CCT) Algorithm, Spectral Power Distribution, SMARTS2 and TRNSYS, Definition and Calculation of the Color Rendering Index

4.1 Chromaticity Modeling

Summaries of colorimety terms are provided below. Attempts were made to model the chromaticity of sunlight and fluorescent bulbs. For spectrums generated by the sun, the model gives reliable chromaticity coordinates. For spectrums that are less smooth and involve sharp spikes, such as fluorescent spectrums, results are inaccurate. Further study of colorimetry is needed and the model needs to be improved.

4.1a Colorimetry

Colorimetry is the branch of color science concerned with specifying numerically the color of a visual stimulus. It is also concerned with the specification of small color differences that an observer may perceive when the differences in the spectral radiant power distributions of the given visual stimuli are such that a complete color match is not observed.

The *trichromatic generalization* states that many color stimuli can be matched in color completely by additive mixtures of three fixed primary stimuli whose radiant powers have been suitably adjusted. The choice of the three primary stimuli is arbitrary with the restriction that none of the primary stimuli can be color matched by a mixture of the other two (e.g. Red, Blue, and Green are valid because red and blue cannot be mixed to make green, blue and green cannot be mixed to make red, and so on).

The *tristimulus space* is a three dimensional space in which a color stimulus Q can be broken down into its component vectors R, G, and B which are called the *tristimulus values* of Q.

Two color stimuli, Q_1 and Q_2, that are each defined by different spectral radiant power distributions, $\int_{380\ nm}^{760\ nm} P_{1\lambda}\, d\lambda$ and $\int_{380\ nm}^{760\ nm} P_{2\lambda}\, d\lambda$, are in complete color match if the tristimulus values match, i.e. $R_1 = R_2$, $G_1 = G_2$, and $B_1 = B_2$.

The tristimulus values of a color stimulus are evaluated using the spectral radiant power distribution of the stimulus and special spectral tristimulus values $\bar{r}(\lambda)$, $\bar{g}(\lambda)$, and $\bar{b}(\lambda)$ called the *color-matching functions*. These values are derived from the concept of an equal-energy stimulus in which across the visible spectrum

$$E_\lambda = \bar{r}(\lambda)R + \bar{g}(\lambda)G + \bar{b}(\lambda)B \qquad \text{and} \qquad E_\lambda = 1$$

Figure 22 displays the color matching functions.

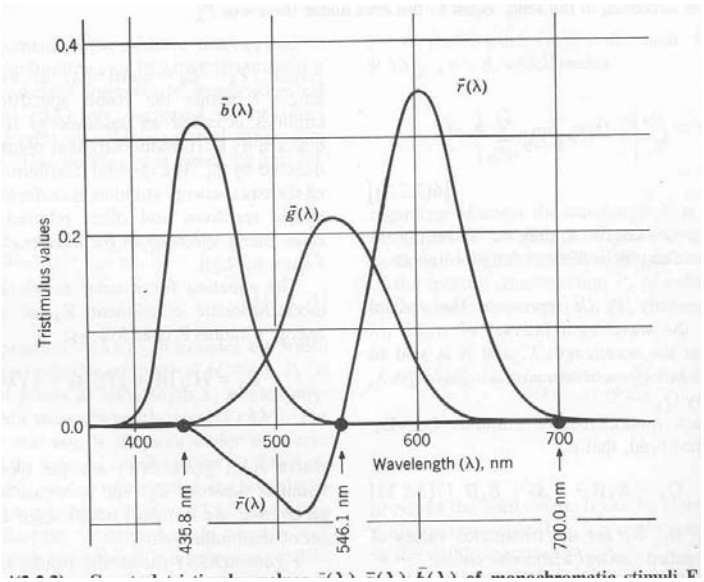

Fig. 22: color matching functions $\bar{r}(\lambda)$, $\bar{g}(\lambda)$, and $\bar{b}(\lambda)$

Using the color matching functions (described below), the tristimulus values R, G, and B of a color stimulus Q are defined as

$$R = \int_{380\ nm}^{760\ nm} P_\lambda \bar{r}(\lambda) d\lambda \quad G = \int_{380\ nm}^{760\ nm} P_\lambda \bar{g}(\lambda) d\lambda \quad B = \int_{380\ nm}^{760\ nm} P_\lambda \bar{b}(\lambda) d\lambda$$

where P_λ is the spectral radiant power distribution of Q at wavelength λ.

Associated with any set of tristimulus values R, G, and B are a set of *chromaticity coordinates r, g, and b* that define the chromaticity of the stimulus independent of its intensity. These values are calculated according to the following equations:

$$r = \frac{R}{R+G+B} \qquad g = \frac{G}{R+G+B} \qquad b = \frac{B}{R+G+B}$$

Chromaticity coordinates can be calculated by different methods and use different nomenclature. The CIE (Commission Internationale de l'Eclairage) 1931 method uses x, y, and z chromaticity coordinates. The r, g, and b coordinates can be changed into x, y, and z coordinates using a straight-forward transformation. In this way, a correlated color temperature (CCT) graph, Fig. 23, can be used to calculated the CCT for a given spectral radiant power distribution's x and y chromaticity coordinates.

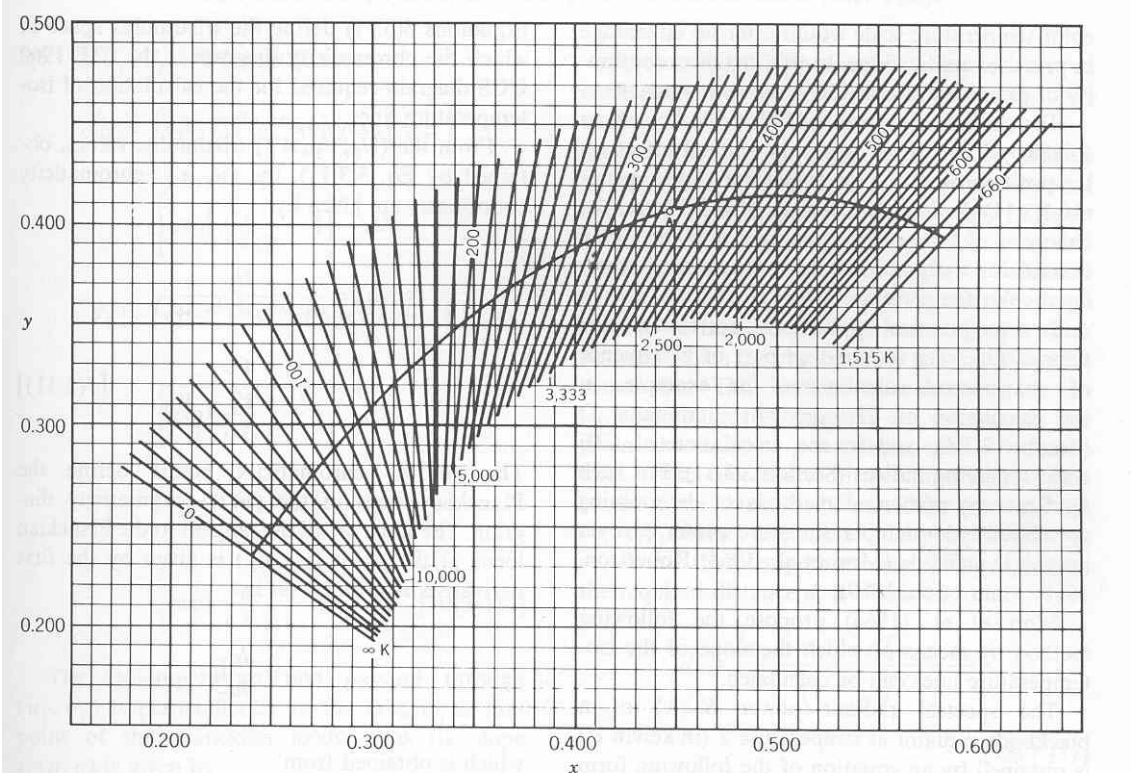

Fig. 23: Calculation of correlated color temperature (CCT) using the x and y chromaticity coordinates of a given spectral radiant power distribution

4.1b Color Matching Functions

The color matching functions may be best understood through the following thought experiment: There are four lights in front of you. Each light emits monochromatic radiation, i.e. light of one wavelength. The radiation that each light emits is summarized below.

light	emits power at wavelength
Q_λ	some λ in visible spectrum
R (red)	700 nm
G (green)	546.1 nm
B (blue)	435.8 nm

The *trichromatic generalization* states that many color stimuli can be matched in color completely by additive mixtures of three fixed primary stimuli whose radiant powers have been suitably adjusted.

What that means is that Q_λ's perceived color can be matched by shining lights R, G, and B together and then modifying their powers until the mixed light is the same color as Q_λ. In this way the color matching functions $\bar{r}(\lambda_Q)$, $\bar{g}(\lambda_Q)$ and $\bar{b}(\lambda_Q)$ for Q_λ are created.

The total color matching functions $\bar{r}(\lambda)$, $\bar{g}(\lambda)$, and $\bar{b}(\lambda)$ are created by shining a light of power equal to Q at other wavelengths and recording the values of $\bar{r}$, $\bar{g}$, and $\bar{b}$ at each of those wavelengths. Sometimes a color matching function can be negative, meaning that the primary

light had to be removed from the mixture and added to the monochromatic light to complete the match. The color matching functions are displayed in Fig. 22.

4.2 Correlated Color Temperature (CCT) Algorithm

A correlated color temperature (CCT) algorithm was written and added to the TRNSYS model. The algorithm was first written in EES and validated by comparing calculated CCT values of sunlight spectrums at various air masses with published data. It was then added to the TRNSYS code. However, TRNSYS calculates larger CCT values than expected. Work continues on discerning the source of the error. Correction of the error may involve changing how TRNSYS modifies the extraterrestrial spectral power distribution (SPD) to generate the SPD at the earth's surface.

The correlated color temperature of a light source measures how "cool" or "warm" a light source appears. Figure 24 lists CCT values for everyday light sources. Though not listed on this figure, daylight around noon is 5000 K, sunset and sunrise are 1800 K, and an overcast sky is about 6500 K.

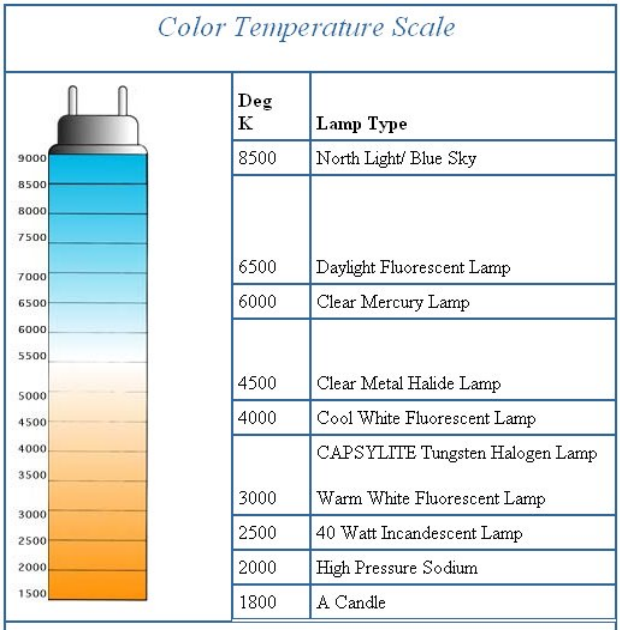

Deg K	Lamp Type
8500	North Light/ Blue Sky
6500	Daylight Fluorescent Lamp
6000	Clear Mercury Lamp
4500	Clear Metal Halide Lamp
4000	Cool White Fluorescent Lamp
3000	CAPSYLITE Tungsten Halogen Lamp Warm White Fluorescent Lamp
2500	40 Watt Incandescent Lamp
2000	High Pressure Sodium
1800	A Candle

Fig. 24: CCT of light sources

The calculation of correlated color temperature involves the calculation of chromaticity coordinates from a SPD using 1931 CIE x,y,z color matching functions at 5 nm bandwidths. The chromaticity coordinates defin0e a point on an isotemperature line graph that, by interpolation, can be used to find the color temperature of a blackbody that produces the same sensation of color as the light source under investigation.

SMARTS2 spectrally models the sunlight delivered to the earth's surface as functions of the characteristics of the intervening atmosphere. One variable that has a large effect on the spectrum of light delivered to the earth's surface is air mass, which is simply the ratio of the atmosphere the sunlight must travel through at the moment of time under investigation to the amount of atmosphere the light travels through at solar noon. Thus, at solar noon, the airmass is 1 and the zenith angle is zero. Air masses of 2, 3, 4, and 5 correspond to zenith angles of 60˚, 70˚, 75˚, and 78˚.

Figure 25 on the following page shows the SPDs predicted by the SMARTS2 spectral model for air masses of 1, 2, 3, 4, and 5. As the color matching functions are only defined in the visible spectrum (380 – 780 nm), the CCT is dependent only on radiation within these wavelength bounds. Figure 26 shows the CCT predicted by the EES CCT algorithm for the different air masses.

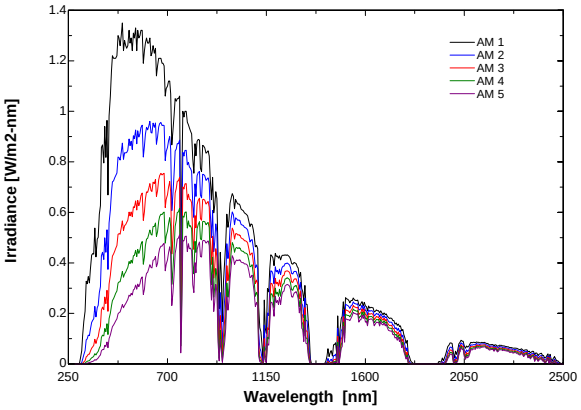

Fig. 25: SMARTS2 generated SPD of sunlight

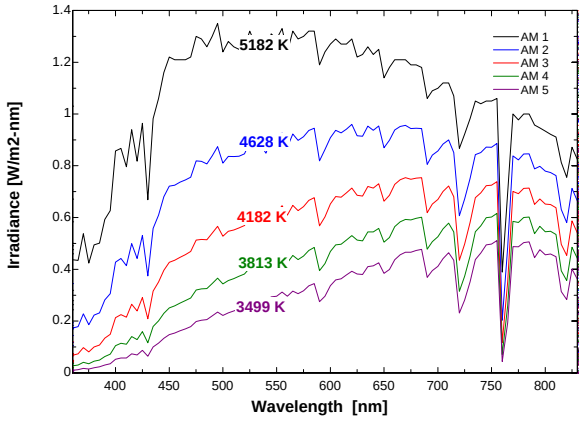

Fig. 26: CCT of SMARTS2 SPDs

The CCT values predicted by the algorithm match well with expected CCT values for sunlight. Verification of the 1800 K CCT near sunrise or sunset would require using an air mass closer to 20. In time a more rigorous verification of the CCT algorithm will be performed.

Next, the CCT code was added to TRNSYS. Table 2 below summarizes some output data from June 1 in Tucson, AZ. CCT1 refers to the correlated color temperature of the sunlight incident on the hybrid lighting system, and CCT2 is the CCT of the light delivered by the HLS.

Table 2: TRNSYS output June 1, Tucson AZ

TIME [HR]	Beam [kj/hr-m2]	Lumens [lumens]	u1 [dim]	v1 [dim]	CCT1 [K]	u2 [dim]	v2 [dim]	CCT2 [K]
3625	0	0	0.0000	0.0000	0	0.0000	0.0000	0
3626	0	0	0.0000	0.0000	0	0.0000	0.0000	0
3627	0	0	0.0000	0.0000	0	0.0000	0.0000	0
3628	0	0	0.0000	0.0000	0	0.0000	0.0000	0
3629	0	0	0.0000	0.0000	0	0.0000	0.0000	0
3630	0	0	0.0000	0.0000	0	0.0000	0.0000	0
3631	0	0	0.0000	0.0000	0	0.0000	0.0000	0
3632	3137	71697	0.2043	0.3219	5431	0.2044	0.3233	5346
3633	3223	94215	0.2031	0.3176	**5767**	0.2033	0.3192	5645
3634	3267	97333	0.2030	0.3167	5828	0.2033	0.3184	5700
3635	3290	98267	0.2030	0.3164	5850	0.2033	0.3181	5719
3636	3300	98574	0.2030	0.3163	5859	0.2033	0.3180	5727
3637	3300	98574	0.2030	0.3163	5859	0.2033	0.3180	5727
3638	3290	98267	0.2030	0.3164	5850	0.2033	0.3181	5719
3639	3267	97333	0.2030	0.3167	5828	0.2033	0.3184	5700
3640	3223	94215	0.2031	0.3176	5767	0.2033	0.3192	5645
3641	3137	71697	0.2043	0.3219	5431	0.2044	0.3233	5346
3642	0	0	0.0000	0.0000	0	0.0000	0.0000	0
3643	0	0	0.0000	0.0000	0	0.0000	0.0000	0
3644	0	0	0.0000	0.0000	0	0.0000	0.0000	0
3645	0	0	0.0000	0.0000	0	0.0000	0.0000	0
3646	0	0	0.0000	0.0000	0	0.0000	0.0000	0
3647	0	0	0.0000	0.0000	0	0.0000	0.0000	0
3648	0	0	0.0000	0.0000	0	0.0000	0.0000	0

In Table 2, one can notice immediately that CCT1 and CCT2 are both too high. Hour 3633 was selected to investigate further because the CCT at this hour should be closer to that expected from an air mass of 4, which is 3800 K. The SPD used by TRNSYS is compared to AM 4 predicted by SMARTS2 in Fig. 27 below.

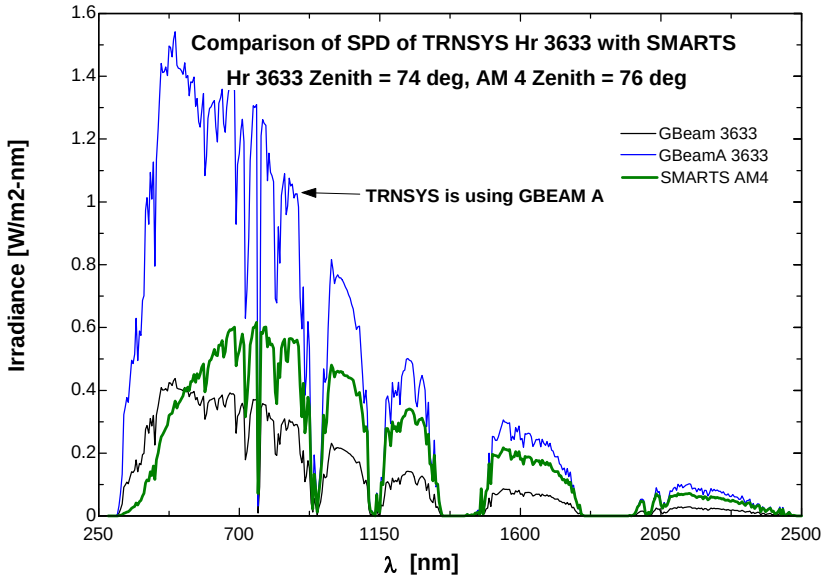

Fig. 27: Comparison of TRNSYS and SMARTS2 SPD

GBeamA is simply the GBeam curve multiplied by a scaling factor; GBeamA and GBeam give the same CCT value. The important difference between the SMARTS plot and GBEAM is the relative position of the peak of the graph. The SMARTS graph peaks closer to 700 nm, while the GBeam graph peaks closer to 480 nm. This yields significant CCT differences: 5767 K TRNSYS, 3813 K SMARTS2.

SMARTS2 is a critically reviewed atmospheric transmission model. An extraterrestrial SPD and decay coefficients are used in TRNSYS to generate its SPD of sunlight. These decay coefficients may have to be modified to give a spectrum more in agreement with SMARTS2 results.

4.3 Spectral Power Distribution

The discrepancy between spectral power distributions (SPDs) of sunlight generated by TRNSYS and SMARTS2 was investigated further. It was believed that the SPD delivered by TRNSYS was already validated. However, another program (EES) was used to generate the spectrums for comparison using the same algorithm that TRNSYS uses. In EES, the spectrums generated by this algorithm and SMARTS match well for a turbidity value of 0.1. However, the SPD generated by TRNSYS does not. It was suspected that there was a difference in the code or data files of the TRNSYS program that causes this unexpected difference.

4.3a Differences in SPD

Figure 28 summarizes the differences in the SPDs generated by SMARTS2 and TRNSYS. Two differences are noteworthy: the magnitude of GBEAMA relative to the SMARTS2 data and the relative shift of maximum power in the spectrums: in GBEAMA the maximum power occurs around 500 nm, while in the SMARTS2 code the maximum occurs closer to 700 nm. For this reason the correlated color temperature (CCT) of the TRNSYS spectrum is closer to 5000 K, while the CCT of the SMARTS2 data is 4000 K.

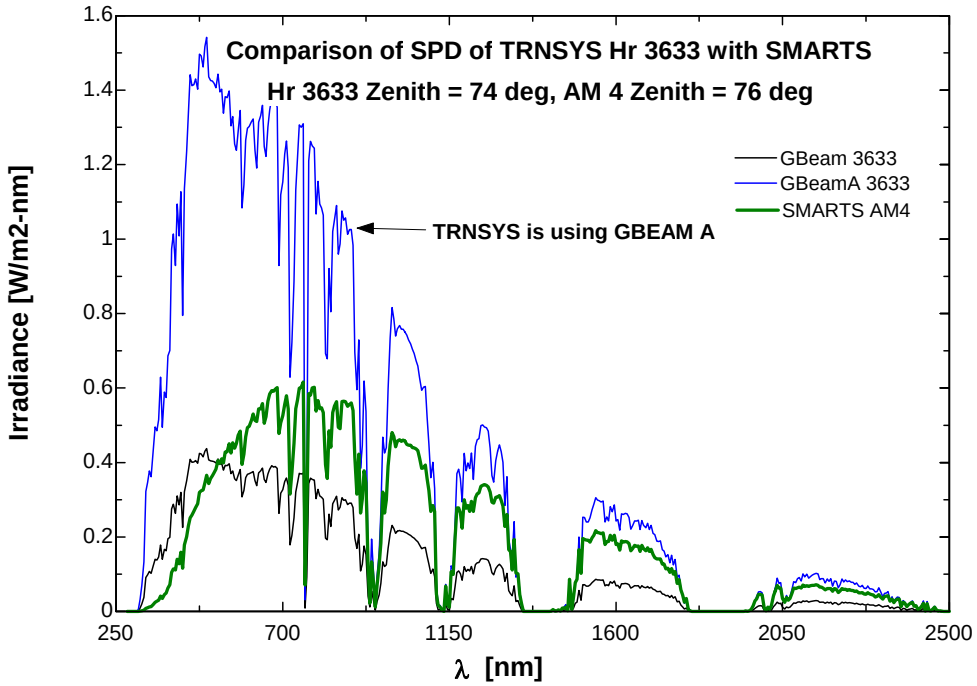

Fig. 28: Comparison of TRNSYS and SMARTS2 SPD

4.3b Validation of the Simplified Decay Coefficient Algorithm

Ideally, the SMARTS2 algorithm would be employed by the TRNSYS code. However, the added complexity and increases in simulation time would most likely compromise the TRNSYS model's ability to serve as a design tool. For this reason, a simplified model of the atmosphere was developed for TRNSYS based on SMARTS2 results for two different turbidity values at a given air mass. Figure 29 shows the extraterrestrial and terrestrial values of the spectrums generated by TRNSYS to create the decay coefficients κ1 and κ2 for an air mass of 2.5.

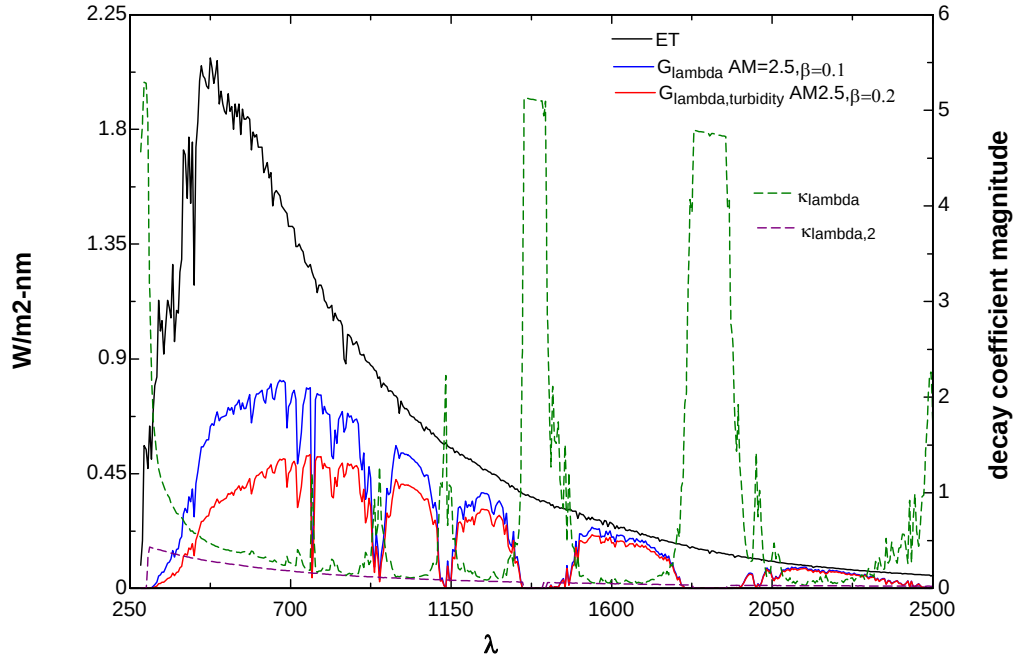

Fig. 29: SPDs generated by SMARTS2 and calculated decay coefficients

The decay coefficient algorithm was added to EES and TRNSYS. Figure 30 shows SPDs generated by EES using the decay coefficients and SMARTS2. They show good agreement.

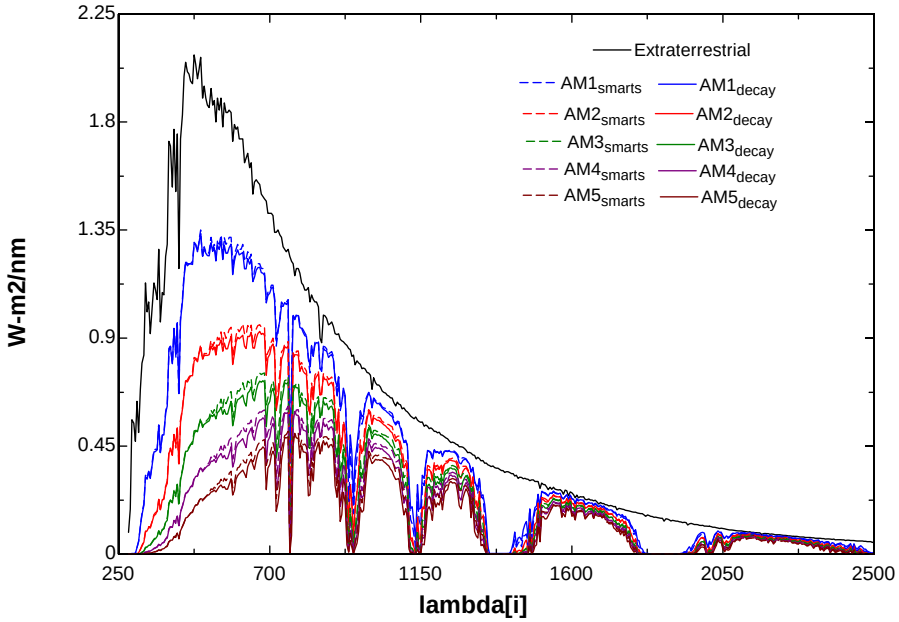

Fig. 30: Comparison of EES and TRSNYS SPDs

Though the EES SPD matches the SMARTS2 spectrum for turbidity values of 0.1, EES and SMARTS2 data for other turbidity values need to be investigated. Another immediate priority is to determine why the EES and TRNSYS SPDs for a given turbidity value and air mass differ significantly and why the GBEAMA value used in TRNSYS has a magnitude that appears, at times, to be larger than ET radiation.

4.3c TRNSYS code error determined

The TRNSYS code was creating incorrect radiation spectral power distributions (SPD) because the SMARTS2 data file used by the code specified the SPD of global horizontal, not beam radiation. This file was exchanged with beam normal SPDs generated by SMARTS2 and now the spectrums and correlated color temperature values generated by TRNSYS are more in line with expected results. However, for better SPD accuracy the SMARTS2 algorithm may be included as a TYPE into TRNSYS in the future.

The scaling factor that the TRNSYS code was using to match the energy under the generated SPD with measured radiation values of the TRNSYS data files was incorrectly formulated. The scaling factor now directly relates the energy under the SPD to the TRNSYS calculated beam radiation values.

The errors have been fixed and new model results have been validated using a simple EES program that estimates the amount of lumens the HLS system should deliver in one year. New model results were generated for publication in the Solar Energy Journal.

4.3d SMARTS2 spectral data file used by TRNSYS

Figure 31 shows SMARTS2 generated spectrums for two turbidity values - 0.1 and 0.2 - at an airmass of 2.25. In his MS thesis, Greg Schlegel indicates that these spectrums can be used to generate decay coefficients to generate SPDs based on turbidity and airmass in the TRNSYS code. In this way the entire SMARTS2 algorithm need not be run for every hour in the simulation.

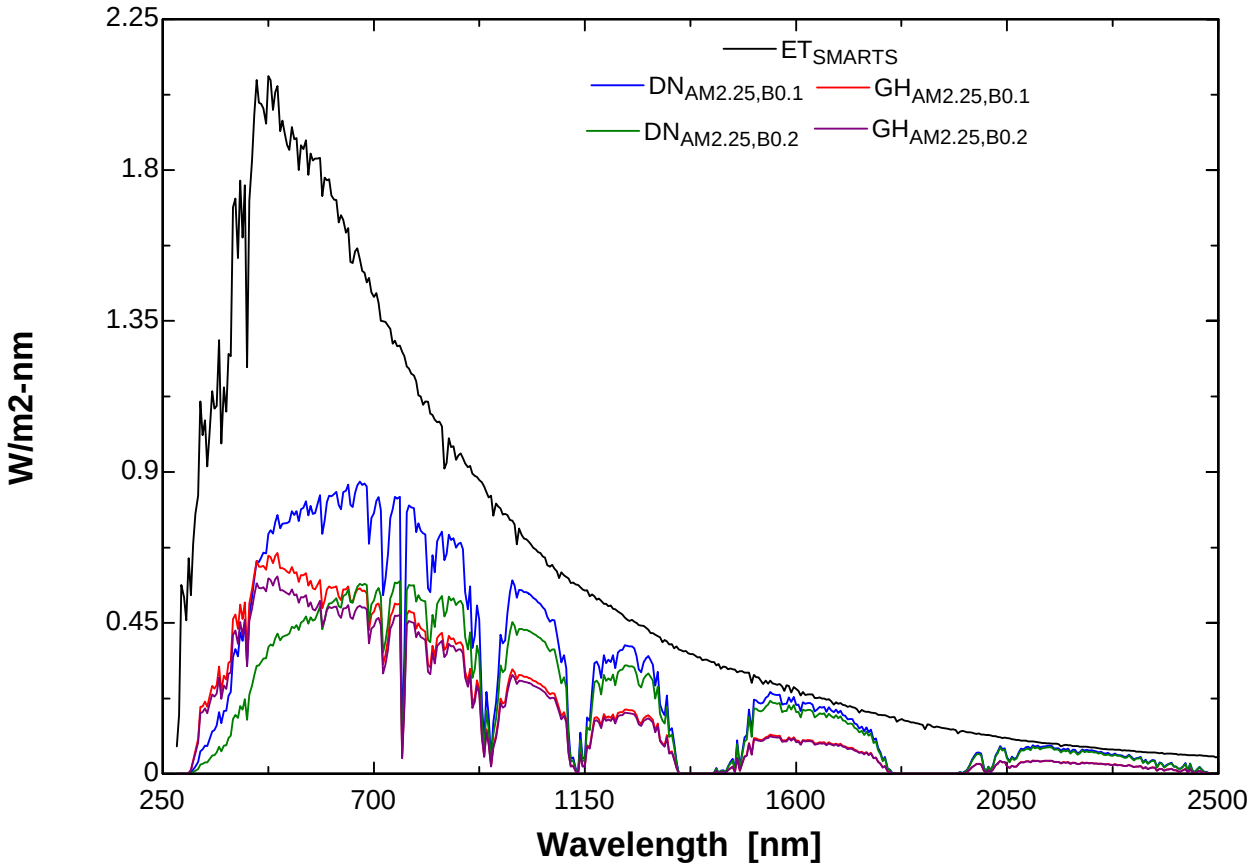

Fig. 31: SMARTS2 generated SPDs used to generate decay coefficients

Global horizontal (GH) and direct normal (DN) SPDs are shown in Fig. 31. The TRNSYS code was incorrectly using the global horizontal spectrums to create spectrums of direct beam radiation. This is why previous spectrums generated by TRNSYS show spectrums severely shifted to the left with large (5800 K - 6500 K) color temperatures. Once the global horizontal files were replaced with the direct normal files, the spectrums yielded more meaningful color temperatures and better matched SMARTS2 results. Figure 32 shows spectrums created by TRNSYS and how well they match SMARTS2 spectrums for turbidity values of 0.1 and 0.2 and an airmass of 2.25.

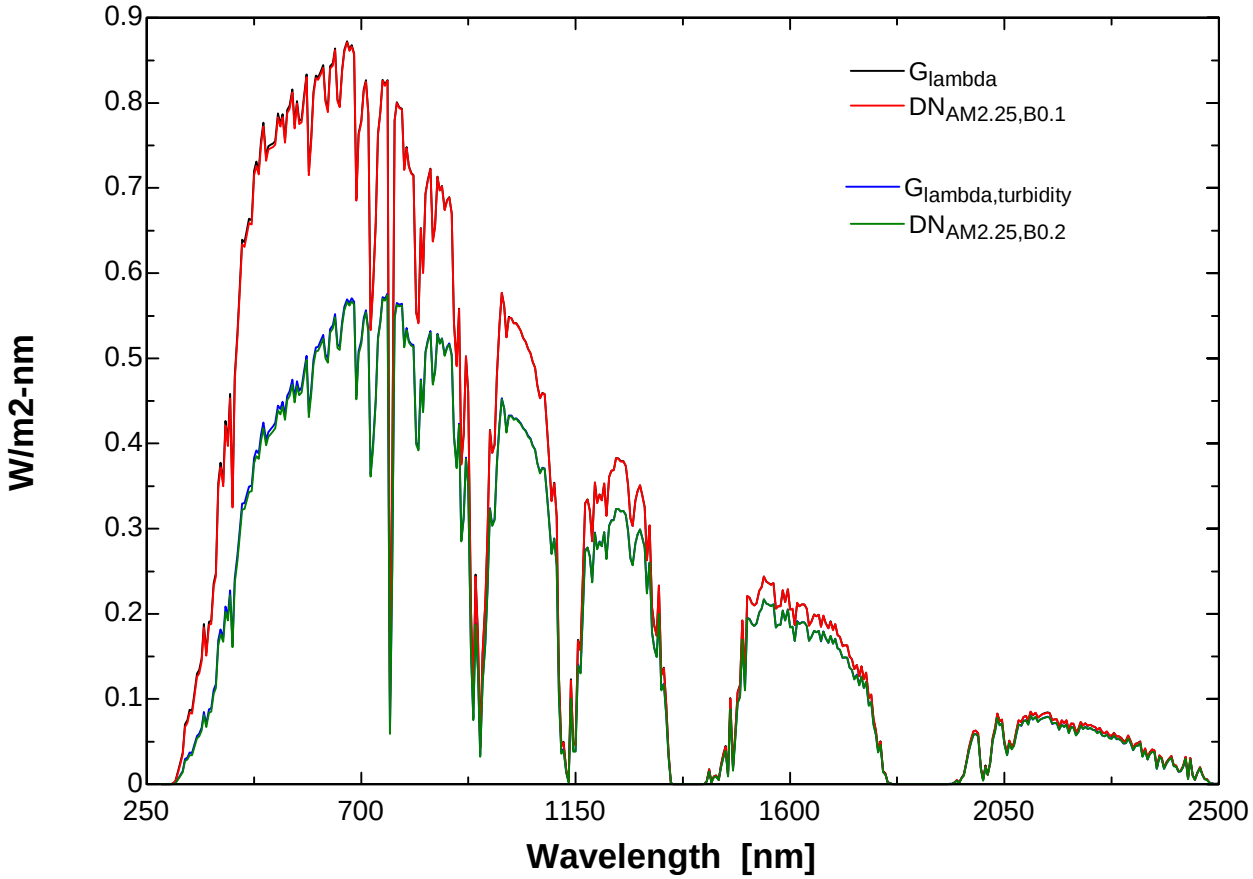

Fig. 32: Comparison of TRNSYS (G_{lambda}) and SMARTS2 (DN) SPDs

4.3e Scaling factor

A scaling factor is used by TRNSYS to match the area under the generated SPD with the beam normal radiation value based on radiation measurements. Previously, the scaling factor was calculated using a ratio of global horizontal radiation values. The SPD was then scaled up or down by this ratio, created a new beam radiation value that most times agreed with the TRNSYS beam normal value.

Sometimes the beam normal values did not match, and in almost all cases it led to an over-prediction of the light entering the HLS, resulting in overly optimistic break-even capital cost values. The scale factor was changed to be a direct ratio of the area of under the SPD to the beam normal radiation value. This change forces the light used by the HLS to be the same magnitude as beam radiation from the weather file. It leads to a slightly smaller BECC: for Honolulu, HI the BECC before corrections was $2800 in 10 years. Now the BECC is $2400.

4.4 Definition and Calculation of the Color Rendering Index

Two lighting indexes, the correlated color temperature (CCT) and the color rendering index (CRI), are used to describe the quality of illumination to a viewer. The CCT has been discussed previously. This discussion focuses on defining the CRI and describing how it is calculated from a light source's spectral power density.

The color rendering ability of a light source is the ability of a light source to render an illuminated object the same color as a reference illuminant. The color rendering index of a light source is a quantitative measure of the degree to which perceived colors of objects illuminated by the light

source match the colors of the same objects illuminated by a standard source. When the light source under investigation renders the colors exactly the same as the reference illuminant, the CRI is 100. Daylight is generally considered to have a CRI close to 100. Incandescent bulbs can have CRIs close to 100, while fluorescent bulbs have CRIs between 50 and 60. A CRI of 80 is considered a minimum for retail applications.

The CRI of a light source can be calculated in the following manner:

1) A reference illuminant needs to be defined. If the correlated color temperature of the light source is less than 5000 K, then the SPD of a Planckian radiator at that CCT should be used as the reference illuminant. If the CCT of light source to be investigated is 5000 K or larger, one of the CIE daylight D SPDs should be used. The chromaticities of the light source and reference illuminant should be as close as possible. The acceptable chromaticity difference between the light source and the reference illuminant is 15 reciprocal megakelvins.

2) A set of 8 test-color samples is specified under terms of spectral radiance factors. These color samples are defined by Munsell values that are functions of the wavelength reflective properties of the samples.

3) The tristimulus values of the test color samples illuminated by the reference illuminant and the light source under investigation are calculated. Calculation of tristimulus values is detailed in the August 2003 report.

4) Most likely the tristimulus values of the reference illuminant and light source under investigation will be different for each of the test color samples. The resultant color shift is a function of the differences in the tristimulus values.

The resultant color shift is defined by

$$\Delta E^*_{uv} = \left[\left(\Delta L^*\right) + \left(\Delta u^*\right) + \left(\Delta v^*\right)\right]^{1/2}$$

where

$$L^* = 116\left(\frac{Y}{Y_n}\right)^{1/3}$$

$$u^* = 13L^*\left(u' - u'_n\right)$$

$$v^* = 13L^*\left(v' - v'_n\right)$$

u', v', u'_n, *and* v'_n are functions of the tristimulus values of the two light sources

5) The calculation of the CRI of one of the eight color samples is

$$R_i = 100 - 4.6\left(\Delta E_i\right)$$

An Ri of 100 for the color sample means that the color of that particular sample was rendered perfectly. The factor of 4.6 in this equation was chosen so the CRI of a standard warm white fluorescent lamp when compared to an incandescent illuminant is 50.

6) The general color rendering index is the average of the color rendering index of the eight color samples

$$R_a = \frac{1}{8}\sum_{i=1}^{8} R_i$$

4.5 Tasks 4.2 and 4.3

In preparation for the BP2 Program review meeting, TRNSYS was run to show completion of UW-M's assigned tasks. These tasks and TRNSYS work showing their completion are summarized below.

4.5a Task 4.2 - Prediction of alpha system performance, through modeling, of various system configurations

Figure 33 shows how light is transmitted through the HLS for a clear summer day in Oakridge, TN around noon. The luminous efficiency, η, is defined as

$$\eta = \frac{Light\ out}{Light\ in}$$

and for the baseline alpha system shown in Fig. 1, η = 48%.

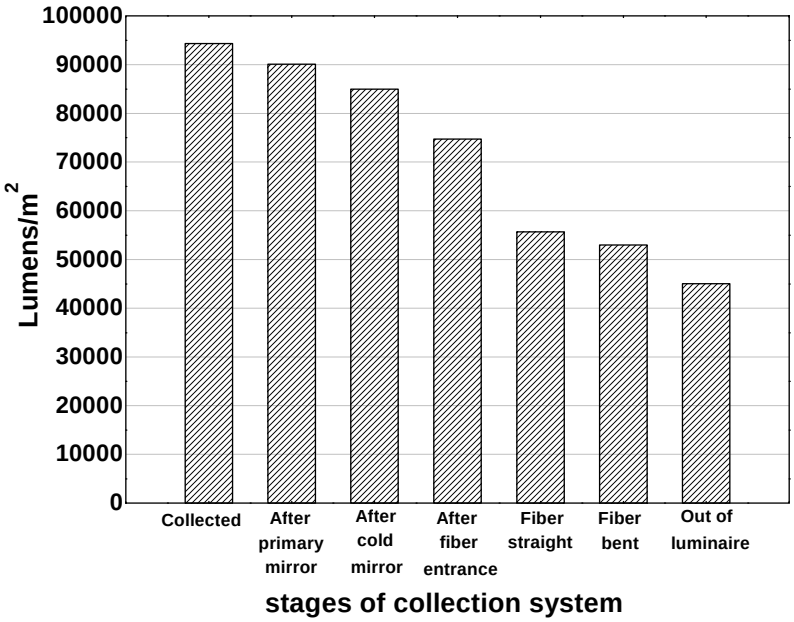

Fig. 33: Transmission of light through HLS

Table 3 shows how changes in some of the parameters of the baseline model change the efficiency. If all improvements are made the efficiency could surpass 60 %.

Table 3: Effect of changing model parameters

Changes to design	η
baseline	**48%**
5m vs. 7m fiber	52%
reduce entrance loss by 50%	51%
elliptical 2nd mirror	51%
elliptical 2nd mirror with 10% packing loss	46%
95% efficient luminaire	53%
all improvements	65%

4.5b Task 4.3 - Compare modeled to predicted performance

Table 4 was presented in the International Solar Energy Society's 2003 conference in Honolulu, HI by Oak Ridge National Lab. It summarizes the measured total luminous efficiency as a function of fiber length for the alpha system. For a system with 7.5 m fiber, the total system efficiency was measured at 48.1%. The TRNSYS model's efficiency for a 7m length of fiber is 48%.

Table 4: ORNL experimental results

Fiber Length (m)	System Efficiency (%)	Chromaticity Value (u',v')	CCT (K)
4.5*	53.5	(.2026, .4979)	5033
5.5*	51.7	(.2016, .4978)	5073
6.5*	49.9	(.2006, .4976)	5111
7.5	48.1	(.1996, .4975)	5150
8.5	45.8	(.1987, .4978)	5182
9.5	44.9	(.1975, .4976)	5243
10.5	42.6	(.1965, .4981)	5268

4.5c Task 4.4 - Prediction of energy savings

The alpha system was modeled annually in TRNSYS for six different geographic locations in the US that were chosen because of their differences in solar insolation, climate, and utility rate

schedules. The total electricity saved is shown in Fig. 34, and the amount of money saved per year per module is illustrated in Fig. 35. The annual energy savings begin to decrease when the modeled building is saturated with light.

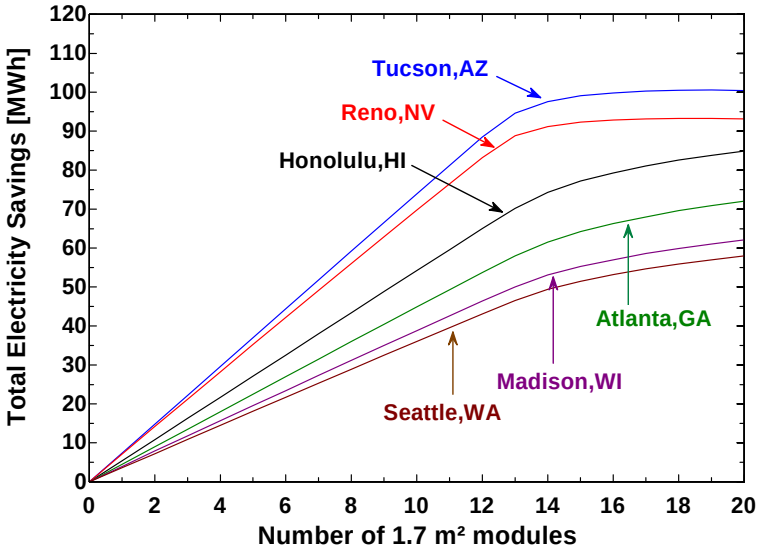

Fig. 34: Annual Electricity Savings

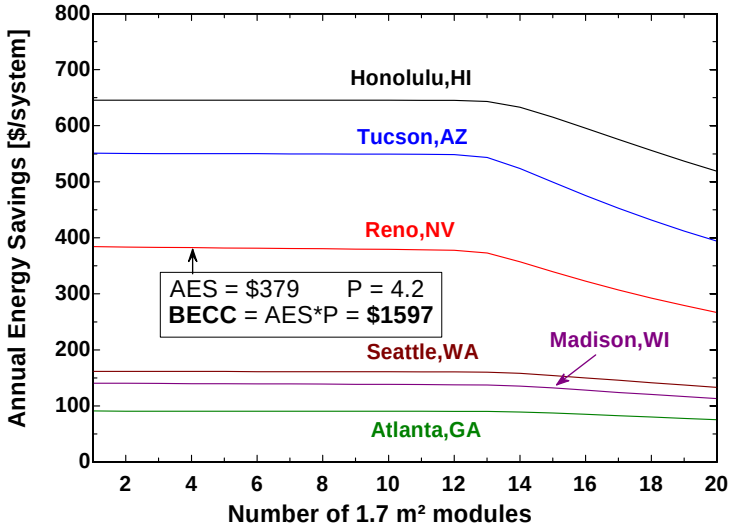

Fig. 35: Annual Energy Savings - 55 lm/W bulbs

5. Bioreactor Re-design, Light Data, Population & Harvesting Testing, and Model Scale Tests

5.1 Lighting Measurements

While the solar collector appears to be functioning well, we are still experiencing minor problems with the light distribution. Not that the organisms will die in this environment, but in the long-term, if an even light distribution can be produced, high productivity can be achieved. Nevertheless, the distribution is clearly good enough to grow organisms (as will be seen), but the uneven quantity of photon distribution should be noted.

To quantify the photon flux in the bioreactor, each of the light sheets was divided into a grid of 3x5 to give 15 readings for each. The sheets are marked A, B, C, D, E, F, G, and H (left to right) when seen from the growth tank side. Each sheet provided 2 sets of 15 readings for both surfaces. For simplicity we have used conventions A(L) and B(R) for each sheet which represent the left and right side of the sheet (again when looked at from the growth tank side).

Let's say we call the membranes 1, 2, 3 …etc.; then #1 will receive light from A(L) and B(R). The locations of these panels in the bioreactor are shown in Figures 36 and 37.

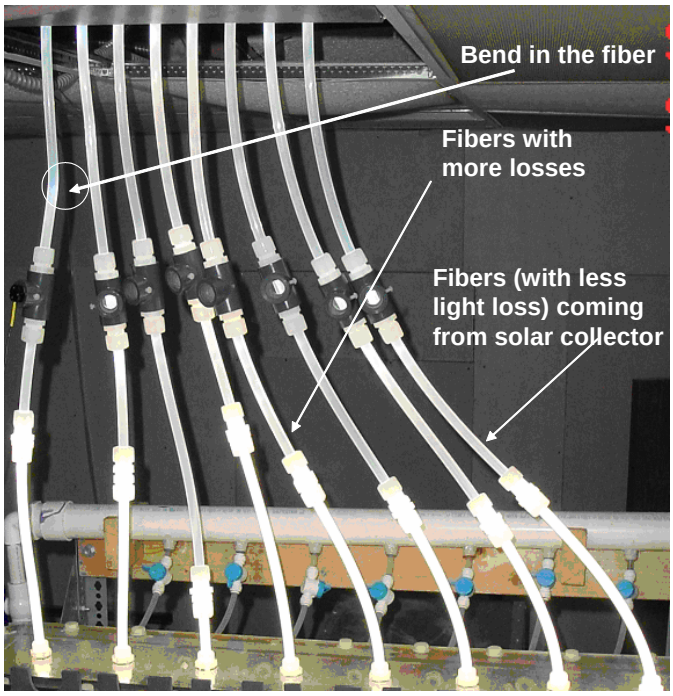

A B C D E F G H

Fig. 36: Lighting panel notes and designations

Fig. 37: Lighting sheets in bioreactor

The readings and the respective graph are shown below.

Table 5: Photon flux measurements (in μmols m^{-2} s^{-1})

A(R)		
43.8	44.6	32.7
50.5	36.4	43.8
25.3	29.7	43.8
29.7	29.0	39.4
46.8	36.4	60.2
B(R)		
52.0	44.6	57.2
44.6	57.2	58.0
38.6	44.6	52.0
43.1	40.9	52.0
72.1	46.1	78.8
C(R)		
55.7	51.3	66.9
46.1	66.1	61.7
37.2	51.3	57.2
43.8	51.3	60.9
97.3	48.3	85.4
D(R)		
45.3	47.6	55.0
54.2	63.2	44.6
39.4	49.0	51.3
44.6	49.8	50.5
51.3	44.6	65.4
E(R)		
50.5	47.6	60.2
40.9	55.0	54.2
42.4	44.6	58.7
40.9	46.1	51.3
64.2	43.1	84.0
F(R)		
57.2	53.5	69.1
44.6	63.9	56.5
43.8	49.8	59.4
44.6	52.8	60.2
63.2	49.0	98.1
G(R)		
58.0	49.8	60.2
46.1	63.9	61.7
47.6	54.2	63.2
46.1	54.2	60.2
33.6	50.5	91.4

B(L)		
69.8	57.2	84.0
67.6	79.5	50.5
63.2	59.4	44.6
67.6	66.1	52.0
117.4	52.8	92.1
C(L)		
58.7	60.9	74.3
62.4	46.8	73.6
49.8	46.1	71.3
61.7	48.3	60.2
150.8	56.5	112.9
D(L)		
61.7	55.7	63.2
53.5	69.1	46.8
53.5	55.7	43.1
58.7	55.7	46.8
91.4	48.3	81.7
E(L)		
66.1	57.2	64.6
48.3	60.9	70.3
58.7	52.8	47.6
57.2	63.9	45.3
134.5	51.3	102.5
F(L)		
67.6	54.2	71.3
67.6	81.0	49.0
63.2	66.9	48.3
63.2	66.1	50.5
125.6	58.0	101.8
G(L)		
58.0	51.3	76.5
61.7	66.1	51.3
56.5	67.6	51.3
54.2	47.6	46.1
138.9	71.3	105.5
H(L)		
55.7	43.8	63.2
53.5	49.8	38.6
49.8	44.6	34.9
52.8	39.4	32.7
173.9	37.2	130.8

Table 6: Maximum, minimum, and average amount of flux deliver by each light sheet.

	A(R)	B(L)	B(R)	C(L)	C(R)	D(L)	D(R)
MAX.	60.2	117.4	78.8	150.8	97.3	91.4	65.4
	50.5	92.1	72.1	112.9	85.4	81.7	63.2
	46.8	84.0	58.0	74.3	66.9	69.1	55.0
	44.6	79.5	57.2	73.6	66.1	63.2	54.2
	43.8	69.8	57.2	71.3	61.7	61.7	51.3
	43.8	67.6	52.0	62.4	60.9	58.7	51.3
	43.8	67.6	52.0	61.7	57.2	55.7	50.5
	39.4	66.1	52.0	60.9	55.7	55.7	49.8
	36.4	63.2	46.1	60.2	51.3	55.7	49.0
	36.4	59.4	44.6	58.7	51.3	53.5	47.6
	32.7	57.2	44.6	56.5	51.3	53.5	45.3
	29.7	52.8	44.6	49.8	48.3	48.3	44.6
	29.7	52.0	43.1	48.3	46.1	46.8	44.6
	29.0	50.5	40.9	46.8	43.8	46.8	44.6
MIN.	25.3	44.6	38.6	46.1	37.2	43.1	39.4
Sum	**592.2**	**1023.9**	**781.6**	**1034.3**	**880.5**	**884.9**	**755.6**
Avg.	39.5	68.3	52.1	69.0	58.7	59.0	50.4

	E(L)	E(R)	F(L)	F(R)	G(L)	G(R)	H(L)
MAX.	134.5	84.0	125.6	98.1	138.9	91.4	173.9
	102.5	64.2	101.8	69.1	105.5	73.6	130.8
	70.3	60.2	81.0	63.9	76.5	63.9	63.2
	66.1	58.7	71.3	63.2	71.3	63.2	55.7
	64.6	55.0	67.6	60.2	67.6	61.7	53.5
	63.9	54.2	67.6	59.4	66.1	60.2	52.8
	60.9	51.3	66.9	57.2	61.7	60.2	49.8
	58.7	50.5	66.1	56.5	58.0	58.0	49.8
	57.2	47.6	63.2	53.5	56.5	54.2	44.6
	57.2	46.1	63.2	52.8	54.2	54.2	43.8
	52.8	44.6	58.0	49.8	51.3	50.5	39.4
	51.3	43.1	54.2	49.0	51.3	49.8	38.6
	48.3	42.4	50.5	44.6	51.3	47.6	37.2
	47.6	40.9	49.0	44.6	47.6	46.1	34.9
MIN.	45.3	40.9	48.3	43.8	46.1	46.1	32.7
Sum	**981.3**	**783.5**	**1034.3**	**865.6**	**1003.8**	**880.5**	**900.5**
Avg.	65.4	52.2	69.0	57.7	66.9	58.7	60.0

Shown below (Fig. 38a-h) are the graphs corresponding to the data in Table 5.

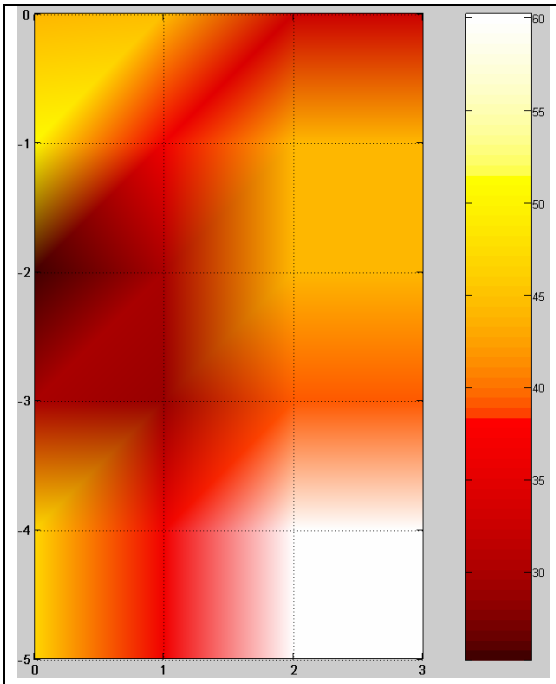
0
-1
-2
-3
-4
-5
0
1
2
3
60
55
50
45
40
35
30

A(R)

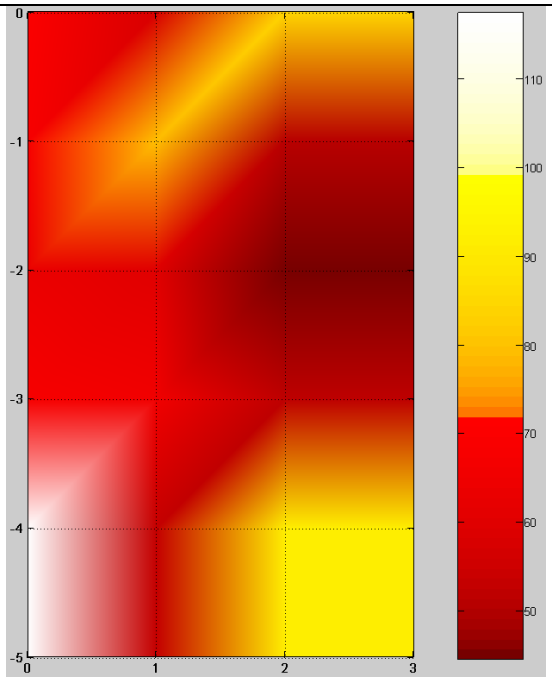
0
-1
-2
-3
-4
-5
0
1
2
3
110
100
90
80
70
60
50

B(L)

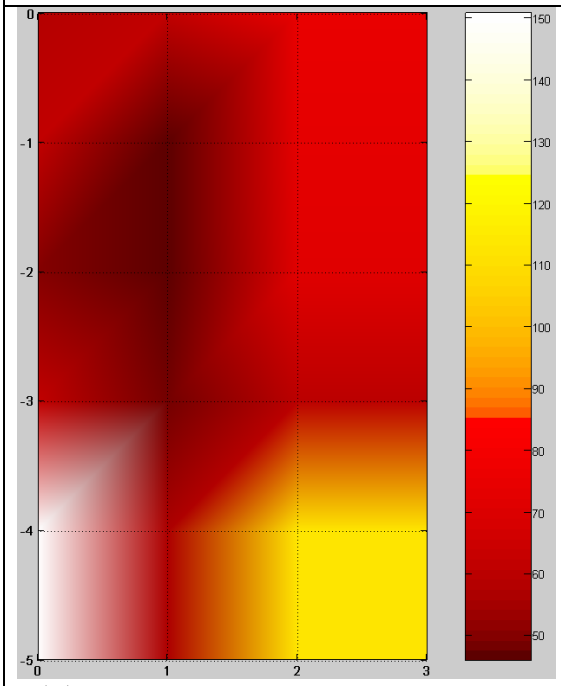
0
-1
-2
-3
-4
-5
0
1
2
3
150
140
130
120
110
100
90
80
70
60
50

B(R)

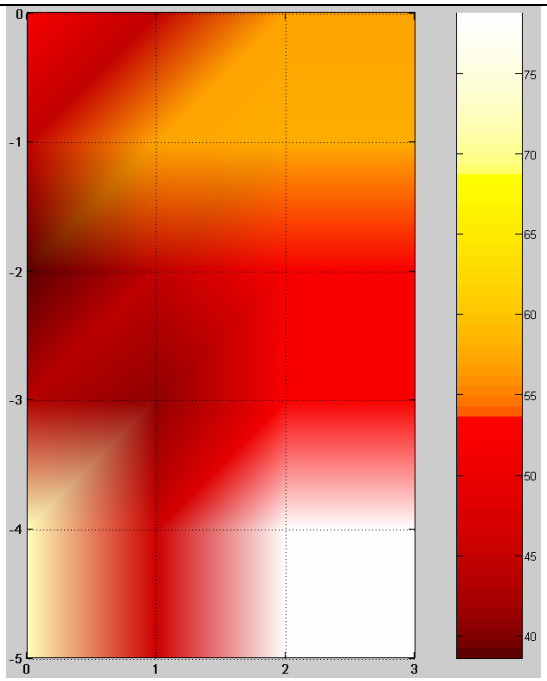
0
-1
-2
-3
-4
-5
0
1
2
3
75
70
65
60
55
50
45
40

C(L)

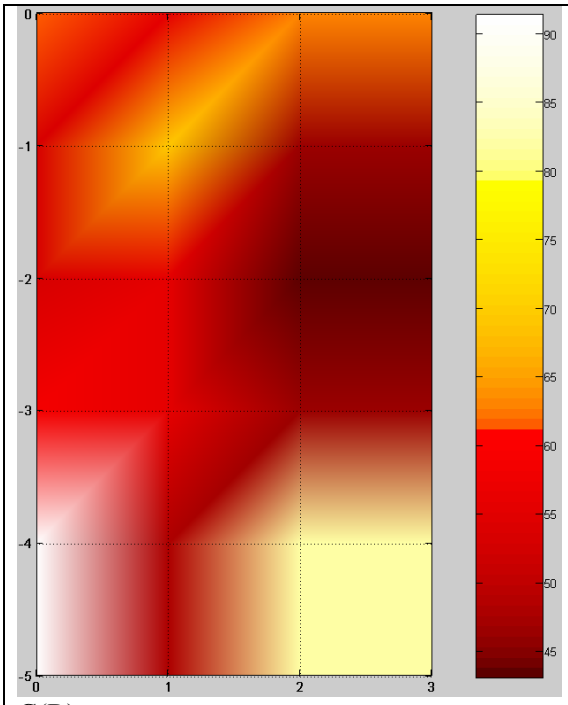
0
-1
-2
-3
-4
-5
0
1
2
3
90
85
80
75
70
65
60
55
50
45

C(R)

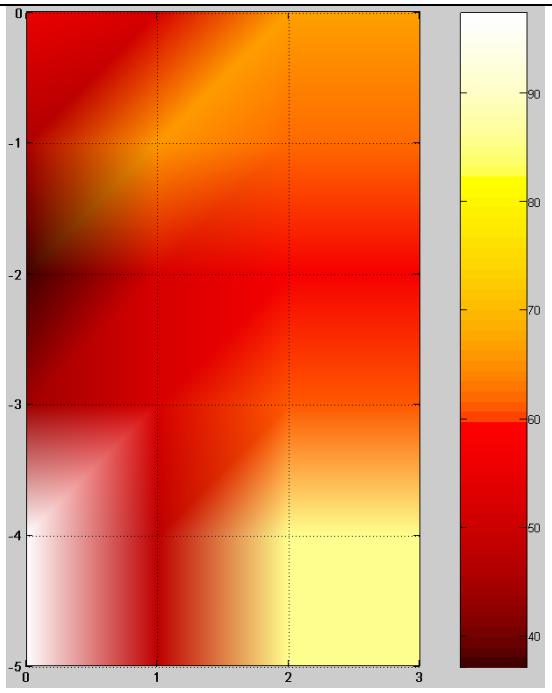
0
-1
-2
-3
-4
-5
0
1
2
3
90
80
70
60
50
40

D(L)

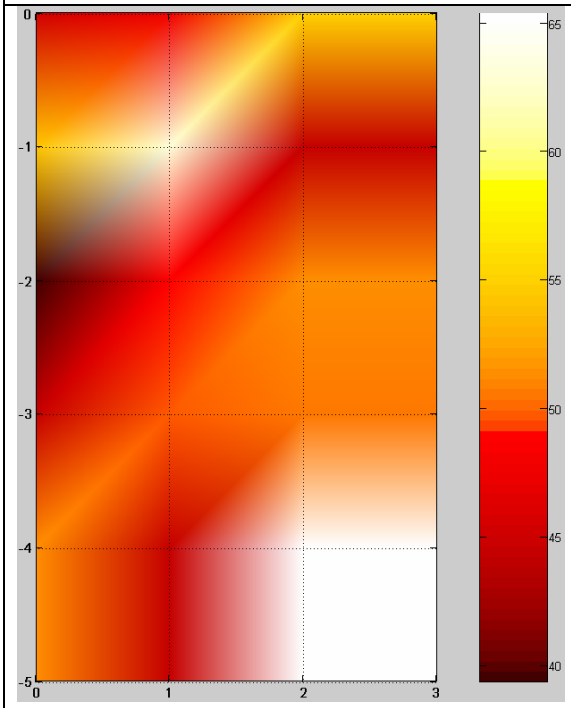
0
-1
-2
-3
-4
-5
0
1
2
3
65
60
55
50
45
40

D(R)

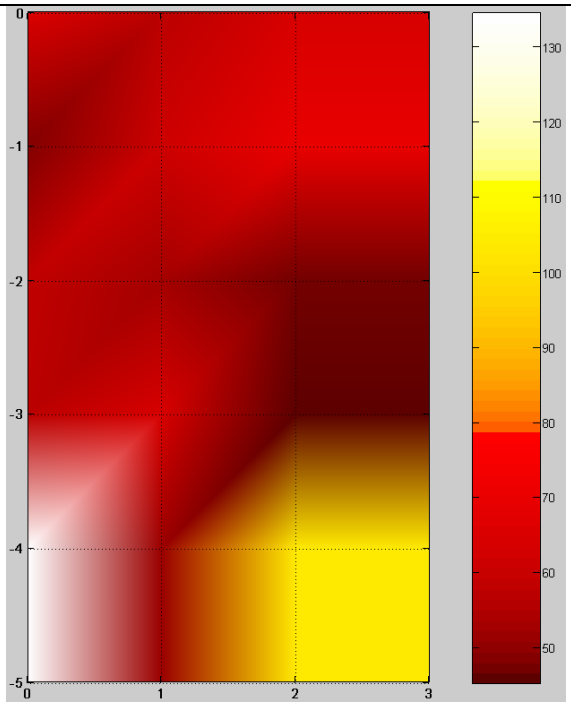
0
-1
-2
-3
-4
-5
0
1
2
3
130
120
110
100
90
80
70
60
50

E(L)

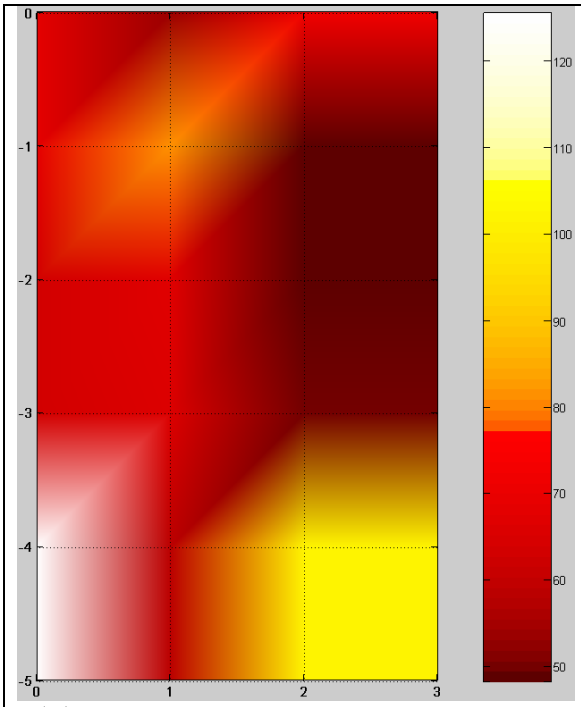
0
-1
-2
-3
-4
-5
0
1
2
3
120
110
100
90
80
70
60
50

E(R)

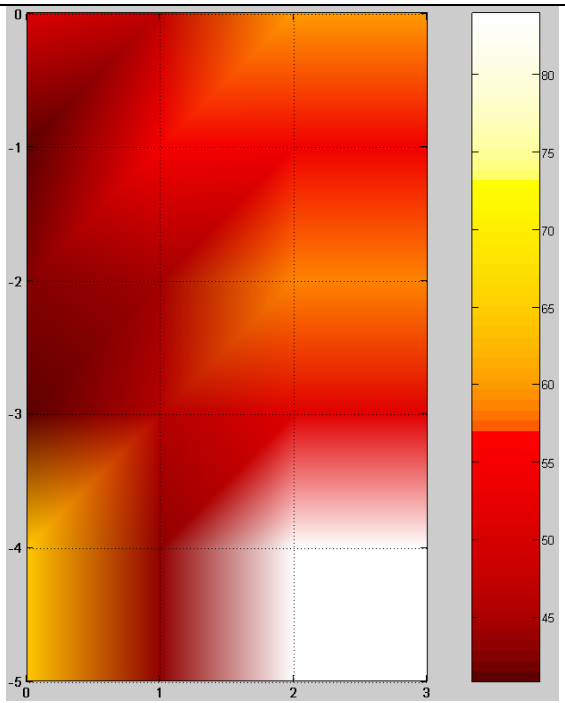
0
-1
-2
-3
-4
-5
0
1
2
3
80
75
70
65
60
55
50
45

F(L)

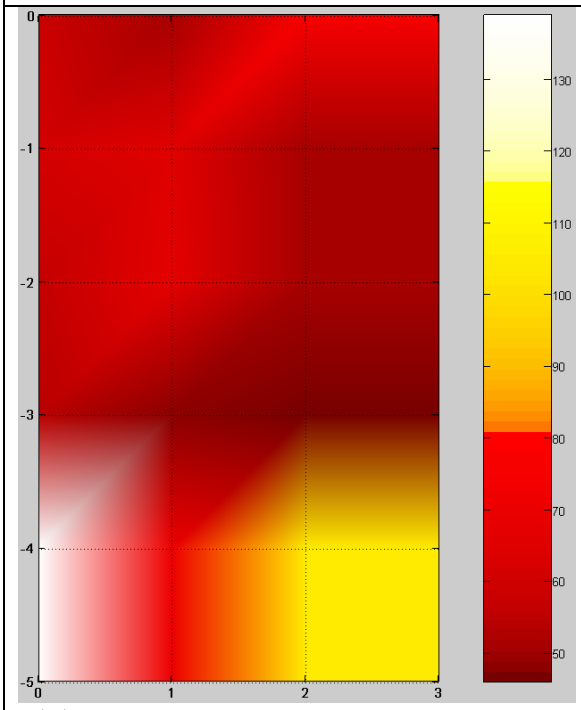
0
-1
-2
-3
-4
-5
0
1
2
3
130
120
110
100
90
80
70
60
50

F(R)

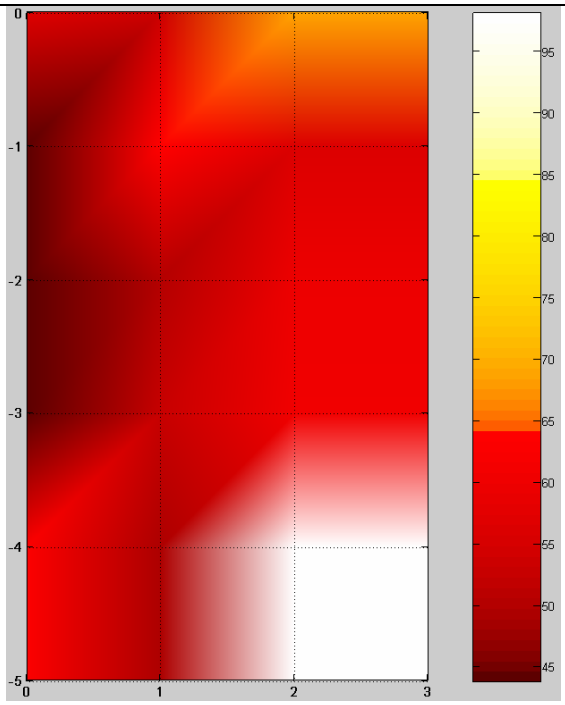
0
-1
-2
-3
-4
-5
0
1
2
3
95
90
85
80
75
70
65
60
55
50
45

G(L)

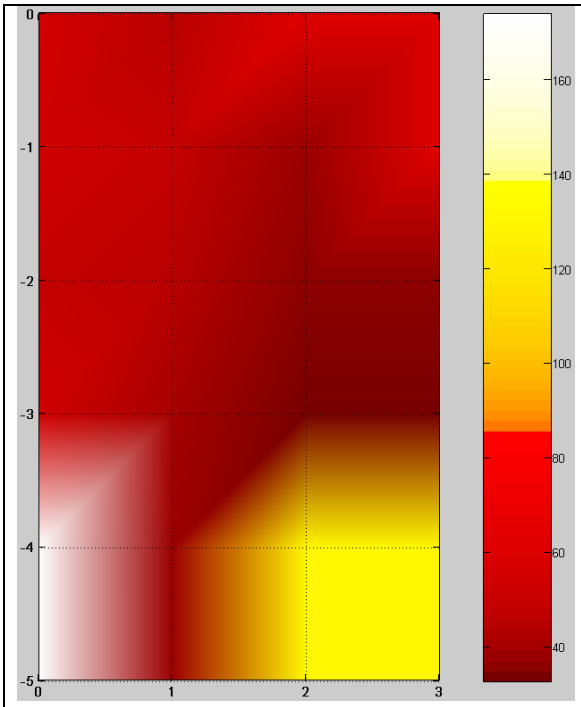

G(R)

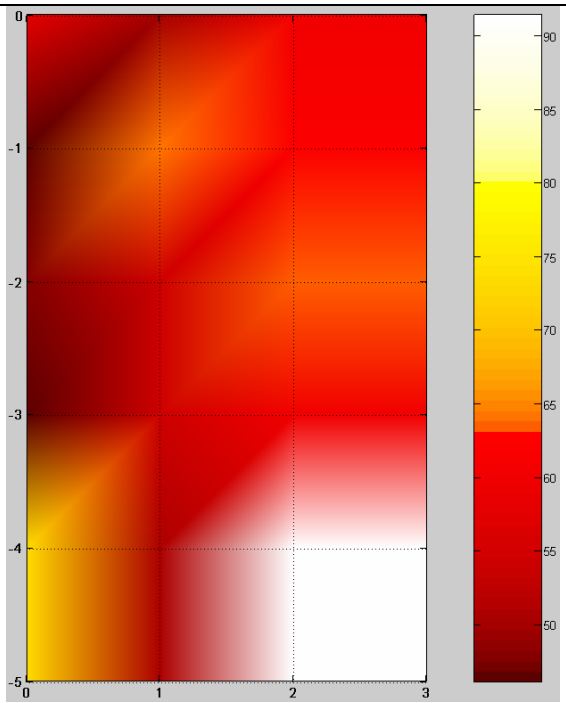

H(L)

The following results can be obtained from the data presented:

1: It can be seen from table 5 that light sheet A delivers the minimum amount of light (Average 39.5 µmols $s^{-1}m^{-2}$). It can be contributed to two factors. As shown in Fig. 36 there is a bend in the fiber coming from the collector. So before entering the light sheets it loses quite a good amount of light. Also the length of the fiber (which loses more light) going into light sheet A is long enough to lose light before entering into the light sheet.

2: Light sheets C and F deliver maximum amount of light (Average 68.9 µmols $s^{-1}m^{-2}$). This is because length of fibers (which loses more light) going into light sheets C and F are having the minimum length.

3: It has been noticed that light intensity delivered from right side of each sheet is less than that of the left side. As shown in Fig. 37 the right side of the sheets have the fixture for holding the fibers. This may contribute to less amount of light from the bends where there is maximum light output.

5.2 Population Testing

Due to a pump failure, the long-term testing was cut short and we were only able to measure shorter-term growth, establishing a system doubling time (biomass production) at approximately 11 days in non-optimized conditions. Figure 39 shows organism coverage on a membrane.

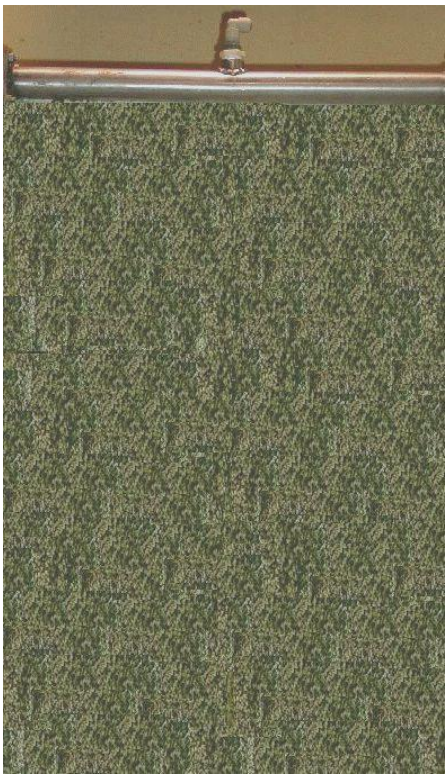

Fig. 39: Algal distribution on membrane (two days dried)

5.3 Redesigned Pumping System for Bioreactor

In the initial system design, we estimated the importance of the subsystems to overall system operation, focusing on maximizing organism growth. Somehow, consideration of catastrophic failure was done on an ad hoc basis, not formally introduced into the design matrix.

In July, we began a 30 day system run of the pilot-scale bioreactor. 40 hours into the test, the water (growth solution) delivery pump failed. One brush on the motor was completely worn. The other brush, amazingly, was as good as new. It became clear that if we are going to run on a continuous basis, the flow loop had to be redesigned to account for primary pump failure.

The new design, shown in Fig. 40, incorporates a secondary pump in parallel with the primary pump that is activated when the differential pressure across the pump drops below 0.5 psid. That way, when the primary pump fails, continuous flow can be maintained, while the primary pump can be isolated and removed for repairs.

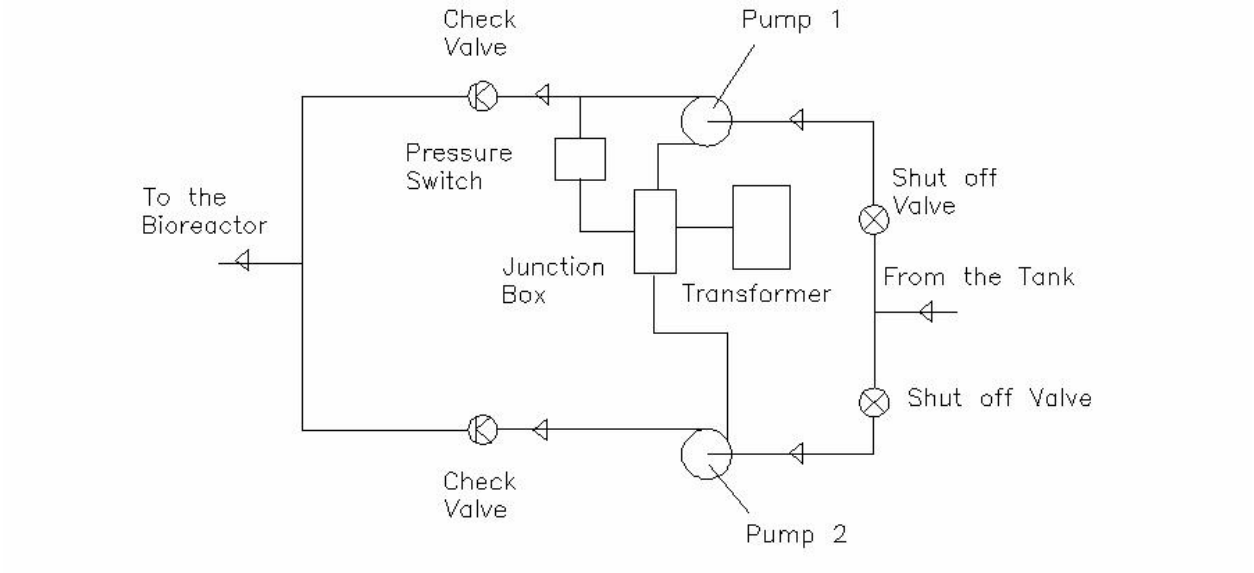

Fig. 40: New flow system schematic

5.4: Bioreactor testing

For the small bioreactor (shown below, before and after harvesting), the mass is doubling approximately every 4 days over 1.5 m^2 of surface area. The pilot bioreactor is also populated, but cloudy weather has limited the growth rates.

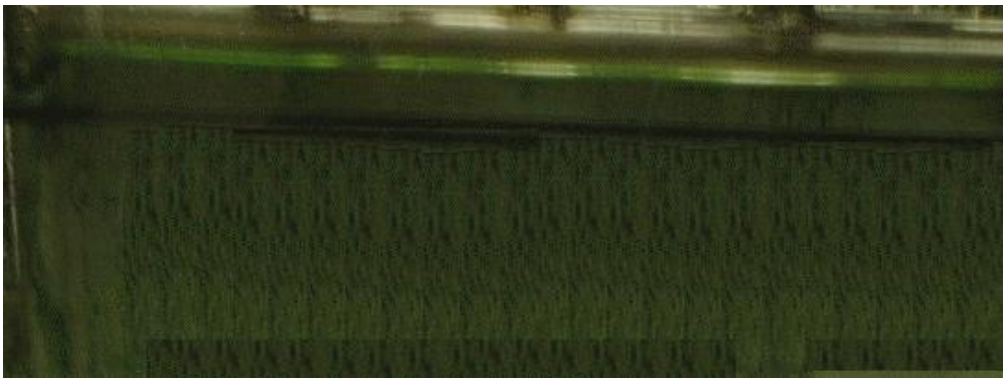

Fig. 41: Bioreactor screen before harvesting

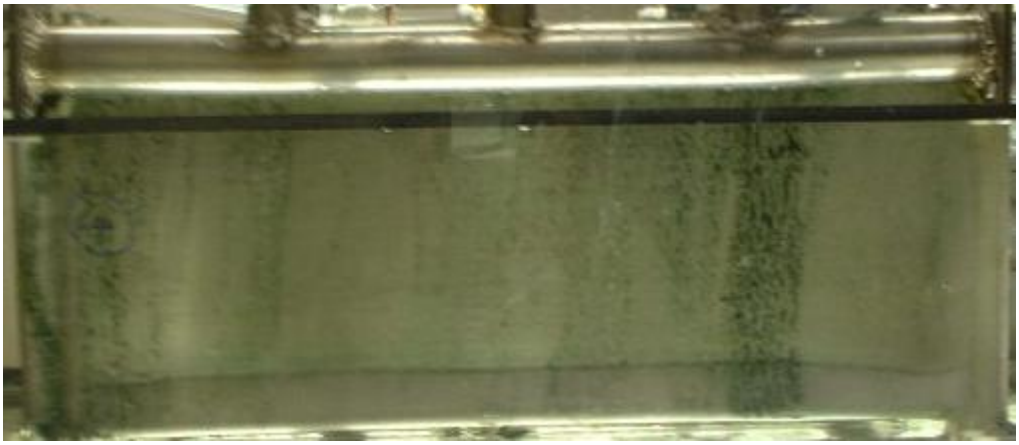

Fig. 42: Bioreactor screen after harvesting

5.5 Model Scale Tests

We have seen very encouraging results from the model scale tests in terms of organism growth rates and we have begun the final tests necessary to meet our project goals. The improved high-flow test system has been used successfully to run several long-term growth tests with periodic harvesting events. The high flow harvesting system performed well. The mass measurement results after a 4-week test show 275% growth over the initial mass loading. This figure would have been higher had there been no leakage and handling losses. Carbon dating of biomass from this test is planned for carbon uptake estimation. The next test will include direct measurement of carbon uptake in addition to organism mass measurements.

5.5a Results and Discussion

Calcium was found to stimulate the generation of cyanobacterial biofilm on artificial substrata. Special calcium-based medium to cultivate cyanobacterial isolates was developed to increase CO_2 trapping and to decrease the contamination of environment with sodium.

The environmental alkalinity was found to be a signal for the morphological changes of highly thermophilic strain Chlorogloeopsis sp. A method for the selection of acid resistant strains of cyanobacteria was also elaborated by our partners at Montana State.

5.5b Growth Rate Testing

With the new header insert put in place and flow irregularities resolved, we did a full productivity test with several harvesting sequences. We used the new harvesting pump, which is capable of 30 gpm, even at differential pressures of 30 psi (indicative of nearly full blockage of the header with organism). The results of mass measurement are summarized in Table 7. We achieved a 275% growth over the initial mass loading. These figures would have been higher had there been no leakages and handling losses.

Table 7: Productivity Test Data

Mass Quantification (Final)

Sr.No	Description	Initial weight (gms)	Final Weight (gms)	Net Weight (gms)
Initial Loading Calculations				
1	Pre-Filter # 1	225.01	229.37	4.36
2	Final-Filter # 1	317.45	319.25	1.8
	Total Initial Mass Loading in 20 liters of solution			**6.16**
	Total Initial Mass Loading in 50 liters of solution			**15.4**
Final Growth Calculations				
	Omnisil Membrane weight			
1	Screen # 1	252.25	260.42	8.17
2	Screen # 2	237.72	245.73	8.01
3	Screen # 3	234.64	241.23	6.59
4	Screen # 4	256.19	260.46	4.27
Filter Weights (in grams)				
1	Pre-Filter # 2	221.52	228.06	6.54
2	Final-Filter # 2	316.75	318.56	1.81
3	Pre-Filter # 3	235.47	239.53	4.06
4	Final-Filter # 3	307.02	308.25	1.23
5	Pre-Filter # 4	233.83	240.18	6.35
6	Final-Filter # 4	313.39	316.99	3.6
7	Pre-Filter # 5	232.47	238	5.53
8	Final-Filter # 5	323.16	324.81	1.65
	Total Final Mass			**57.81 grams**
	Total Mass Growth			**42.41 grams**

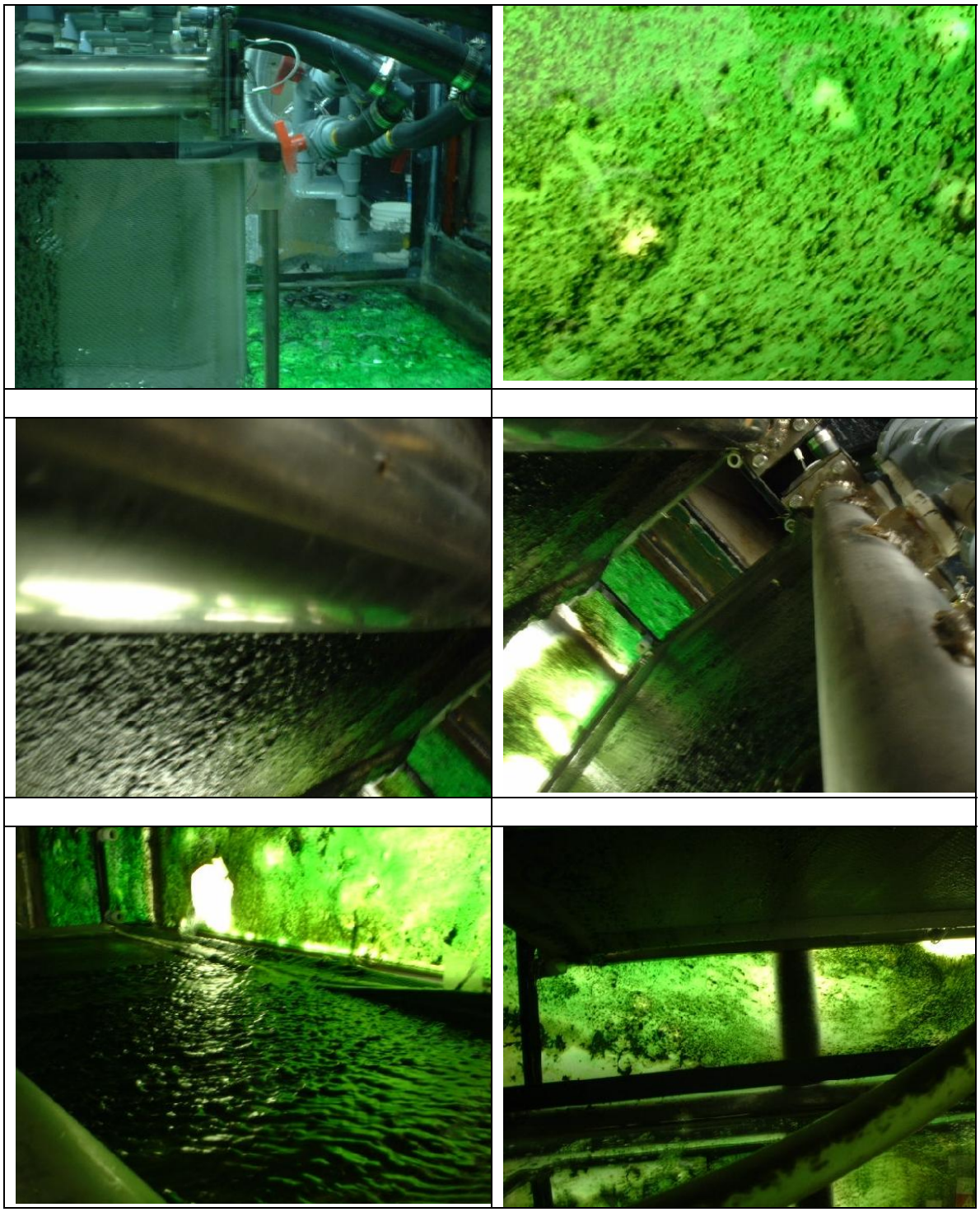

Fig. 43: Pictures from CRF-II organism growth mass measurement test

6. Selection of Thermophilic Algal Species and Development of Laboratory-Scale Bench Top Photobioreactor

6.1 Selection of Thermophilic Algal Species

The selection of thermophilic algal species for CO_2 sequestration was focused on an unidentified strain of *Nostoc* sp. (1.2. S.C.(2)) (Figure 44), a thermophilic species isolated from Yellowstone National Park by Dr. Keith Cooksey of Montana State University and whose samples were provided by Dr. David Bayless of Ohio University.

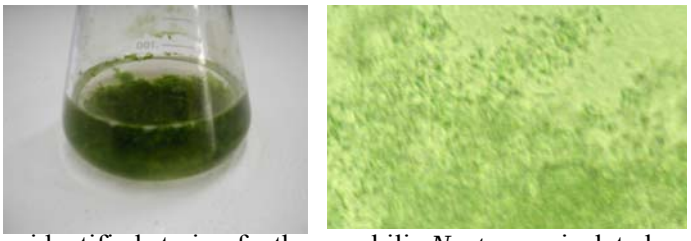

Fig. 44: An unidentified strain of a thermophilic *Nostoc* sp. isolated from Yellowstone National Park

6.1a Chlorophyll Fluorescence

Measurements of chlorophyll fluorescence for *Nostoc* sp., a measure of photosynthetic efficiency, were conducted using a chlorophyll meter (chlorophyll fluorescence package, Qubit systes, Ontario, Canada) (Figure 45). The samples were grown in a heated water bath with a constant temperature of 50 ºC, an average light intensity of 83.3 μmol m^{-2} s^{-1} and a photoperiod of 18/6. Algal samples were suspended in 30-mL algal cuvettes at a concentration of 1.1 g/L. The samples were dark-adapted for 30 minutes, and measurements were conducted under ambient temperature (27 ºC). Based on the chlorophyll fluorescence reaction, the efficiency of quantum yield (F_{PSII}) was calculated using the following equation:

$$F_{PSII} = F_V/F_m = (F_m - F_o)/ F_m$$

where, F_{PSII} is the efficiency of quantum yield, F_m is peak fluorescence, and F_o is minimum fluorescence.

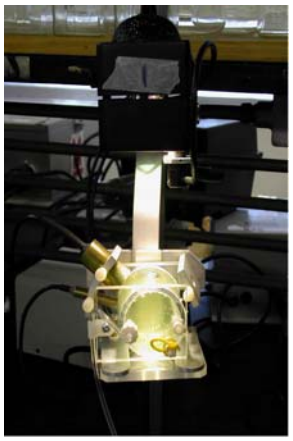

Fig. 45: Fluorescence Package, Qubit Systems (Ontario, Canada)

The results, shown in Table 8, yielded an efficiency of quantum yield for *Nostoc sp.* of 0.667, exceeding the value for *Chlorella vulgaris* of only 0.522. Note that under optimal condition, the maximum attainable value is 0.8. This indicates the high photosynthetic efficiency of *Nostoc sp*., which is indicative of its high CO_2 fixation capacity.

Table 8: Efficiencies of quantum yield for two cyanobacteria

Algal Species	F_{PSII}
Nostoc sp.	0.667
Chlorella vulgaris	0.522

6.1b Growth Rates

Experiments showed that *Chlorella vulgaris* (UTEX 259) did not tolerate a growing temperature of 35 °C or 50 °C. Previous studies reported that some strains of *Chlorella* are thermotolerant (e.g., *Chlorella pyrenoidosa* growing at 39°C). Hirata et al. (1996) reported that an unidentified *Chlorella* sp. (UK001), which was isolated from a spring in Ohita prefecture, Japan, could grow at 40 °C. Hanagata et al. (1992) also reported that an unidentified *Chlorella* sp. (strain K35), also isolated from Japanese fresh water environment, could grow at 40 °C. The *Chlorella vulgaris* (UTEX 259) used in this study had relatively lower optimum temperature than those species.

Figure 46 shows the average final dry weights of *Chlorella vulgaris* at high (212.2 µmol m^{-2} s^{-1}) and low (102.5 µmol m^{-2} s^{-1}) light conditions at 25 °C. The results showed that the means were statistically indistinguishable at the 95% confidence level.

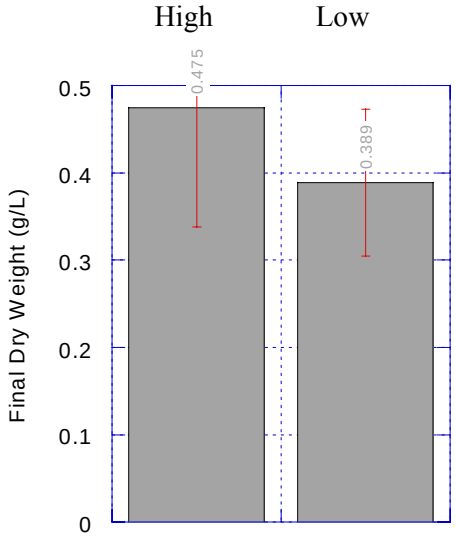

Fig. 46: Average final dry weights of *Chlorella vulgaris* at high (212.2 µmol m^{-2} s^{-1}) and low (102.5 µmol m^{-2} s^{-1}) light conditions at 25 °C. The error bars shown are standard errors

A growth study for the thermophilic *Nostoc* species under elevated CO_2 concentration (5% v/v) and elevated temperature (50 ºC) was conducted using two light conditions, i.e., high level (70.2 ± 2.60 µmol m^2 s^{-1}) and low level (36.9 ± 0.97 µmol m^2 s^{-1}). Each light level had 14 samples. Figure 47 shows the schematic diagram of the experimental system.

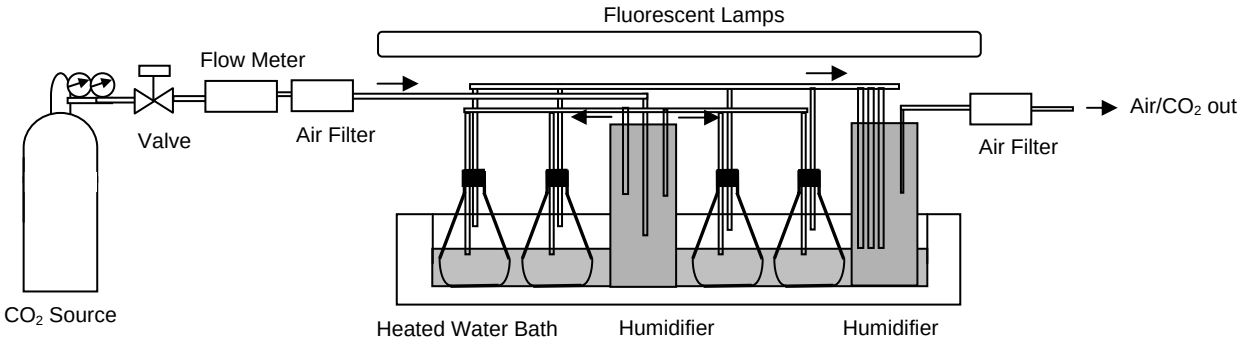

Fig. 47: Schematic diagram of experimental system

Figure 48 shows the average dry weights for the two light treatments after 8 days under elevated temperature (50 ºC) and elevated CO_2 concentration (5%). The error bars shown in Figure 46 are standard errors. The two light treatments are statistically indistinguishable in terms of average dry weight at the 95% confidence level.

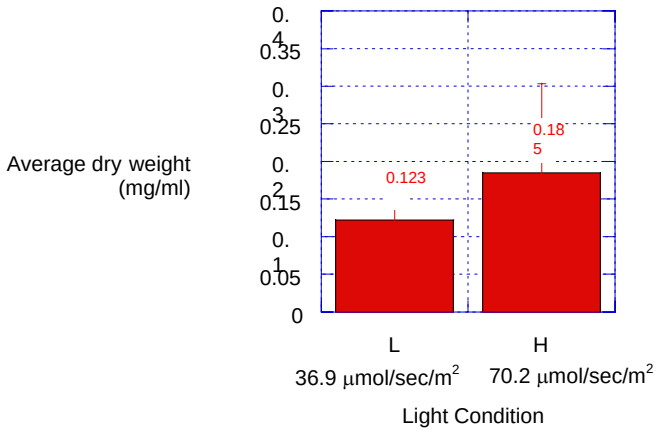

Fig. 48: Average dry weight of two light treatments after 8 days under elevated temperature (50 ºC) and elevated CO_2 concentration (5%)

Since Chlorella vulgaris could tolerate a much higher light intensity of 212.2 µmol m^{-2} s^{-1}, growth experiment for *Nostoc sp.* under higher light intensities was conducted. Three light intensities -- 203.0, 100.1, 246.1 µmol m^{-2} s^{-1} -- were used. Fluorescent lamps were partially covered with a shading material to attain lower light intensities. The experiment was conducted under elevated CO_2 concentration (1% v/v) and elevated temperature condition (50 ºC) for 8 days. Two

replications were harvested every other day, and the biomass sample in BG-11 solution was oven-dried at a temperature of 105 °C.

Figure 49 shows the changes in dry weights of *Nostoc sp.* over the experimental period under the various treatments. Figure 50 provides the average final dry weights on day 8. The maximum average dry weight was observed under the light intensity of 200 µmol m^{-2} s^{-1}, significantly exceeding the average dry weights at 100 and 246 µmol m^{-2} s^{-1}. Table 9 shows the average growth rates for the three light intensities.

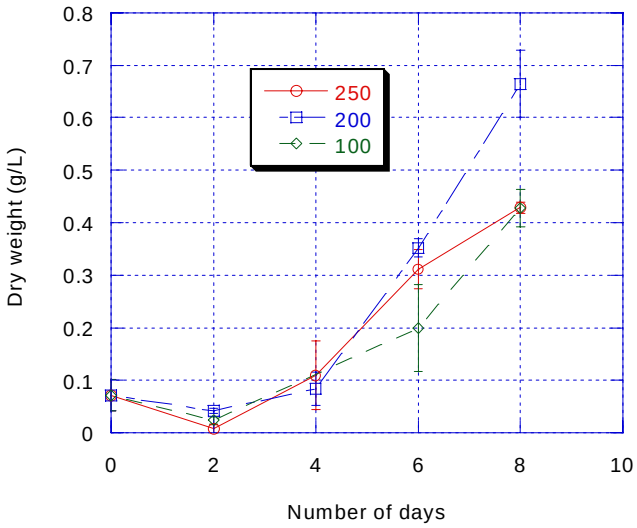

Fig. 49: Dry weight changes over time for *Nostoc sp.* at three light intensities in µmol m^{-2} s^{-1}

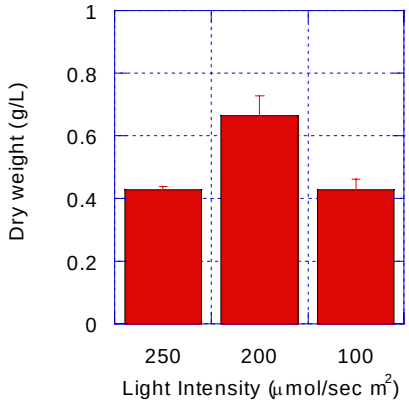

Fig. 50: Average final dry weights for *Nostoc sp.* on day 8

TABLE 9: Average growth rates of *Nostoc sp*. at three light intensities

Approx. Light Intensity ($\mu mol\ m^{-2}\ s^{-1}$)	Average Growth Rate (mg/L day)
250	53.59
200	83.05
100	53.48

6.2 Laboratory-Scale Bench-Top Photobioreactor

The laboratory-scale bench-top photobioreactor was constructed (Figures 51 and 52). The size of the reactor is 24"W x 15 ¾" H x 11 ½"L. A small pump (Beckett Corporation, Irving, Texas), with 60GH capacity, is used to deliver the nutrient solution (BG-11) through ¾-inch PVC pipe onto the screen. Black aluminum screens (18" W x 10" L) are used as the growing substrate. The angle of the screen frames can be changed. The screen itself can be easily changed so that different growing materials could be used as desired. Three screens are enclosed within a transparent airtight closure. The piping system also serves as the structure to hold the screen. Plexiglas cover was used so that photosynthetic radiation can be attenuated.

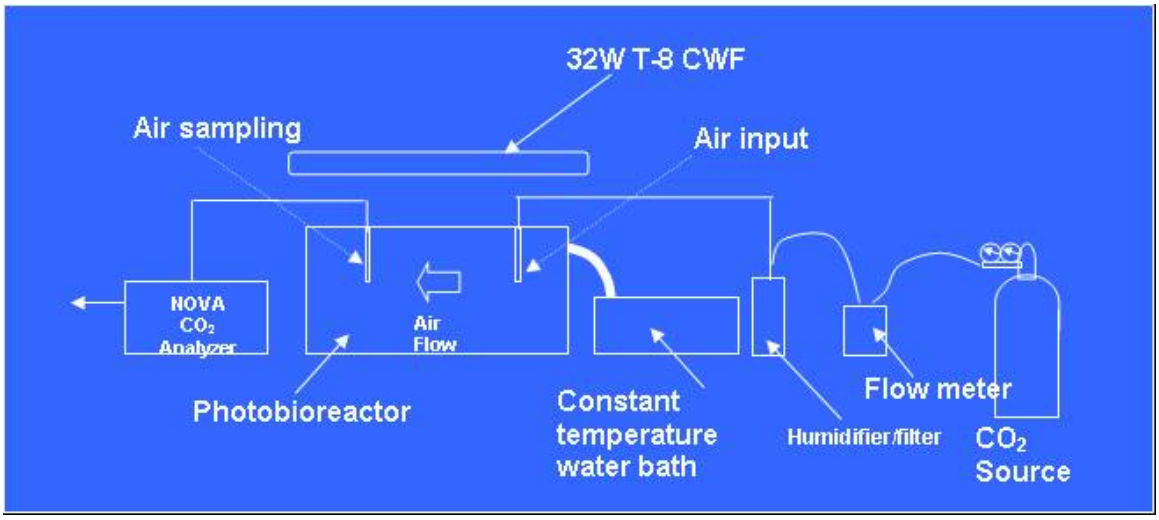

Fig. 51: Schematic of the photobioreactor set up

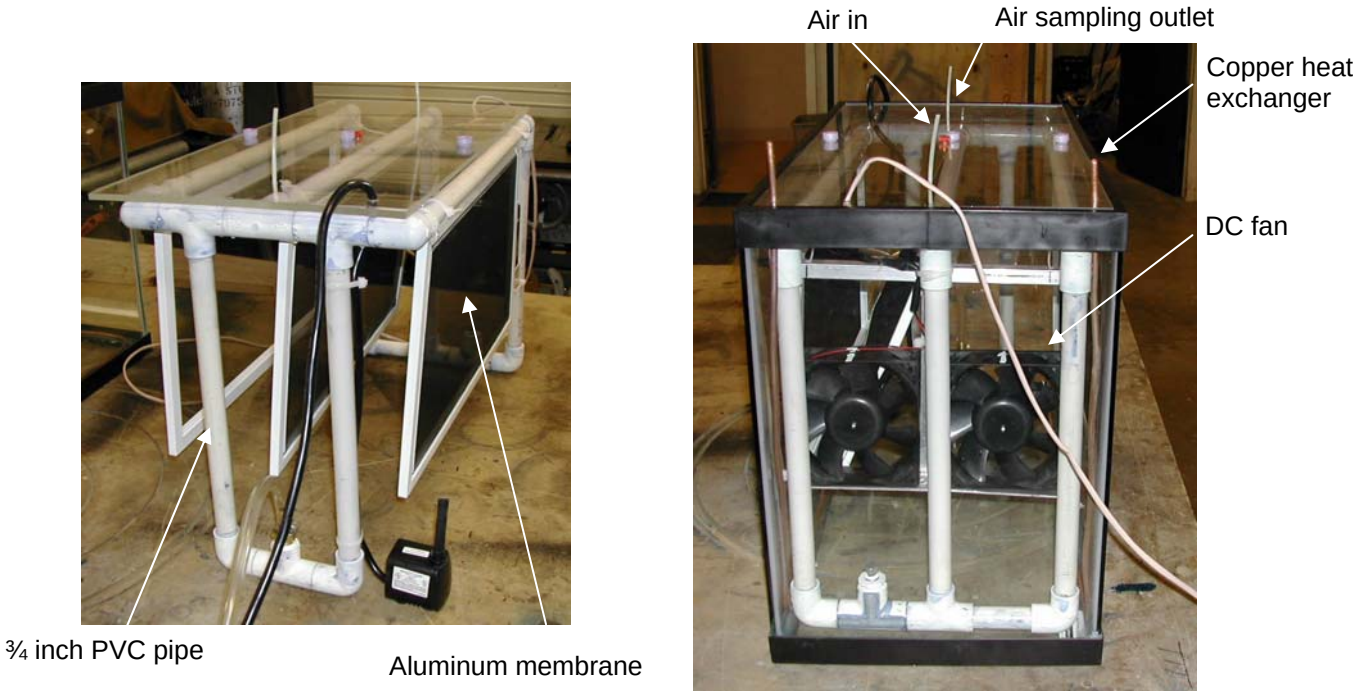

Fig. 52: Photobioreactor details

Wind speed within the chamber can be controlled using two DC fans (FBA12G, Panasonic) and a DC power supply. A wind speed of 1.5 m/s is attainable. The wind speed can be easily controlled by simply changing the voltage supplied. Temperature within the photobioreactor is controlled using a constant water bath (National appliance co., Portland, Oregon) and copper tubings. Data are monitored in real-time (Figure 53). A multi-channel programmable datalogger (21X micrologger, Campbell Scientific, Inc., Logan, UT) is used to monitor the data. Currently, multiple-point temperature data are monitored using copper-constantan thermocouples.

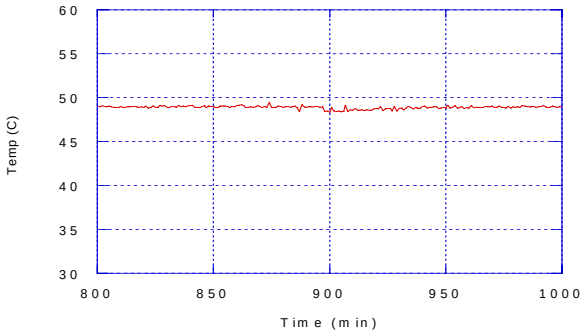

Fig. 53: Time movement of actual temperature within the photobioreactor

An experiment with elevated CO_2 concentration (5% v/v) and elevated temperature (50 ºC) was conducted (Figure 54). The initial loading of *Nostoc* sp. was 22.5 mg (dry weight) per membrane and 67.5 mg total.

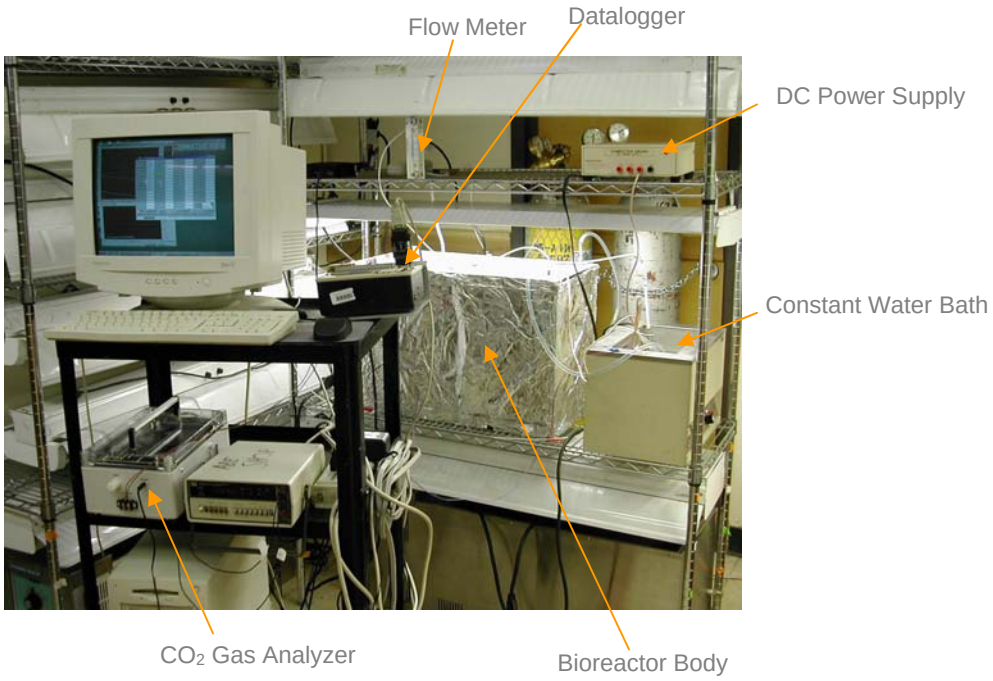

Fig. 54: Photobioreactor in operation

The *Nostoc* strain survived at high temperature (50 ºC), elevated CO_2 (5% v/v) and low light intensity (130 µmol m^{-2} s^{-1}). There were no visible signs of contamination. However, biomass growth on the membrane surface was limited. Although aluminum membrane was selected for its light weight, high corrosion resistance and easy availability, it was not suitable for use as a membrane matrix. Currently, an experiment using the heat-tolerant fabric Omnisil 1000 (Thermal Material Systems, Inc., NV) as the membrane matrix is being conducted. Further studies on initial biomass loading and nutrient circulation rate will be examined.

7. Collector/reciever and light deliver

7.1 Collector/Receiver System (Task 1)

Several accomplishments were made during this time period. They are listed below.

- Completed formulating specifications for low-cost primary reflector and requirements for reflector and tracking system.
- Contacted potential suppliers of low cost optically acceptable mirrored dishes and reflective films for adhesion to the dish.
- Met with ORNL researchers in San Diego to discuss specifications and approaches for the primary mirror/tracking system.
- Evaluated a spun aluminum, thermo formed plastic dish, and stamped steel. Received samples material samples from dish manufacturers.
- Procured and began testing of a Fortec low cost stamped steel dish.
- Procured Reflechtech polymer reflective film. Adhered the film to the Fortec dish and developed testing procedures for optical accuracy.
- Begin the design and search for all components for the low cost optically acceptable dish, tracking system and controls.
- Began the design and search for all components for the low cost optically acceptable dish, tracking system and controls.
- Began assembling components for the low cost optically acceptable dish, tracking system and controls.
- Sent our FORTEC dish to UNR for high flux fiber testing and other dish testing.
- Ordered two more FORTEC dishes for SAIC testing and UNR testing.
- Purchased an Edtek dish, tracker and controls. Met with Ed Horne of Edtek at the Oak Ridge meeting and discussed his system.
- Prepared cost estimates for the original system as a bench mark and low cost system (see Appendix C.

7.2 Requirements for Hybrid Solar Lighting Dish-Tracker System

Appendix D contains requirements for the dish-tracker subsystem of the hybrid solar lighting system. The requirements may be divided into several types:

- Environmental
- Optical
- Operational
- Mechanical

Environmental requirements relate to the outdoor exposure of the system, and take into account such things as temperature extremes, resistance to weathering, and protection of the system against environmental hazards such as snow and wind loads. Optical requirements relate to the basic requirements of delivering a certain amount of solar light to the aperture of the optical fibers. They affect such things as the reflectance of the mirrors, mirror accuracy, and dish concentrator size. Operational requirements include those related to tracking the sun, power requirements, and interfaces. Mechanical requirements also include the interfaces to the building roof, to the fiber bundle, and other mechanical connections.

For the complete report, please see Appendix D.

7.3 Fiber Receiver

Two options were looked at for the fiber receiver. The first and most promising option is a bundle of small diameter fibers thermally compressed together to eliminate packing losses. Another option was using 3M's large core fibers to make a bundle, but this bundle obviously has large gaps between fibers that decrease the efficiency. However, it is relatively simple to make and allows for a fiber to run from the collector to the luminaire with no couplings.

7.3a Small fiber bundle

ORNL continued development of the fiber receiver by investigating new integrating rod configurations and continued development of the new fiber optic bundle light distribution system (Fig. 55) by improving the packing fraction losses in initial prototypes. Also, ORNL continued evaluation of the 2nd generation collector components with on-sun tests at its new facility (ORNL – Engineering Technology Facility Bldg. 5800). Tests to measure flux profile at the fiber end-faces were completed and new non-imaging optic concentrators are now being evaluated to more uniformly insert visible sunlight into the polymer fiber optic bundle. Work also continued on identifying cost-drivers and associated methods for reducing system level costs. Production estimates were received for controllers, tracking mechanisms, and two different primary mirror fabrication methodologies. Results from both activities will be provided at the quarterly meeting in Oak Ridge.

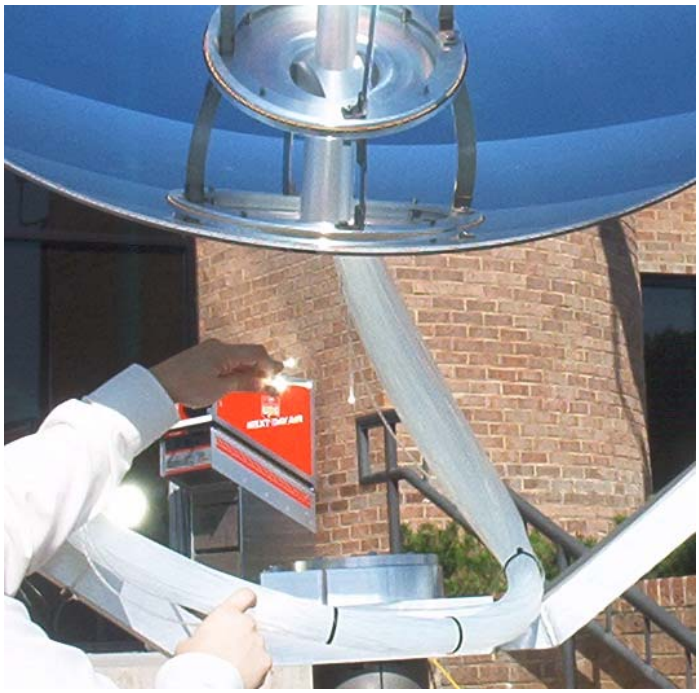

Fig. 55: Small-fiber bundle

7.3b 3M Fiber Bundle

A bundle of 3M fibers was made for the new Edtek mirror at UNR. This bundle of nine fibers is a test to see if a cheap fiber bundle comprised of large-core fibers can be effectively used, despite the packing fraction losses (roughly 28%). A 1.6" square quartz rod will be place in front of the bundle to reduce the IR flux and act as a non-imaging device so the center fiber does not receive more than the outer fibers.

Fig 56: 3M fiber bundle

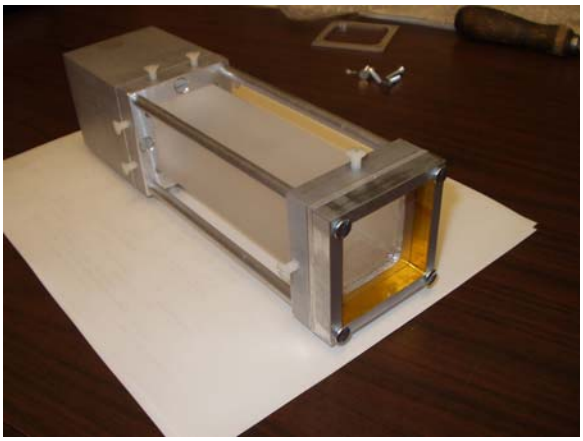

Fig 57: 3M fiber bundle holder with quartz non-imaging rod

7.4 Alpha Collector/Receiver System

A tour of Edtek's facility resulted in excitement for the new dish, but not much information about the coating or performance of the tracker. At the onset, Ed Horne said that he had a new coating for his mirrors that he was very excited about, but he would not disclose any information about it whatsoever. He will be supplying the dishes with this new coating with a only a one year guarantee, but he is confident that they will weather superbly and degradation won't be an issue. The tracking system was demonstrated with a 100W light bulb, but the system was indoors so they were not able to demonstrate it on-sun.

Some specs on the system presented during the tour. These may differ from the delivered systems:

- Primary mirror + stiffeners (as shown in Fig. 58) weigh 28 lbs.
- The useful aperture of the 56" diameter mirror is 52".
- The primary mirror comes with a 5" diameter hole in the bottom for their mounting rings.
- In the demonstrated configuration, the elevation had 135^{o} of freedom and the azimuth had 200^{o}. However, this could change depending on the configuration of the mirror mount and the type of azimuth drive they use.
- They are investigating two different systems for the azimuth drive. Whichever one performs best will be shipped to ORNL and UNR for evaluation.
- The system will be equipped with an anemometer so it can weathervane in high winds.

Fig. 58: Edtek Primary Mirror

The Edtek Alpha system, as shipped to UNR and ORNL, is shown in Fig. 59. This system has the optical sun sensing device mounted on the back side of the secondary hyperbolic mirror. This allows the dish to pick up the sun early in the morning because it is not in the shadow of the primary mirror.

Fig. 59: Edtek Alpha System as shipped to ORNL and UNR

8. Non-Energy Benefits of Daylighting

During the month of October, the experiment proposed to find the non energy benefits of daylight was finalized at the meeting in ORNL on October 8th 2003.

A summary of the proposed human factors experiment is described below.

8.1 Setup and procedure

In this experiment, human subjects will see two different lighting arrangements in an office setting. They are:

A. - A windowless office with electric lighting only
B. - A windowless office with daylight from the HSL.

Each subject will answer a short questionnaire that will give an idea of their mood. Then they will be shown Office A first, followed by office B. After experiencing Office A for a short time, doing some basic office tasks, each subject will be asked how much they would like to have such an office for their place of work for the next year. They will also be told that the cost for renting Office A is $10 per square foot per month. The same question will be asked for all the office B but, in addition, the subject will be asked how much they think the office they have just experienced would be to rent, bearing in mind that Office A costs $10 per square foot per month to rent.

The estimated rental cost per square foot per month serves two purposes. First, it gives an idea of the financial value attached to having a view out and a having daylight. Second, it helps determine the importance of daylight in the office.

The subjects will also answer the same questionnaire on mood after going through the setups. This will help understand the effect of the lighting systems on their mood.

The whole experiment will be done for two sets of subjects. The first set will go through the experiment without knowing that office B was illuminated with daylight. The second set would be made aware that office B is illuminated with daylight before they answer the questionnaire. This way, we can also quantify human bias for daylighting.

8.2 Variables in the experiment:

- Independent variable -
  - Light delivery system (daylight / electric light)
  - Knowledge of the daylight system
- Dependent variable
  - Preference (color appearance, rendering etc)
  - Monetary value (rental value)
  - Performance (simple tasks)
- Constant
  - Minimum maintained illuminance at task plain
- Tasks
  - Simple numerical verification tasks
  - Look at color chips, colorful magazines, newspapers
  - Answer questionnaire regarding preference

8.3 Subjects:

At least twenty subjects will take part in the two experiments. These subjects will be either naïve office workers from the location of the experiment, who are willing to participate in the experiment, or can be hired from a temporary office worker agency. Both will have extensive experience of current office lighting practice.

8.4 Location:

In the meeting at ORNL, it was decided that the experiment should be held either at the existing facility at ORNL or at the new installation at UNR, Nevada. Later communications suggested that the setup of the HSL at UNR would take a couple of months and may be ready only by Feb 2004. Hence it was decided that the experiment should be done at the ORNL facility.

A detailed procedure and the questionnaire for the subjects is being worked on by the Lighting Research Center.

9: UNR Solar Energy Lab and Alpha System Test Facility

9.1 Facility

The team at UNR has acquired a new laboratory on top of the Engineering Laboratory Center (ELC) at UNR. This laboratory is a small room on top of the main building, adjacent to an elevator shaft. The room is approximately 10' x 20', with a 13' high ceiling. Outside the room it is 14' to the roof line, and there are several large I-beams that we will be mounting a platform to for the collectors. The fiber optic collector will be mounted directly above the I-beam closest to the building, and the high-lumen system will be mounted on the other I-beam shown in the foreground of the picture. A structural engineering firm designed the solar experiment platform. The total installed cost of the platform was around $18,000. The completed platform is shown in Fig. 60.

Fig. 60: UNR Solar Experiment Platform

A web cam viewing that platform can be seen at the following link: http://webcam401.me.unr.edu

9.2 Instrumentation

A flow sheet of the data acquisition system (DAS) of the UNR solar energy lab is shown in Fig. 61. The data acquired is for monitoring the thermal management and light transmission properties of the Alpha and High-Lumen test system.

The thermal management instrumentation consists of thermocouples measuring primarily the temperature of the fibers at the entrance region, where they are joined to the quartz. The light transmission will be measured with a 4" integrating sphere, a spectrometer for measuring lumens, and a spectroradiometer for measuring irradiance. The direct normal irradiance will be measured directly, and either the total lumens per square meter (lux) will be measured directly or calculated from the irradiance measurements. In the lab, the lux can be measured with the spectroradiometer. The power consumed by both tracking systems will be measured to provide a comparison between the two different systems. The power consumed by the luminaires in the lab will also be measured so that energy savings can be calculated.

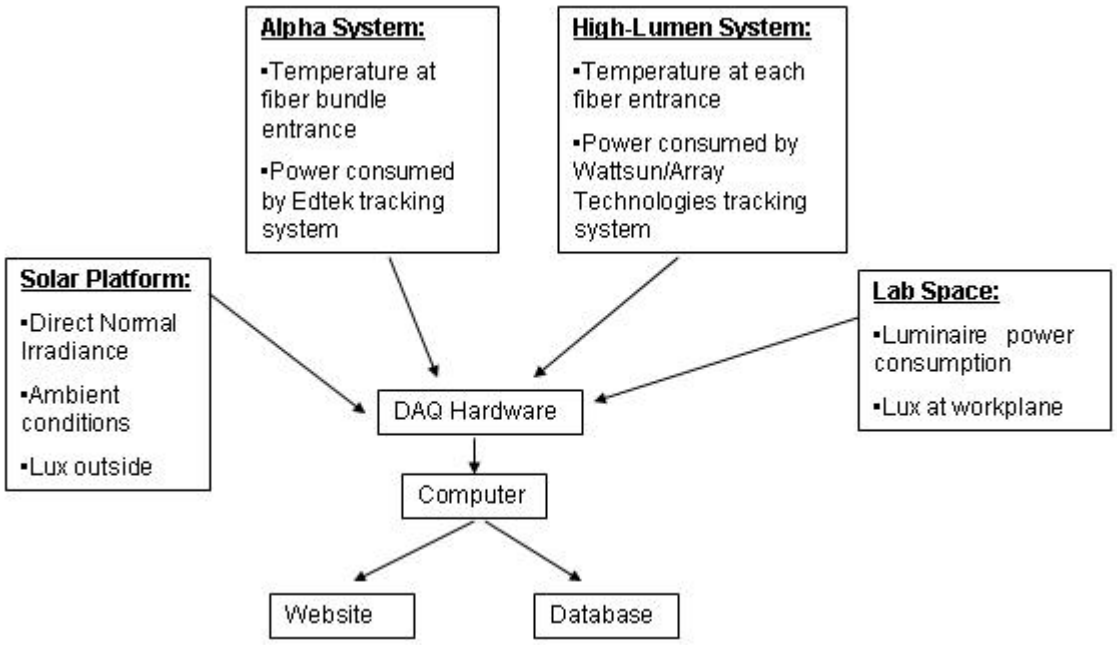

Fig. 61: Data flow chart

CONCLUSIONS

During the reporting period, the project team made advancements in the design of the Alpha system and small-fiber bundle, updated and added components to the TRNSYS Full-Spectrum Solar Energy System model, tested the TPV array and non-imaging device, made changes and advancements in the high-lumen test system, and made changes to the fiber transmission models.

A test plan was developed for both the high-lumen tests and the study to determine the non-energy benefits of daylighting. The photobioreactor team also made major advancements in the testing of model scale and bench top lab-scale systems. Accomplishments for this period are:

1. Work was performed on the high-lumen test system and mechanical durability test device. Different brands of fibers were selected and acquired for both tests, and bending fatigue tests are underway. The high-lumen test system has undergone some revisions, and tests are not underway yet. A test plan has been laid out that outlines the steps that will be taken to perform the tests and analyze the data that is obtained.

2. Tests of the TPV array were performed and a publication was generated and submitted to the ISEC conference. The TPV array generated 26.7W and demonstrated 12% conversion efficiency. The results were compared with laboratory test data, and when the intensity differences of the light sources and characteristics of the cells are taken into consideration, the laboratory and outdoor tests are in agreement.

3. The light transmission of arbitrary lengths of fiber optic cables was investigated and models are being built with FORTRAN code and TracePro. The effects of interface roughness on light transmission were investigated, a sensitivity analysis of light transmission through a straight optical fiber was performed, and it is shown that the core-cladding interface roughness term is necessary for approximating experimental results. A study of light transmission using results generated from FORTRAN code is also shown.

4. Updates and additions were also made to the TRNSYS model. Chromaticity modeling, correlated color temperature (CCT), and spectral power distribution were studied and are being added to the TRSNSYS system model. Definition and calculation of the color rendering index is also presented.

5. Bioreactor light distribution tests, population and harvesting tests, and model scale tests were performed. There are very encouraging results from the model scale tests in terms of organism growth rates and the final tests necessary to meet our project goals have been started.

6. A bench top lab-scale membrane-based photobioreactor was developed. This system is designed to grow microalgae on a membrane surface. Experiments were described and results presented. An unidentified Nostoc-type species is also characterized.

7. Several manufacturers were investigated for new, lower cost concentrating and tracking components. A lower-cost system, built by Edtek, Inc., was chosen for the Alpha system. An extremely low-cost stamped steel mirror, by Fortec, was purchased and analyzed for use in a beta or gamma system. A small-fiber bundle was optimized for use in the Alpha system, along with a non-imaging device. A simple large-fiber bundle was also built and will be tested soon.

8. A test plan for the experiment proposed to find the non energy benefits of daylight was finalized and is presented. Details of how the experiment will be performed and the location of the experiment are discussed.

9. A solar energy lab at UNR was acquired for use as the Alpha system test facility. A large platform was built to mount the Alpha system and High-Lumen test system adjacent to

the lab. The team is now designing the data acquisition system in order to monitor the light transmission, thermal management of the fibers, luminaire power consumption, and power consumption of the two different tracking systems.

DISTRIBUTION

- NETL AAD Document Control
- Frank "Tex" Wilkins, DOE
- Lew Pratsch, DOE
- Joel S. Chaddock, NETL
- Bonnie Dowdell, NETL
- David J. Bayless, Ohio University
- William Beckman, University of Wisconsin, Madison
- Clinton Berry, TN Dept. of Economic & Community Dev. Energy Division
- Joel L. Cuello, University of Arizona
- Roger Davenport, Science Applications International Corporation
- David R. Dinse, TVA Public Power Institute
- Dan Dye, University of Nevada, Reno
- Lewis Fraas, JX Crystals Inc
- Jason B. Keyes, JX Crystals Inc.
- Sandy Klein, University of Wisconsin
- Dave McNeil, Nevada Energy Office
- Jeff Muhs, Oak Ridge National Laboratory
- Nadarajah Narendran, Rensselaer Polytechnic Institute (RPI)
- Jennifer Sahlin, 3M
- Ramesh Raghavan, RPI
- Robert Schnell, Honeywell Laboratories
- Robin W. Taylor, Science Applications International Corporation

APPENDIX A

HIGH LUMENS SCREENING TEST SETUP FOR OPTICAL FIBER USED IN HYBRID SOLAR LIGHTING SYSTEM

Jeanette Kretschmer
University of Nevada, Reno
Mechanical Engineering
Mail Stop 312
Reno, NV 89557
PH: (775) 784-6735
FAX: (775) 784-1701
jkretsch@unr.edu

ABSTRACT

A research team led by Oak Ridge National Laboratory has designed a Hybrid Solar Lighting System for transporting daylight to building interiors via optical fibers [3]. Light carrying capacity, flexibility, and cost are important design factors for choosing an appropriate fiber, and these factors have pointed to the use of large-core plastic fibers. For the hybrid approach to be practical, the fibers must perform well for approximately 10 years, thus long-term transmission data is needed.

This paper describes the design and analysis of two experimental apparatuses. One of these two has been chosen to evaluate the long-term optical performance of three different brands of large core fiber as a screening test for the Hybrid Lighting System. The test setup must supply a specified amount of lumens, protect the fiber from heat, and allow for periodic degradation measurements to be taken easily. This is a comparison and screening test only.

INTRODUCTION

The experiment objective is to compare the transmission and attenuation of three different types of optical fibers when exposed to concentrated sunlight for a period of several months. The data will be used to recommend a fiber for use in the Hybrid Solar Lighting System. The Hybrid Solar Lighting System calls for each fiber to carry approximately 8,000 lumens, therefore the selected testing apparatus must be capable of supplying a minimum of 8,000 lumens to each fiber. Each fiber must be adequately protected from infrared (IR) wavelengths to remain below its respective maximum rated operating temperature. The selected fiber brands to be tested are: 3M, Poly Optic and Lumenyte.

In this paper, a test plan is presented that meets the project requirements. The design of the two test systems is shown as well as the performance results for one of the configurations. Test preparation steps required regardless of the apparatus are also discussed, such as investigation of the quartz and the polishing method exercised on the optical fibers.

NOMENCLATURE

n_0 refractive index of air
n_1 refractive index of fiber core
R Fraction of incident light lost due to Fresnel reflection

METHOD

Test Plan

A 10 meter length of fiber will be placed in the testing apparatus and exposed to concentrated sunlight for three months or until steady state is reached. Test data will include fiber temperature at various distances from the entrance surface, overall lumen output and spectral transmission in the 250nm to 900nm range. At the end of the test the cutback method will be used and again both overall lumen output and spectral transmission will be measured at each length. In order to generate a useful transmission graph, it is recommended that transmission be measured at 2nm to 5nm wavelength intervals [2]. The transmission data will be taken for each length of fiber and written to an Excel sheet for post processing.

The 10 meter length was chosen because that is the length used in the Hybrid Solar Lighting System and because it should be a long enough segment to offer an opportunity to monitor color shift. One of the benefits of daylighting is that white light is supplied instead of the lower color temperatures supplied by most artificial lights, thus color shift needs to be monitored to ensure that a possible benefit is not being lost. The cutback method will be used at the end of each test because it has been adopted as the standard approach for measuring attenuation in optical fibers [2].

Instrumentation

Transmission at various wavelengths is measured using a spectroradiometer by StellarNet Inc. Overall lumen output is measured using a four inch integrating sphere and a hand-held spectrometer by Labsphere, as illustrated in Fig.1. The photopic curve is the commonly accepted definition of the wavelengths the average human eye responds to. The lumen is a measurement of wavelengths in the visible region, weighted by the photopic curve, so a good way to measure overall transmission is the number of lumens at various distances down an optical fiber [2].

Figure 1. Spectrometer and integrating sphere

A Cogent high intensity discharge light with voltage regulator will be the light source used for testing after the fiber has been removed from the testing apparatus. This source will be allowed 10 minutes warm up time to stabilize.

Test Apparatus #1

The first of the two test apparatuses is shown in Fig. 2 and includes a 35 inch diameter Fresnel lens, a supporting truss, a hot mirror, an IR cutoff filter, and a quartz rod to protect the fiber from heat. The entire system mounts to a solar tracking device.

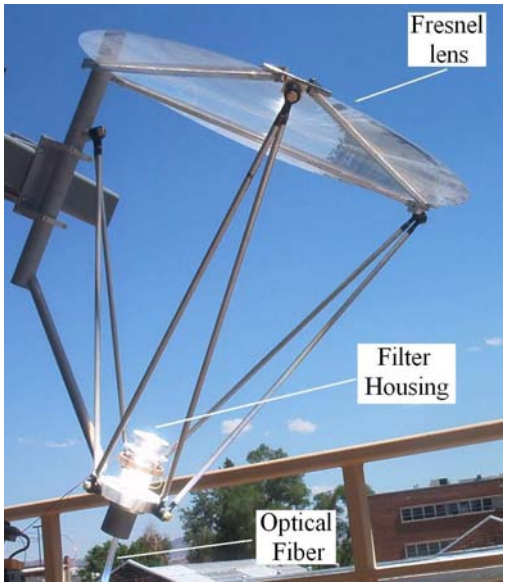

Figure 2. Fresnel Testing Apparatus

Theoretical Performance

The theoretical plausibility of this test setup was verified using a simple TracePro model and Microsoft Excel. TracePro is an optical modeling program that allows the user to draw three dimensional objects and then apply optical properties. The Tracepro model includes an ASTM standard solar source for air mass 1.5, a hot mirror, an infrared (IR) filter, a quartz rod and the initial surface of the optical fiber. TracePro traced the rays and then created a flux report. The number of watts striking the entrance surface of the fiber in the visible region were summed up in Excel, and then that number was multiplied by 200 lumens/watt which is the standard number for filtered sunlight. By this method, the theoretical number of lumens available is substantially more than the 8,000 lumen minimum, as displayed in Table 1.

Surface	Incident Watts	Lumens
Fresnel	546.80	109,360.66
Hot Mirror	212.72	42,544.69
IR Filter	176.70	35,340.05
Quartz Rod	122.98	24,595.22
Fiber Entrance	118.06	23,611.41

Table 1.Theoretical lumens

Actual Perfromance

The Fresnel testing apparatus was set up with a piece of quartz (no fiber attached) and several lumen readings were taken on different clear days. These readings indicated that the Fresnel system was only able to consistently supply approximately 6,000 lumens to the exit surface of the quartz, which would be the entrance of the fiber. The major difference in the theoretical and actual results is believed to come from imperfections in the Fresnel lens. This is a relatively cheap, low quality piece of plastic and the large diameter and harsh outdoor environment leaves much room for defects in the lens, scratches, dirt etc. There is also a small amount of blockage (shown in Fig.2) caused by the assembly holding the lens that was not accounted for in the model.

Test Apparatus #2

The second test apparatus, shown in Fig. 3, utilizes a parabolic mirror rather than a Fresnel lens. Instead of testing one fiber per system, four fibers are placed in a bundle. A cold mirror, IR cutoff filter and quartz rod are still used to control the temperature at the fiber entrance, but one rectangular piece of quartz is used rather than individual cylindrical pieces. This quartz rod doubles as a non-imaging device to help ensure that all the fibers are illuminated evenly.

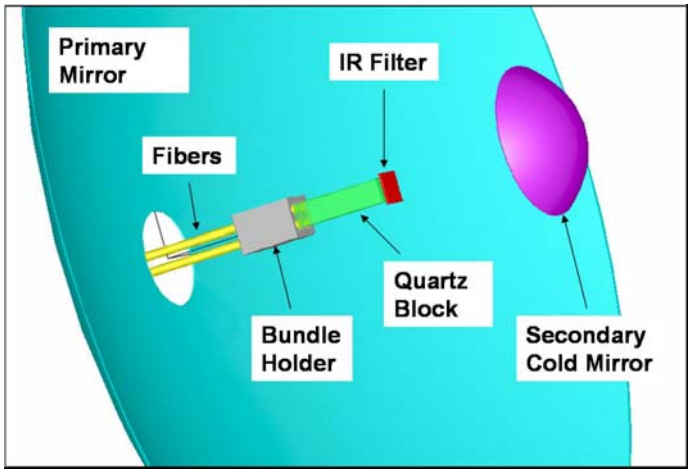

Figure 3. Test Apparatus #2

A model of test apparatus #2 was created in TracePro and the theoretical results, shown in Table 2, are very encouraging. This system is still in the construction stage and performance data is not yet available. However, unlike the Fresnel test setup, it is expected that the model of the second apparatus will better represent the experimental setup due to higher quality optical components, especially the primary and secondary mirrors.

Surface	Incident Watts	Lumens
Primary Mirror	846.77	169,353.68
Secondary Mirror	820.62	164,123.02
IR Filter	550.24	110,048.61
Quartz Exit	524.33	104,866.58
Fiber #1 Entrance	50.89	10,178.00
Fiber #2 Entrance	50.47	10,094.00
Fiber # 3 Entrance	50.12	10,024.00
Fiber # 4 Entrance	50.76	10,152.00

Table 2. Theoretical lumens

EXPERIMENT COMPONENTS AND TEST PREPARATION

Change in temperature from entrance surface to exit surface of quartz rod

Heat is an obvious problem when using plastic fibers to transport solar light. To combat this problem, a hot mirror and IR filter are used to cut out the near IR, and a quartz rod is used to help cut out the longer IR wavelengths. The length of the quartz rod used in the final testing will depend on the actual available energy from the chosen testing apparatus. However, a small experiment was performed to gain an understanding of the temperature difference between the entrance and exit surfaces of quartz rods of different lengths. Figure 4 summarizes the results of this experiment normalized by the entrance temperature. A higher normalized temperature value corresponds to a greater temperature drop along the length of the quartz. As shown, the trend is that the difference between the entrance and exit temperatures is greater with longer quartz.

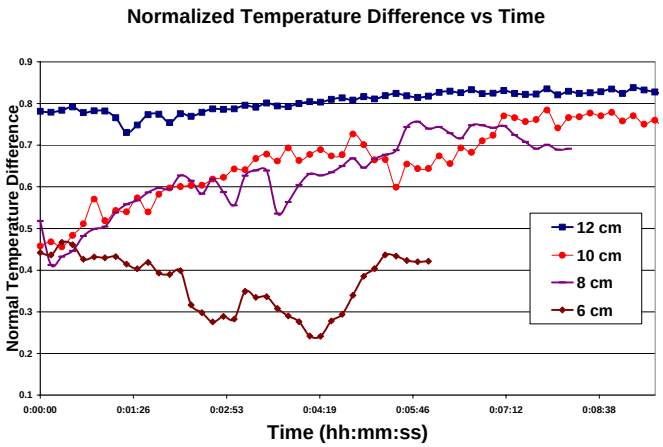

Figure 4. Graph of normalized temperature difference between entrance and exit surface of quartz rod.

Lumen loss in fused quartz rod

Since the length of the quartz rod is inversely proportional to the temperature at the entrance of the fiber, it is important to know the effect the quartz has on light transmission. An experiment was performed to measure the lumens lost in various lengths of the fused quartz rod. The rods were connected to a Cogent light source as shown in Fig. 5.

Figure 5. Cogent light/ quartz setup.

Two trials were performed and the results are shown below in Table 3. As shown in Table 3, there is so little visible light lost through the quartz that it is difficult to even accurately measure. Variations in measurements could be due to the quartz being placed at slightly different distances from the light source or at slightly different depths into the integrating sphere.

Quartz Test Using Cogent Light Source 12-8-03		
Quartz Length (cm)	Trial 1 Lumens	Trial 2 Lumens
4	80	80.3
6	81.8	80.3
8	80.5	79.9
10	80.9	80.3
12	80.3	80.3

Table 3. Lumen loss through fused quartz rod.

Fresnel Reflection and Bonding

Fresnel reflection occurs at the surface of the fiber. Some light that strikes the surface of the fiber is reflected even when the incidence angel is within the numerical aperture of the fiber. This is caused by a change in the index of refraction as light travels from air to the fiber. When two fibers or a piece of fused quartz and fiber are joined together, they are sometimes separated by a small air gap, causing Fresnel reflection to occur twice in each junction [1]. The formula below (taken from [1]) calculates the

fraction of incident light that is reflected, where n_1 is the refractive index of the fiber core and n_0 is the refractive index of the separating medium (air).

$$R = \left(\frac{n_1 - n_0}{n_1 + n_0} \right)^2 \qquad (1)$$

Using a fiber core refractive index of n_1= 1.498 and assuming air to have a refractive index of n_0 = 1.0, the Fresnel reflection between air and the fiber is about 4%. The refractive index of the quartz is similar to that of the fiber, so the junction causes a loss of roughly 8%.

To help reduce the losses caused by this junction, the quartz and fiber were fused together. A device was constructed that holds the fiber and quartz in alignment and then presses them together (see Fig. 6). The device was then placed in the Fresnel testing apparatus and the available heat fused the two together. A small experiment was performed to test the bond between the quartz rod and the fiber. The holding device was set up and the quartz and fiber were pressed together but not bonded. The quartz was then connected to the cogent light source and the lumen output was measured to be 2780 lumens. The quartz and fiber were then placed in the Fresnel testing setup and given enough time to bond. After bonding the reading was 2900 lumens, an increase of about 4%.

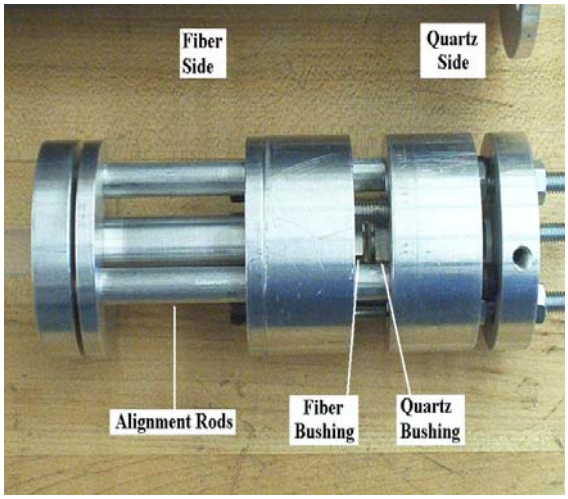

Figure 6. Holding device for fusing quartz rod and plastic fiber.

Fiber Polisher

All fibers used in the testing are polished using the same equipment and sequence. The fiber polisher, shown in Fig. 7, consists of a threaded tube just large enough in diameter for the fiber to fit though. The fiber is clamped in place at the bottom where a plastic collar protects the fiber from being damaged while clamped. Fine threads on the tube allow for small vertical adjustment of the fiber. The polisher has variable disc speed and eccentricity.


Figure 7. Fiber polisher

The polishing sequence begins with cutting the fiber using a PVC cutter. Then a coarse sandpaper is used to create a square end on the fiber. This step is

followed by a finer sandpaper and then by a sequence of 3M polishing pads, which have 30, 15, 9, 3 micron finishes. They are used in that order and everything is kept irrigated by a pressurized water tank. This procedure consistently produces a high-quality polish on the fibers.

CONCLUSIONS

The Fresnel lens test setup supplies enough concentrated light for much of the necessary preliminary testing, but does not consistently supply 8,000 lumens to the fiber. As 8,000 lumens was one of the experiment requirements, this setup will not be used for the actual testing. Instead, the parabolic mirror and fiber bundle approach will be used. This method also saves space and money since all three fiber types can be tested at once using the same mirror.

REFERENCES

[1] Integrated Publishing, Updated Nov 2003, "Reflection Losses," http://www.tpub.com/neets/tm/108-2.htm

[2] Poppendieck, M.P.,1998, "Test Methods for Optical Fiber," Proceedings of SPIE Conference on Illumination and Source Engineering, Vol. 3428, pp 90-97.

[3] Wood, B.D., and Muhs, J., 2002, "Adaptive Full-spectrum Solar Energy Systems", NETL Report # 41164R02

APPENDIX B

DEMONSTRATION OF THERMOPHOTOVOLTAICS FOR A FULL-SPECTRUM SOLAR ENERGY SYSTEM

(Submitted to the ASES 2004 Solar Conference)

Dan Dye*, University of Nevada, Reno
Mailing Address:
Mechanical Engineering
Mail Stop 312
University of Nevada, Reno
Reno, NV 89557
PH: (775) 784-6735
FAX: (775) 784-1701
Email: dye@unr.edu
***corresponding author**

Byard Wood, Utah State University
Mailing Address:
Mechanical and Aerospace Engineering
Utah State University
Logan, UT 84322-4130
PH: (435) 797-2866
FAX: (435) 797-2417
Email: byard.wood@usu.edu

Lewis Fraas, JX Crystals, Inc.
Mailing Address:
1105 12th Avenue NW, suite A2
Issaquah, WA 98027
PH: (425) 392-5237
FAX: (425) 392-7303
Email: lfraas@jxcrystals.com

Jeanette Kretschmer, University of Nevada, Reno
Mailing Address:
Mechanical Engineering
Mail Stop 312
University of Nevada, Reno
Reno, NV 89557
PH: (775) 784-6735
FAX: (775) 784-1701
Email: jkretsch@unr.edu

Keywords: thermophotovoltaic; infrared; full-spectrum

ABSTRACT

A non-imaging (NI) device and thermophotovoltaic (TPV) array for use in a full-spectrum solar energy system has been designed, built, and tested [1,2,3]. This system was designed to utilize the otherwise wasted infrared (IR) energy that is separated from the visible portion of the solar spectrum before the visible light is harvested. The IR energy will be converted to electricity via a gallium antimonide (GaSb) TPV array. The experimental apparatus for the testing of the IR optics and TPV performance is described. Array performance data will be presented, along with a comparison between outdoor experimental tests and laboratory flash tests. An analysis of the flow of the infrared energy through the collection system will be presented, and recommendations will be made for improvements. The TPV array generated a maximum of 26.7 W, demonstrating a conversion efficiency of the IR energy of 12%.

INTRODUCTION

A solar concentrating system that concentrates visible daylight into fiber optic cables was built at Oak Ridge National Laboratory (ORNL) [4,5,6]. This system, referred to as the benchmark system, has demonstrated effective collection and distribution of the visible portion of the solar spectrum, but has thus far been filtering out and wasting the IR spectrum to keep it from burning the fiber optics. The IR spectrum is passed through the secondary mirror, while the visible light is reflected into the fiber optics. The concept is to use the IR spectrum to generate electricity via a GaSb TPV array making the system a full-spectrum solar energy system. Fig. 1 shows the concept of the full-spectrum system.

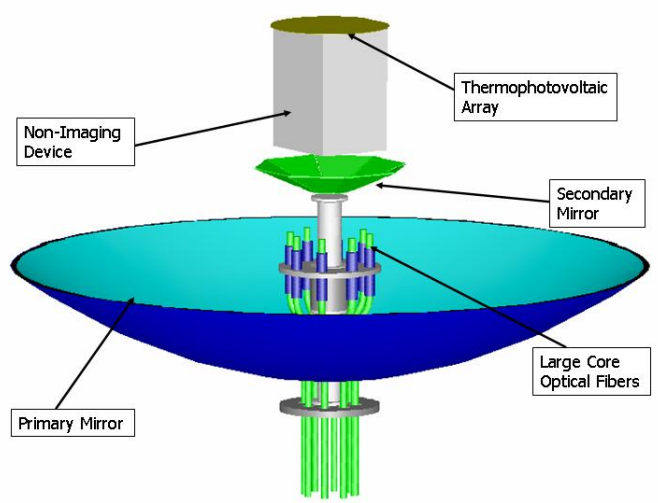

Figure 1: Full-spectrum solar collector

The goal of this research was to demonstrate that the otherwise wasted IR portion of the solar spectrum could be converted into electricity, without reducing the performance of the visible light collection system. Using this approach, the total system performance is increased since more of the incident irradiance is converted into a useful product, be it daylight or electricity.

This paper describes tests performed at the University of Nevada, Reno (UNR) to determine the performance of the TPV array under concentrated conditions. The design of the secondary optics, the experimental setup, and performance results and conclusions will be presented. An energy flow analysis is presented that shows the losses through the individual optical components.

EXPERIMENTAL SETUP

The experimental apparatus consists of a solar tracking and concentrating system, a TPV array, and a cooling circuit. The system was designed to perform similarly to the ORNL benchmark system, but to test the performance of the TPV array only. However, the system was also designed such that the IR optics could be integrated into the ORNL system without degrading its performance. Essentially, the IR optics and TPV array are located at the antenna of the primary mirror and fit in the shadow of the secondary mirror, as shown in Fig. 2.

Figure 2: IR-TPV Test System

The system consists of the following components:

- Dual-axis solar tracking system
- 46” diameter aluminum primary mirror
- Spectrally-selective cold mirror
- 96% reflective aluminum front-side mirrors inside non-imaging device
- Liquid cooling system to cool the TPV array during testing
- GaSb TPV array
- Instrumentation to measure:
  - Direct normal irradiance
  - Temperature
  - Voltage
  - Current

The solar collector shown in Fig. 2 uses a 46” diameter paraboloidal mirror to concentrate the solar irradiance. A secondary mirror using Navitar Coating’s High Efficiency Cold Mirror (HECM) coating redirects the visible light and transmits the IR energy, and a NI device distributes the flux over the TPV array. The design of the NI device is important because it must uniformly distribute the flux over the surface of the TPV array [7,8]. A side-view of the TPV array mounted at the end of the NI tube is shown in Fig. 3. Fig. 4 shows the NI tube, cooling supply and return lines, and cold mirror.

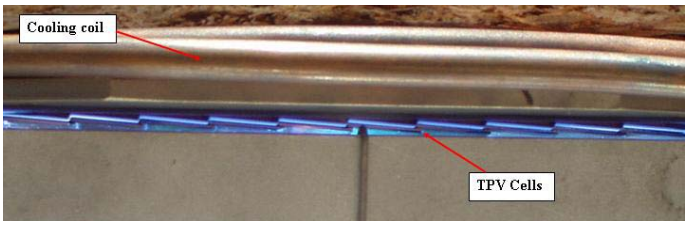

Figure 3: TPV Array Inside NI Tube

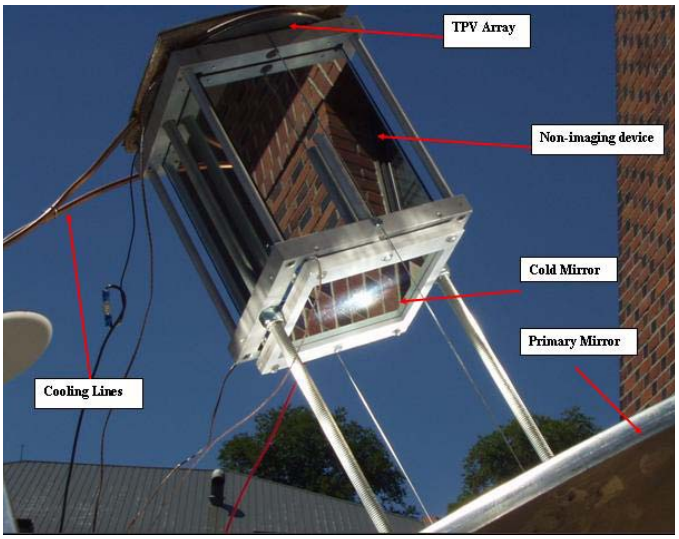

Figure 4: NI Device

The TPV array, shown in Fig. 5, is comprised of 100 GaSb cells that are responsive from $0.7 < \lambda < 1.8$ µm. The active area of the array is approximately 180 cm^2. The cells are wired in series; therefore the array requires uniform irradiation in order to generate its maximum power, thus requiring the use of the NI device.

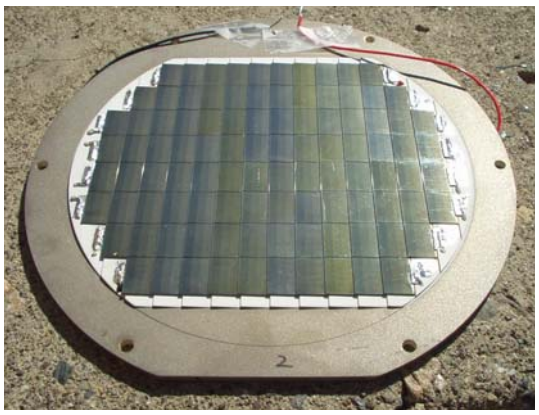
Figure 5: 100 Cell GaSb TPV Array

The cooler the array is operated, the more efficiently the cells will perform. Using a 50/50 mixture of ethylene glycol and water, the chiller and cooling system was able to keep the TPV array between 31° C and 36° C throughout the day, when ambient temperatures were between 28° C and 35.5° C during the tests. A copper cooling coil was pressed against the backing plate of the TPV array, using a thermally conductive paste to assist in the heat transfer. This combination was able to cool off the array enough to perform the tests. Without the cooling circuit, tests showed temperatures at the TPV plane above 160° C, far in excess of the melting point of the solder used in the array.

Voltage and current were measured with Fluke hand-held multimeters, the temperature and direct normal irradiance was recorded using a Fluke Hydra Data Bucket, and an Eppley Labs Normal Incidence Pyrheliometer (NIP) Radiometer was used to measure the irradiance. After tests the data was analyzed in Excel and MathCad.

RESULTS

Tests were performed three times during the day of September 26th, and both current and voltage data were measured. A plot of current versus voltage for the test that generated the highest power is shown in Fig. 6. A plot of power versus voltage from the same data set is shown in Fig. 7. The other two tests produced very similar results; the maximum power was only a few percent less.

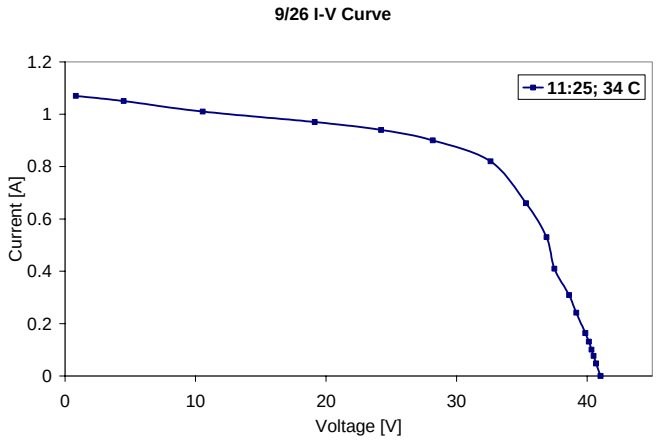

Figure 6: I-V Curve

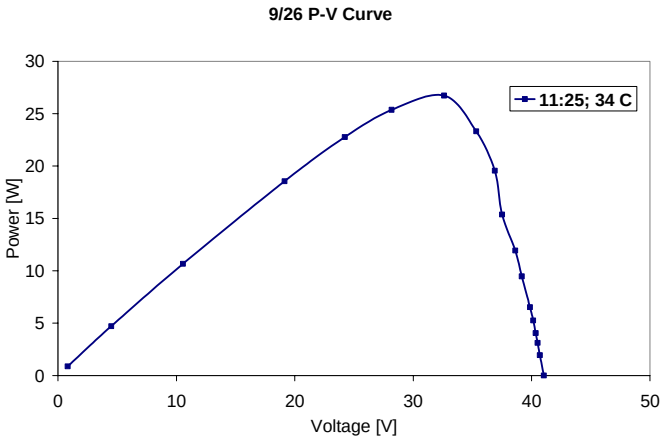

Figure 7: P-V Curve

In the original flash tests of the TPV array performed at JX Crystals, the temperature was 25° C and the array produced 177 W, with V_{oc} = 47.7 V and I_{sc} = 5.7A. This is shown in Table 1. Under the outdoor test conditions in Reno, the array temperature was 34° C, the array generated 26.7 W, with V_{oc} = 41.03 V and I_{sc} = 1.07 A.

The drop in V_{oc} can be explained by the fact that the cell voltage drops approximately 1.7 mV/C per cell, and because of the lower flux density than in the flash tests. The voltage drop due to the higher temperature of the UNR tests corresponds to a drop of 1.5 V. The voltage drop due to the lower flux density of the UNR tests corresponds to a drop of an additional 4 V. This would predict V_{oc} = 42.2 V, which is only 3% higher than the V_{oc} obtained experimentally. The difference in performance between the indoor flash tests and outdoor tests could also be due to thermal gradients across the TPV array surface caused by non-uniformity of the flux, as well as reflective losses due to a portion of the rays striking the surface at high incident angles.

Table 1: GaSb TPV Array Test Results

	UNR	JX Crystals
Isc	1.07 A	5.7 A
Voc	41.03 V	47.72 V
Imax	0.82 A	5.13 A
Vmax	32.6 V	34.52 V
Pmax	26.73 W	177.16 W
Approximate Incident IR	227 W	1,250 W
Efficiency	12%	14%
Temp Condition:	34° C Outdoor Test	25° C Indoor Flash Test

The data from the NIP was used to estimate the IR irradiance. The total direct normal irradiance measured by the NIP was multiplied by 53% to estimate the portion in the range from 0.7 to 1.8 μm. This approximation comes from the ASTM Standard for Air Mass 1.5, where the energy in this range is 53% of the total energy available. Using this source and known spectral properties of the mirrors and filters, the flow of the IR energy is estimated.

This energy flow is given in Fig. 8. In this chart, it is obvious that there is room for improvement in the collection system. The most obvious flaw is the transmission percentage through the secondary mirror. The cold mirror coating, in the range $0.7 < \lambda < 1.8$ μm, transmits 61% of the IR energy concentrated by the primary mirror. This could be improved upon by choosing a different coating, but the coating is highly reflective in the visible spectrum which is the most desirable for the visible optics. Other coatings could be tested for higher transmittance in this region, as long as they didn't decrease the reflected visible light. There are also losses inside the NI tube and on the TPV surface due to flux uniformity, but this system has been optimized to give the best balance between uniformity and transmittance. It would be possible to transmit more IR energy to the TPV array, but if it is non-uniform, the extra energy would be wasted.

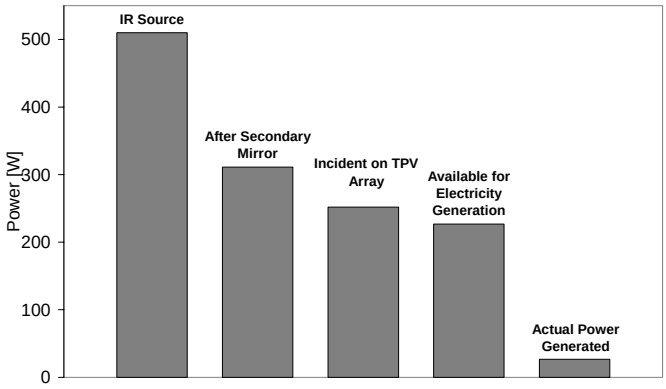

Figure 8: Energy Flow Chart

CONCLUSIONS AND RECOMMENDATIONS

A system that can utilize otherwise wasted IR energy in the visible benchmark collector has been demonstrated. This system uses a TPV array to convert the wasted IR energy into electricity, but since it fits in the shadow of

the secondary mirror, it will not hamper the performance of the visible daylight collection system. The extra power, 27 W in this case, serves to increase the overall efficiency of the full-spectrum collector/receiver system.

Without the losses through the secondary mirror and NI device, the TPV array would have the potential to generate more than twice as much power. However, this IR energy system, in combination with the visible lighting system, can better utilize the solar spectrum than standard day-lighting systems or photovoltaic cells alone. While the system is not designed for optimum performance in the IR spectrum, 27 W is more than enough power to charge the batteries to run the solar tracking system. If the TPV array can charge the batteries for the tracker without requiring additional PV arrays or power lines ran up to the roof, then it could be very advantageous in the implementation of this unique approach to solar energy.

Future work on this project should focus on better transmitting cold mirror coatings. Also, passive cooling systems should need to be investigated to reduce the parasitic losses from the active cooling system.

ACKNOWLEDGEMENTS

This project is funded in part by:
Cooperative Agreement
DE-FC26-01NT41164

Thanks are due to the Energy Systems Laboratory at the University of Nevada, Reno, Oak Ridge National Laboratory and all team members involved in this project.

REFERENCES

[1] Dye, D., Wood, B.D., Fraas, L.M., and Muhs, J., 2003, "Optical Design of an Infrared Non-Imaging Device for a Full-Spectrum Solar Energy System," Proceedings of the ASME International Solar Energy Society Conference, Hawaii

[2] Dye, D., and Wood, B.D., 2003, "Infrared Transmission Efficiency of Refractive and Reflective Non-Imaging Devices for a Full-Spectrum Solar Energy System," Nonimaging Optics: Maximum Efficiency Light Transfer VII, Proceedings of SPIE

[3] Fraas, L.M., Daniels, W.E., and Muhs, J., 2001, "Infrared Photovoltaics for Combined Solar Lighting and Electricity for Buildings," Proceedings of 17th European Photovoltaic Solar Energy Conference

[4] Muhs, J., 2000, "Design and Analysis of Hybrid Solar Lighting and Full-Spectrum Solar Energy Systems," American Solar Energy Society, SOLAR 2000

[5] Muhs, J., 2000, "Hybrid Solar Lighting Doubles the Efficiency and Affordability of Solar Energy in Commercial Buildings," CADDET Energy Efficiency Newsletter, No. 4, pp. 6-9

[6] Wood, B.D., and Muhs J., 2002, "Adaptive Full-Spectrum Solar Energy Systems", NETL Report # 41164R02

[7] Dye, D., and Wood, B.D., 2003, "Non-Imaging Devices for Uniform Irradiance on Planar Surfaces for Parabolic Concentrators," Proceedings of ASES, SOLAR 2003

[8] O'Gallagher, J.J., Winston, R., and Gee, R., 2001, "NonImaging Solar Concentrator with Near Uniform Irradiance for Photovoltaic Arrays," Nonimaging Optics: Maximum Efficiency Light Transfer VI, Proceedings of SPIE Vol. 4446

APPENDIX C

COST COMPARISONS FOR HYBRID SOLAR LIGHTING SYSTEMS

Comparison of Hybrid Lighting Prototype Costs

	Benchmark	Alpha	Beta
Primary Mirror	$ 5,072	$ 3,500	$ 250
Secondary Mirror	$ 2,251	$ 2,251	$ 2,251
Tracking Mechanism	$ 11,400	$ 11,450	$ 2,450
Fiber Optics Holder	$ 3,720	$ 3,720	$ 3,720
Fiber Assembly	$ 7,540	$ 7,540	$ 7,540
System Total	$ 29,983	$ 28,461	$ 16,211

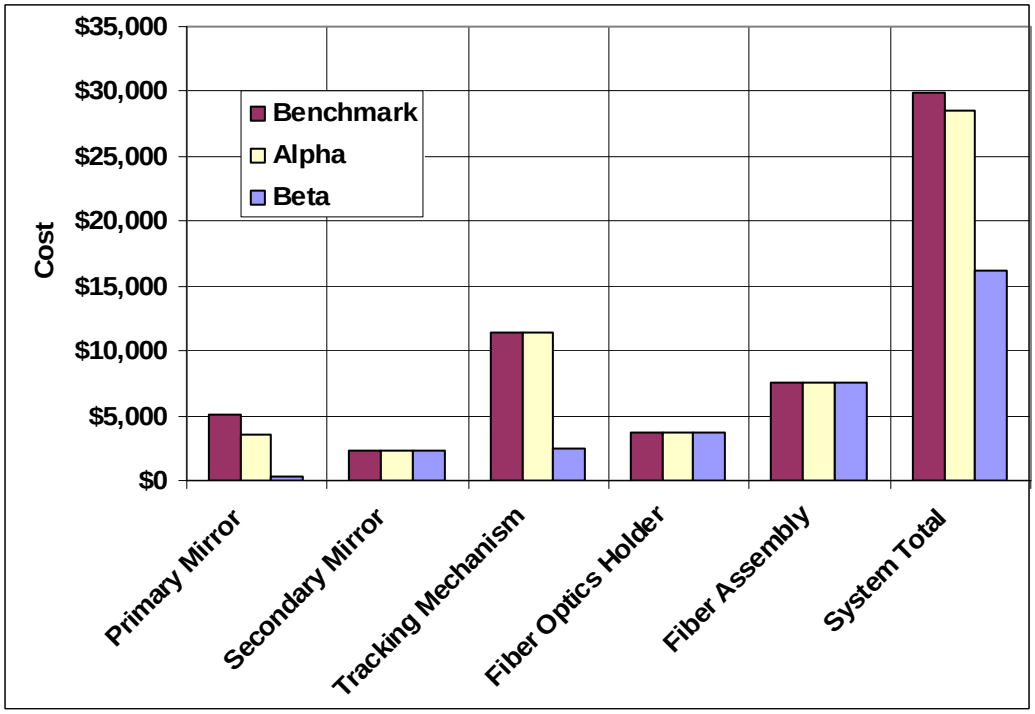

Cost Estimate -- Benchmark Hybrid Lighting System

Subsystem

	Component	Subsystem Cost	Component Cost	Source
Primary Mirror		**$ 5,072**		
	Mirror		$ 2,400	ROC Glassworks
	Mirror Mount		$ 2,672	Various
Secondary Mirror		**$ 2,251**		
	Mirror Segments		$ 360	S&S Optical
	Mirror coatings		$ 625	Navitar
	Mirror Mount		$ 1,266	Various
Tracking Mechanism		**$ 11,400**		
	Tracker Mechanism		$ 2,295	Array Tech
	Tracker Controls		$ 1,655	Enhancement Electronics
	PV Cells and Battery		$ 500	Enhancement Electronics
	Mounting Post		$ 300	Dixie Roofing
	Conduit		$ 150	Edmundson Electric
	Roofing Installation		$ 6,500	Dixie Roofing
Fiber Optics Holder		**$ 3,720**		
	Quartz Rods		$ 150	Internal
	Hot Mirrors		$ 200	Andover Corp
	Support Mechanism		$ 3,370	Various
Fiber Assembly		**$ 7,540**		
	Bellows		$ 160	MMC
	Mounting Parts		$ 4,580	Various
	Optical Fiber		$ 2,800	3M

System Total	**$ 29,983**

Source: Performance Summary, Benchmark Prototype System, 6/15/03

Cost Estimate -- Hybrid Lighting System using Ed-Tek Concentrator

Subsystem

	Component	Subsystem Cost	Component Cost	Source
Primary Mirror		**$ 3,500**		
	Mirror		$ 3,500	EdTek
Secondary Mirror		**$ 2,251**		
	Mirror Segments		$ 360	S&S Optical
	Mirror coatings		$ 625	Navitar
	Mirror Mount		$ 1,266	Various
Tracking Mechanism		**$ 11,450**		
	Tracker & Controls		$ 4,000	Ed-Tek
	PV Cells and Battery		$ 500	Enhancement Electronics
	Mounting Post		$ 300	Dixie Roofing
	Conduit		$ 150	Edmundson Electric
	Roofing Installation		$ 6,500	Dixie Roofing
Fiber Optics Holder		**$ 3,720**		
	Quartz Rods		$ 150	Internal
	Hot Mirrors		$ 200	Andover Corp
	Support Mechanism		$ 3,370	Various
Fiber Assembly		**$ 7,540**		
	Bellows		$ 160	MMC
	Mounting Parts		$ 4,580	Various
	Optical Fiber		$ 2,800	3M

System Total	**$ 28,461**

Sources: Performance Summary, Benchmark Prototype System, 6/15/03
Ed-Tek quotes for single systems

Cost Estimate -- Hybrid Lighting System using Satellite Dish

Subsystem	Component	Subsystem Cost	Component Cost	Source
Primary Mirror		**$ 250**		
	Substrate		$ 100	Fortec
	Reflective Film		$ 50	Reflectech
	Reflector Install Labor		$ 100	SAIC
Secondary Mirror		**$ 2,251**		
	Mirror Segments		$ 360	S&S Optical
	Mirror coatings		$ 625	Navitar
	Mirror Mount		$ 1,266	Various
Tracking Mechanism		**$ 2,450**		
	Tracker Mechanism		$ 500	SAIC
	Tracker Controls		$ 1,000	SAIC
	PV Cells and Battery		$ 500	Various
	Mounting Hardware		$ 300	Various
	Conduit		$ 150	Edmundson Electric
Fiber Optics Holder		**$ 3,720**		
	Quartz Rods		$ 150	Internal
	Hot Mirrors		$ 200	Andover Corp
	Support Mechanism		$ 3,370	Various
Fiber Assembly		**$ 7,540**		
	Bellows		$ 160	MMC
	Mounting Parts		$ 4,580	Various
	Optical Fiber		$ 2,800	3M

System Total	**$ 16,211**

Sources: Performance Summary, Benchmark Prototype System, 6/15/03
SAIC estimates for controls/tracker mech.
Fortec & Reflectech purchase prices
Based on non-structural roof mount

Cost Estimate -- Hybrid Lighting System

Assumptions:

System uses weighted tray/bar system for non-penetration roof mount
6' Pressed-steel dish
SAIC dish controller system with self-calibration
Azimuth turntable/elevation jackscrew
Self-powered with battery backup
Cost-reduced fiber mount & secondary mirror designs

System Total Cost $ 12,857

Subsystem

Component	Qty	Unit	Unit Cost	Total Cost	Source
Primary Mirror				**$ 307**	
Mirror substrate and mount, with shipping	1	ea	$ 100	$ 100	Fortec 1.8m dish
Reflective film	30	sq.ft	$ 3	$ 90	Reflectech
Reflector install labor	3	hr	$ 30	$ 90	SAIC
2"x2"x1/4"x10' square steel tube	2	ea	$ 14	$ 27	American Metals
				$ -	
Secondary Mirror/PV Array				**$ 1,685**	
Mirror segments	1	set	$ 360	$ 360	S&S Optical
Mirror coatings	1	lot	$ 625	$ 625	Navitar
Mirror mount	1	ea	$ 200	$ 200	Estimated
PV cell array, 50 Watt output	50	W	$ 10	$ 500	JX Crystals, $10/W
				$ -	
Tracker/Controls				**$ 1,077**	
Controller, microprocessor	1	ea	$ 100	$ 100	Zworld Rabbit
Interface board (similar to Disney)	1	ea	$ 200	$ 200	SAIC
Wiring & sensors (limits, tilt, DC power)	1	lot	$ 200	$ 200	SAIC
Linear actuator, 600lb, 24"	1	ea	$ 60	$ 60	Rick's Satellite Movers
DC gearmotor, 24VDC, 26RPM, 11 in-lb	1	ea	$ 51	$ 51	MMC 894/6331K34
Spur gear, 32-tooth	1	ea	$ 14	$ 14	MMC 942/7300K16
Gear rack, acetal, 20 deg, 500mmx16mm	2	ea	$ 21	$ 41	MMC 942/7300K12
Gear rack clamps	1	pkg 10	$ 12	$ 12	MMC 942/7300K21
Track roller, flanged, 1"D, 625lb radial, 325lb thrust	6	ea	$ 31	$ 183	MMC 985/6318K17
Battery charge controller	1	ea	$ 100	$ 100	Solar PV
Battery, 12VDC, 17AH, sealed AGM	2	ea	$ 57	$ 115	MMC 763/7448K76
				$ -	
Fiber System				**$ 9,289**	
Fiber mount	1	ea	$ 1,000	$ 1,000	Fabricated, estimate
Hot mirror	1	ea	$ 200	$ 200	Andover Corp
Optical fiber, 8 ea @10m long	80	m	$ 35	$ 2,800	3M
Troffer, Lithonia 4', T8	8	ea	$ 59	$ 472	UNR actual cost
Dimmable Ballast, Advance Mark VII, T8	8	ea	$ 72	$ 572	UNR actual cost
Flourescent Bulb, T8	32	ea	$ 3	$ 85	UNR actual cost
Lumenyte 4' extraction fiber	16	ea	$ 200	$ 3,200	UNR actual cost
Wattstopper LS-201 sensor	8	ea	$ 120	$ 960	UNR actual cost
				$ -	
Installation				**$ 500**	
Hole for fibers	1	ea	$ 200	$ 200	Roofing contractor
Setup labor	6	hr	$ 50	$ 300	Estimated
				$ -	

APPENDIX D

REQUIREMENTS FOR THE HYBRID SOLAR LIGHTING DISH-TRACKER SYSTEM

Table of Contents

Introduction

Hybrid solar lighting (HSL) is a concept whereby visible solar light is concentrated, transmitted through optical fibers, and re-distributed inside a building to provide daylighting to interior spaces. In the same system, the infrared portion of the solar spectrum is separated and focused onto PV cells to produce electricity. In the nominal configuration, a reflective solar dish concentrator approximately 1.5m in diameter is mounted on the roof of a building to concentrate the solar light, and the light is focused onto 12 optical fibers, each fiber feeding one "troffer" lighting fixture inside the building. The solar dish concentrator tracks the sun in order to keep the sunlight focused on the aperture of the optical fibers throughout the day.

This document contains requirements for the dish-tracker subsystem of the hybrid solar lighting system. The requirements may be divided into several types:

- Environmental
- Optical
- Operational
- Mechanical

Environmental requirements relate to the outdoor exposure of the system, and take into account such things as temperature extremes, resistance to weathering, and protection of the system against environmental hazards such as snow and wind loads. Optical requirements relate to the basic requirements of delivering a certain amount of solar light to the aperture of the optical fibers. They affect such things as the reflectance of the mirrors, mirror accuracy, and dish concentrator size. Operational requirements include those related to tracking the sun, power requirements, and interfaces. Mechanical requirements also include the interfaces to the building roof, to the fiber bundle, and other mechanical connections.

Environmental Requirements

The dish-tracker system shall operate normally within the following ranges of environmental conditions.

Temperature Limits

-40C to 50C Ambient temperature during operation

Altitude

0 to 5000m Altitude

Relative Humidity

0 to 100% Relative humidity, including condensing conditions

Wind

50 mph Maximum wind speed for normal operation

120 mph Maximum survival wind speed

Rain/Snow

All components shall be protected from rain and snow, including blowing rain and snow. NEMA 4 or IP65 protection of all exposed electrical components is required.

Dust

All electronics and mechanical components shall be protected from blowing dust and sand.

Insolation

1100 W/sq.m Maximum direct-normal solar insolation

All components shall be designed for, or protected from, exposure to concentrated solar radiation and solar UV radiation.

Service Life

The system shall be designed for a normal service life of 20 years. Within that service life, degradation of performance of 20% shall be deemed acceptable.

Optical Requirements

The basic purpose of the dish-tracker system is to deliver a certain amount of light energy to the optical fiber bundle (and PV array). The following requirements are based on a nominal system feeding 12 fibers, each 12mm in diameter and capable of accepting a maximum of 8000 Lumens of light, or approximately the visible portion from 80W of incident sunlight under bright-sun conditions. This requirement translates into a requirement to deliver 960W of solar power to an aperture approximately 40mm in diameter, or an average solar flux of 764 kW/sq.m (about 750 "suns").

The illumination requirement does not specifically limit the size or required accuracy of the dish concentrator. Instead, it defines a combination of size and accuracy needed to deliver the desired energy to the fibers. A larger dish, with lower accuracy, can provide the same amount of light (albeit with more spillage) as can a smaller, more-accurate dish. The following figure illustrates the relationship between dish size and the required accuracy to provide 1500W of solar power to a 50mm (2") diameter target (e.g., ~750 suns). As shown, a dish of 1.5m diameter can have no more than 4mrad of RMS surface error to supply this power, but a dish of 2.0m diameter can have as much as 9mrad of slope error to achieve the same result. Another consideration in this comparison is that the focal spot size increases with the size of the dish, so a smaller dish needs to be tracked more accurately to keep its spot on the aperture of the fibers. A larger, less-accurate dish requires a less-accurate tracking system in order to meet the requirement.

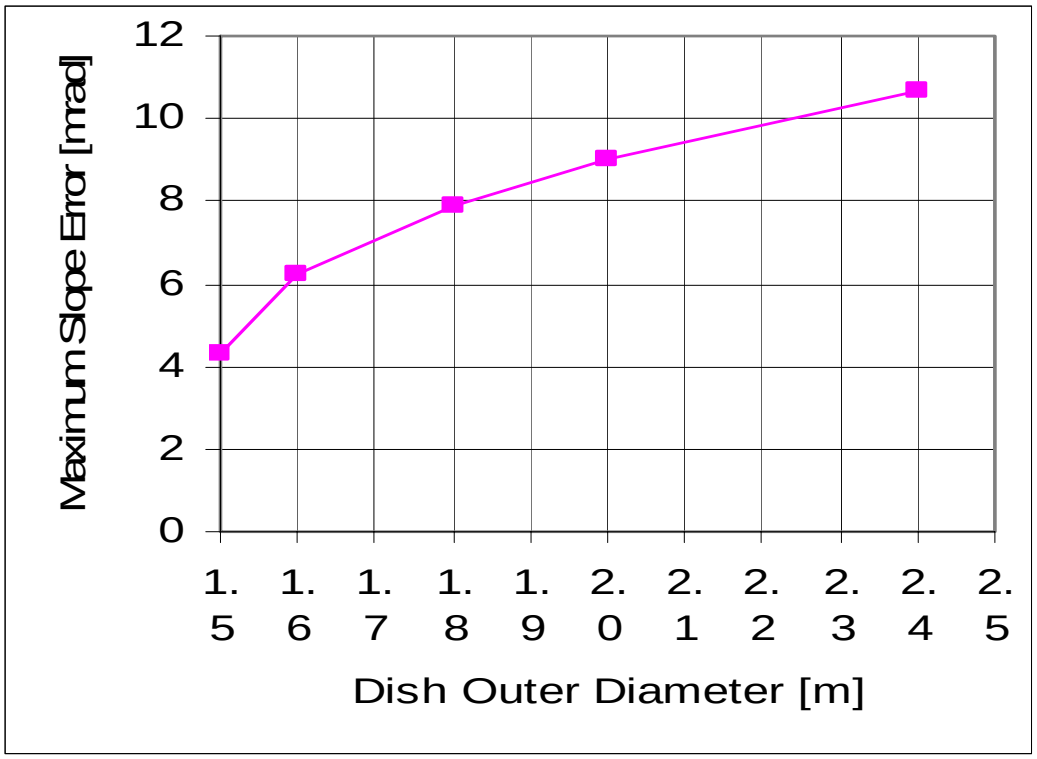

Solar Concentration

750 Net average solar concentration ratio over 50mm diameter fiber aperture (based on visible light portion of the solar spectrum, net after reflection and other losses)

96000 Lumens of light delivered to 50mm diameter fiber aperture at 1000 W/sq.m direct normal insolation

Incidence Angle

20 degree Maximum incidence angle of solar radiation onto fiber bundle aperture

Tracking Accuracy

Tracking accuracy shall be sufficient to maintain the solar concentration on the aperture of the optical fiber at nominal values at all times when conditions are within operational limits.

Autonomy

The system shall operate autonomously, without any operator intervention once initially installed and aligned.

Power

The dish-tracker system shall be self-powered from the PV array on the hybrid solar lighting system. A rechargeable battery shall provide backup and emergency power.

Alignment

Once aligned, the system shall self-calibrate its tracking to maximize the solar energy delivered to the optical fibers and PV array.

Maintenance

The system shall require no more than one hour of routine maintenance per year.

Control

The only operational control shall be a single dry contact closure to remotely enable operation of the system.

Operation

When enabled, the system shall automatically acquire and track the sun from sunup to sundown. When disabled, during high winds, and at night, the system shall move to a face-up stow orientation.

Mounting

The system is designed to be skid-mounted on a flat roof structure without requiring major structural roof penetrations.

Weight

The system shall not exceed 200lb, excepting ballast used for roof mounting.

The system shall not exceed 20lb/sq.ft of roof loading.

Control Interface

System control shall be via a 2-conductor cable to a dry contact closure. The cable shall be sized to be suitable for 1A, 24VDC operation with less than 1VDC voltage drop.

Fiber Bundle

The weight of the fiber bundle shall be supported at roof level with sufficient free length above the roof to accommodate all motion of the tracker.